ASSESSMENT OF LANDUSE INDUCED LAND SURFACE TEMPERATURE CHANGES IN THE GREATER ACCRA REGION, GHANA

By

Mathias Agbozo

(BA, Geography and Resource Development)

A Thesis submitted to the Department of Geomatic Engineering, Kwame Nkrumah University of Science and Technology, Kumasi in partial fulfilment of the requirements for the degree of

MASTER OF PHILOSOPHY IN GEOGRAPHIC INFORMATION SYSTEMS

AUGUST 2019

DECLARATION

I hereby declare that this submission is my own work and that, to the best of my knowledge and belief, it contains no material previously published or written by another person nor material which to a substantial extent has been accepted for the award of any other degree or diploma at Kwame Nkrumah University of Science and Technology, Kumasi or any other educational institution, except where due acknowledgment is made in the thesis.

……..	……	……..
Student (PG9264217)	Signature	Date

Certified by

……..	……	……..
Supervisor	Signature	Date

Certified by

……..	……	……..
Head of Department	Signature	Date

DEDICATION

I dedicate this research work to the Almighty God and my brother.

ACKNOWLEDGEMENT

This research work could not have been completed if not for the assistance of many individuals.

First and foremost, I would like to express my sincere gratitude to my supervisor Dr. Samuel A. Andam-Akorful, for his insight and guidance towards the successful completion of this research work.

I would also like to express my appreciation to Bright Addae for your inspiration and contribution towards the success of my study and research work.

I would also wish to give a special thank you to my family for their support and my fiancée for her prayers and support throughout the duration of my studies.

Immense appreciation to friends and colleagues especially Mr David Nunoo for his kind heart and Kennedy Darko for the support. My final thanks go to the management of Sambus Geospatial Limited.

ABSTRACT

This study explored the application of geospatial technology in understanding change pattern of Land use/Land cover (LULC) and associated Land Surface Temperature (LST) variability in the Greater Accra region between 1986 and 2018. Landsat satellite imagery between the months of December and February (dry season) were used for LULC analysis and LST Estimation. MODIS LST data for 1986, 2002 and 2018 were also utilized for the validation of satellite derived LST.

The aim of this research was to investigate how LULC changes affects LST. The results of analysis show that LULC in Greater Accra region has changed significantly over the 32-year period. Four major LULC types identified were; vegetation, built-up, bare land and waterbody. Bare land cover type indicated decrease from 1986 to 2018 of 60.22%. Water bodies experienced varying trend of 7.84% decrease representing 9.11 Km^2. Vegetation cover indicated 16.20% increase in 2002 and 28.02% decrease in 2018. This amounted to a total of 11.82% decrease in vegetation cover. On the contrary, built-up increased by 654.03% (724.3 Km^2) between 1986 and 2018. LST was observed to have increased by 3.05℃ over the 32-year period of this study across the Greater Accra region. with the highest LST of 36.95℃ and the lowest of 20.19℃, both recorded in 2002. The trend however indicated a significant increase between 1986 and 2002 but a decrease in LST from 2002 to 2018. The increasing trend in LST over time was found to be consistent with the observed urban expansion of the study area. High temperatures are also more apparent along the coastal belt of the region stretching northwards as development spread in the same direction. Total change in LST for the entire period of the study show increases of 3.53℃, 3.04℃, 2.78℃ and 2.65℃ for bare land, vegetation, built-up and waterbody land use/land cover types respectively. LULC association with LST shows that bare land experienced the highest negative change of 60.22% and this corresponded to the highest increase in LST of 3.53℃ over the same period. Correlation analysis and Coefficient of variation indicated largely that, MODIS LST data validated derived LST from Landsat satellite imagery. Trend of both LST values follow identical pattern with few instances where derived LST is greater than MODIS LST. Both NDBAI and NDBI exhibited a positive correlation with LST. NDVI demonstrated a negative linear correlation while NDWI indicated the strongest negative linear correlation with LST. Land use/Land cover change can be linked to rising Land Surface

Temperature Changes in the Greater Accra region of Ghana. The research stresses the need to ensure effective land use planning by relevant regulatory bodies to control urban development and address anthropogenic causes of surface temperature changes.

TABLE OF CONTENT

DECLARATION II

DEDICATION III

ACKNOWLEDGEMENT IV

ABSTRACT IV

TABLE OF CONTENT V

List of Figures VIII

List of Tables X

List of Abbreviations and Acronyms XI

1 Chapter One: Introduction 1

1.1 Background 1

1.2 Problem Statement 3

1.3 Objectives 4

1.4 Research Questions 4

1.5 Structure of Thesis Report 4

2 Chapter Two: Literature Review 5

2.1 Land Surface Temperature (LST) 5

2.2 Urban Heat Island (UHI) 7

2.3 Remote Sensing (RS) Approach to LST Estimation 8

2.4 Land Use/Land Cover Classification 10

2.4.1 Random Forest Classifiers 11

2.4.2 Random Forests and RS Satellite Imagery 12

2.5 Driving Factors of Land Use/Cover Change 12

2.6 LST Trend and LULC Change 13

3 Chapter Three: Approach and Methodology 15

3.1 Study Area 15

3.1.1 Physical Characteristics and Administrative Structure 15

3.1.2 Climate 17

3.1.3 Vegetation Cover 17
3.1.4 Demographic and Economic Characteristics 17
3.2 Data Type and Source 19
3.2.1 Landsat Satellite Images 19
3.2.2 MODIS Land Surface Temperature Data 20
3.2.3 Vector Datasets 21
3.3 Methods 21
3.3.1 Satellite Image Pre-processing 21
3.3.2 Land use/Land cover Classification 21
3.3.3 Change Detection Analysis 25
3.3.4 Land Surface Temperature (LST) Estimation Algorithm 25
3.3.5 Land Surface Temperature Validation 28
3.3.6 Correlation Analysis 29
4 Chapter Four: Results and Discussions 29
4.1 Land Use/Land Cover Patterns 30
4.1.1 Land use/Land cover Mapping and Analysis 30
4.2 Results of LULC Accuracy Assessment 33
4.3 Land Use/Land Cover Change (LUCC) Dynamics in the Greater Accra Region 36
4.3.1 Vegetation Cover 39
4.3.2 Bare and Open Land Cover Change 41
4.3.3 Urban and Built Environment Expansion 44
4.3.4 Waterbodies 46
4.4 Land Surface Temperature Analysis 48
4.4.1 Land Surface Temperature Validation 48
4.4.2 Spatio-Temporal Dynamics of Land Surface Temperature Distribution 52

4.4.3 Measure of Association in the Spatial Pattern of LST 57
4.5 Relationship between LST and LULC Types 60
4.5.1 Zonal Statistical Analysis between LULC Types and LST 60
4.5.2 Correlation Analysis between LST and LULC Types 62
5 Chapter Five: Conclusions and Recommendations 72
5.1 Conclusions 72
5.2 Recommendations 73
References 73

Appendices ..... - 1 -

List of Figures

Figure 3-1 Map of Greater Accra Region 16
Figure 3-2 Methodology Flowchart 19

Figure 3-3 Random Forest Model 24

Figure 3-4 Major Steps in Estimating LST 26

Figure 4-1 LULC Classification Map of 1986 32

Figure 4-2 LULC Classification Map of 2002 33

Figure 4-3 LULC Classification Map of 2018 34

Figure 4-4 Percentage Change in LULC Types 38

Figure 4-5 Graphical Representation of LULC Change 38

Figure 4-6 Vegetation Cover Trend 39

Figure 4-7 Percentage Change in Vegetation Cover..... 40

Figure 4-8 Bare land Cover Trend 41

Figure 4-9 Percentage change in Bare land 42

Figure 4-10 Percentage Change in Built-up..... 43

Figure 4-11 Percentage Change in Built-up..... 44

Figure 4-12 Waterbody LULC Trend 45

Figure 4-13 Percentage Change in Water bodies 46

Figure 4-14 Spatial Distribution of LST Validation Sample Sites 49

Figure 4-15 Correlation between Derived LST and MODIS LST for 2002 49

Figure 4-16 Correlation between Derived LST and MODIS LST for 2018 50

Figure 4-17 Spatial Distribution of Land Surface Temperature in 1986 53

Figure 4-18 Spatial Distribution of Land Surface Temperature in 2002 54

Figure 4-19 Spatial Distribution of Land Surface Temperature in 2018 56

Figure 4-20 Spatial Autocorrelation for 1986 57

Figure 4-21 Spatial Autocorrelation for 2002 58

Figure 4-22 Spatial Autocorrelation for 2018 58
Figure 4-23 LULC type and Average LST 60
Figure 4-24 Relationship between LST and NDVI in 1986 63
Figure 4-25 Relationship between LST and NDVI in 2002 63
Figure 4-26 Relationship between LST and NDVI in 2018 63
Figure 4-27 Relationship between LST and NDBAI in 1986..... 65
Figure 4-28 Relationship between LST and NDBAI in 2002..... 65
Figure 4-29 Relationship between LST and NDBAI in 2018..... 65
Figure 4-30 Relationship between LST and NDBI in 1986 66
Figure 4-31 Relationship between LST and NDBI in 2002 67
Figure 4-32 Relationship between LST and NDBI in 2018 67
Figure 4-33 Relationship between LST and NDWI in 1986 68
Figure 4-34 Relationship between LST and NDWI in 2002 69
Figure 4-35 Relationship between LST and NDWI in 2018 69

List of Tables

Table 3-1*:* Research Approach 18
Table 3-2 Details of Landsat Satellite Images 20
Table 3-3 Description of LULC types 22
Table 3-4: Thermal Conversion Constants used for LST Estimation 27

Table 3-5 Estimation of Atmospheric Transmittance 29

Table 4-1 LULC Types and Coverage Extent of 1986 32

Table 4-2 LULC Types and Coverage Extent of 2002 33

Table 4-3 LULC Types and Coverage Extent of 2018 34

Table 4-4 Accuracy Assessment of LULC Maps 35

Table 4-5 Producer Accuracy 36

Table 4-6 Extent of Change in LULC Types 37

Table 4-7 Cross-Table Validation of LST 47

Table 4-8 Accuracy Assessment of LST Validation..... 50

Table 4-9 Comparison of Landsat and MODIS Specifications 51

Table 4-10 Land Surface Temperature Statistics 52

Table 4-11 Land Surface Temperature categorized by Land use/Land cover type 59

Table 4-12 Comparison between LULC Change and LST Change between 1986 and 2018 60

List of Abbreviations and Acronyms

AMA – Accra Metropolitan Assembly

AVHRR - Advanced Very High-resolution Radiometer

CBDs – Central Business Districts

CERSGIS – Center for Remote Sensing and Geographic Information Services

DIRS - Digital Imaging and Remote Sensing Laboratory

DN – Digital Number

EEA - European Environment Agency

GHGs – Green House Gases

GIS – Geographic Information System

GST - Ground Surface Temperature

IPCC – Intergovernmental Panel on Climate Change

LST – Land Surface Temperature

LUCC – Land Use/Land Cover Change

LULC – Land Use/Land Cover

MMDAs - Metropolitan, Municipal and District Assemblies

MNDWI – Modified Normalized Difference Water Index

MODIS - Moderate Resolution Imaging Spectral-diometer

NDBAI Normalized Difference Bare Land Index

NDBI – Normalized Difference Built-up Index

NDVI – Normalized Difference Vegetation Index

NDWI - Normalized Difference Water Index

NIR – Near Infrared

PHC - Population and Housing Census

PuHT - Peri-Urban Heat

RF – Random Forest

RS – Remote Sensing

RuCT - Rural Cool Troughs

SWIR – Short Wave Infrared

TIR – Thermal Infrared

TMA – Tema Metropolitan Assembly

TOA – Top of the Atmosphere

UAV – Unmanned Aerial Vehicle

UHI – Urban Heat Island

UNEP – United Nations Environment Programme

USGS – United States Geological Survey

UTM - Universal Transverse Mercator

WGS - World Geodetic System

WHO – World Health Organization

WMO - World Meteorological Organization

1 Chapter One: Introduction

1.1 Background

Concerns over changing climatic conditions is unequivocal in recent times. Climate change conditions is among the major challenges facing the world in this modern age. It adds substantial stress to the environment and the society due to its repercussions felt by both human and natural systems (Adedeji *et al.* 2014; Serdeczny *et al.* 2017). Hille (2016) identifies global surface temperature as one of the two key climate change indicators. Earth's climate has warmed by approximately 0.6ºC over the past hundred years, each decade has experienced successively warmer surface temperatures compared to the previous decade from 1850 (Walther *et al.* 2002; Stocker *et al.* 2013). Africa is among the continents that are likely to suffer the impact of changing climate (Intergovernmental Panel on Climate Change, 2014; Niang *et al.* 2014). Surface temperature changes in Sub-Saharan Africa has not been any different from global trends. A study carried out by Collins (2011) on temperature variability over Africa, found significant increasing temperature trends between 1979 and 2010.

Increasing temperatures has been exacerbated in cities by Urban Heat Islands (UHI) effect. The phenomenon of urban heat island (UHI) shows that temperatures in built-up regions differ in few degrees higher compared to those in non-urbanized regions. ―Recent studies show that a number of cities in the world have observed an upsurge in urban temperatures‖ (Manu *et al.* 2006). Many researchers including Voogt and Oke (1997) have linked anthropogenic activities to UHI. The effects of urban heat-island (UHI) is one key example of human influence on local climate (Hinkel *et al.* 2003).

Urbanization trends resulting in increasing size of cities and deterioration of urban environment has been a source of growing worry for future cities (Enete and Okwu, 2013). Approximately 2% of the entire landmass of the earth constitute urban regions, which are inhibited by approximately half of the world's population (Van Vliet, 2001). The urbanization rate especially in most of the emerging countries is significant over recent decades due to the pursuit of fast economic development (Li *et al.* 2009). It has rapidly increased in the past century and is projected to further increase. Rapid growth of population and the incessant exploitation of the world's resources over the years have been the main factors instigating land-use/cover change (LUCC) on global scale (Zhou and Wang, 2011). Kleemann *et al.* (2017) reported that, population growth particularly in

rural communities constitute a significant factor of LUCC in Ghana. The dynamics of Land use and land cover (LULC) affect the land surfaces‘ ability to reflect or absorb in varying proportions solar radiation (Appiah *et al.* 2017). LUCC typically affect land surface temperatures (LST) (Asmat *et al.* 2016 cited in Appiah *et al.* 2017).

The most appropriate tool for the systematic assessment of heat islands at city and regional scales is remote sensing, it allows the analysis of surface temperature maps and processing of images revealing the distribution of other parameters influencing UHI (European Environment Agency, 2010). Thermal Infrared (TIR) imagery is significant in several applications such as LST estimation (Liu and Zhu, 2012). Thermal bands from satellites have been used in several studies to estimate surface temperature (Bakar *et al.* 2016). Several authors have used the TIR satellite remote sensing as proxy for calculating LST through the estimation of land surface reflectance properties (Srivastava *et al.* 2010; Liu and Zhang, 2011; Rajeshwari *et al.* 2014 cited in Appiah *et al.* 2017). Thermal infrared (TIR), the Enhanced Thematic Mapper Plus (ETM+) and the Landsat Thematic Mapper (TM) data have been used likewise for local-scale reports of urban heat island (Chen *et al.* 2002; Weng, 2001).

Previous research works have shown that, integration of Remote Sensing (RS) and Geographic Information System (GIS) can be combined as tool for estimating the LST impact on rapid builtup growth development (Liu and Weng, 2008). Widyasamratri *et al.* (2013) in his study to assess the rate as well as the intensity of urbanization in Jakarta, Indonesia, established the correlation between UHI and urbanization. In another study by Bakar *et al.* (2016), the relationship between LUCC revealed a negative correlation between vegetation cover and LST concluding that Modified Normalized Difference Water Index (MNDWI), Normalized Difference Vegetation Index (NDVI) and Normalized Difference Built-up Index (NDBI) indices could serve as pointers to monitor the impact of LCLU on LST.

In Ghana, the correlation between LULC and LST has been assessed for few cities. However, there exist limited research and comprehensive understanding of long-term LST trend in the Greater Accra region at large. The insight offered by the long-term spatiotemporal study of LST is necessary for urban thermal environment and microclimate characterization. The study was therefore intended to investigate LUCC relationship with LST in the Greater Accra Region of Ghana.

1.2 Problem Statement

The World Meteorological Organization (2017) report on temperature shows that 2015 to 2017 have been the top three warmest years and it constitute a long-term warming trend. Reports of heat waves have also been rampant in recent times, buttressing observed increasing temperature trends. Mora *et al.* (2017) predicts more extreme cases in the coming decades, in frequency and over much greater portion of the planet. The planet earth recorded

The impacts of increasing temperature trends have been identified by several studies. For instance, increasing thermal stress poses significant threats to human health (European Environment Agency, 2011). UHI effect increases the hazard of outdoor environment discomfort and injuries related to heat stress which pose threat to the health of those living in the cities (Ebi *et al.* 2004; Mathies *et al.* 2008; Barredo, 2009; Hajat *et al.* 2010; Enete *et al.* 2013).

WHO (2007) report on ―Improving Public Health Responses to Extreme Weather/Heat-Waves, EuroHEAT‖ emphasizes the fact that, hot weather can kill and cause illness. Higher temperatures in the urban areas also increase daily energy consumption requirement for cooling, especially during peak electric demand periods in the Central Business Districts (CBDs). Increased energy consumption is also linked to the release of more greenhouse gas due to the combustion of fossil fuel, thus perpetuating the cycle (EEA, 2010).

In local climates of many cities, a major contributing factor to increasing temperatures has been identified as LUCC (Peng *et al.* 2018; Mushore *et al.* 2017; Chen *et al.* 2006; Pei *et al.* 2016; Buyadi *et al.* 2013; Zhou and Wang, 2011). Urban growth has accounted for changes in LULC and impacted LST (Wang *et al.* 2018; Zhao *et al.* 2017).

Land use/cover pattern in Ghana have experienced fundamental change due to accelerated economic development. For example, infrastructure development in Accra has been very high with built-up areas increasing by 59% between 1985 and 2010 (Yeboah *et al.* 2017). Due to the seriousness of LUCC on environment, impact studies has been undertaken leading to the conclusion that the changes can have momentous impact on climate and local weather (Yeboah *et al.* 2017; Landsberg, 1981). This underpins the need to understand the LST trends and its association with the changes in land use in the Greater Accra of Ghana. The insight from this study seeks to present valuable actionable information for variety of application in addressing the rising

temperature conditions in our cities. This knowledge on the impacts of changing urban landscape on microclimatic conditions of cities is imperative for spatial decision making in especially urban design and land use planning for sustainable development.

1.3 Objectives

Main:

The aim of this study is to investigate how Land Use/Cover changes affects Land Surface Temperature (LST) in the Greater Accra Region of Ghana.

Specific:

1. To identify the changing pattern of LULC over the past thirty-two (32) years.
2. To understand LST variability in the Greater Accra region.
3. To analyze LST variations associated with LULC changes.

1.4 Research Questions

1. What is the trend of LULC in the region?
2. Is there spatial variation in Land Surface Temperature?
3. What is the relationship between LULC types and LST?
4. Can LST changes be explained by the changing nature of LULC in the region over the years?

1.5 Structure of Thesis Report

The thesis structure was organized in five interrelated chapters. Chapter one outlined the following: research background; aim and objectives of the research; research question as well as problem definition. The second chapter reviewed relevant papers and other literature on GIS and RS application in LULC and LST research. The third Chapter gives description to the study area, data sources, research techniques and general methodological approach used in the study. Chapter four presented the results after the data analysis and discussion on the findings of the research. Finally, the fifth chapter focused on the research limitations, recommendations and the conclusion.

2 Chapter Two: Literature Review

The attention of climate researchers has for the last decade been drawn to regional and local climate under human influences to ascertain the upsurging change in driving factors of climate (Adegoke *et al.* 2003). The change in the surface thermal environment is one of the key components of regional climate change. The global average data of combined ocean and LST confirms a warming of 0.85˚ C (0.65 to 1.06) from 1880 to 2012 (Stocker *et al.*, 2013). Many observed increases in the average temperature on the global scale have been linked directly to the emission of greenhouse gases (GHG) (Hegerl *et al.*, 2007). Anthropogenic causes have been on the rise since the era of pre-industry, driven mainly by population and economic growth which influence LULC. The impact of human influences has been the main cause of the upsurge in LST since the middle of the twentieth century.

2.1 Land Surface Temperature (LST)

A number of factors have been linked to micro climatic warming and heat rise. The major factor is the rise in LST. According to Bense, *et al.* (2016), LST defines the skin temperature of the surface –referring to canopy surface temperature of vegetation (*i.e.* for densely vegetated area) and soil surface temperature (*i.e.* for bare soil). The skin temperature or land surface is referred to as the temperature that comes from the surface of the canopy layer. For meager vegetated ground, LST defines the temperature of the canopy, body of the vegetation as well as surface of soil (Qin and Karnieli, 1999). LST is defined by the temperature radiating from the surface of the earth – controlling water exchange with temperature and surface heat (Yuan and Bauer, 2007).

The difference that exist between Ground Surface Temperature (GST) and LST effect is not only based on the regular recurrence of shortwave radiation from the sun and the influence of the characteristic layer and surface of the soil/litter. Thus, the main bias or deviation can be brought about especially when using products of LST since the inadequate reflection of the buffering effects of vegetation, snow cover as well as upper soil layers (Luo *et al.*, 2018).

LST is among the significant phenomena that control the chemical, physical and the biological courses of the earth and an important factor in urban climate study (Pu *et al.* 2006). In other words, land surface temperature constitutes a significant phenomenon in understanding the physical courses of water balance and surface energy. It is considered as a complete force underpinning the

exchange of turbulent heat and long-wave radiation at the atmosphere-surface interface (Brunsell and Gillies, 2003; Zhang *et al.* 2008; Anderson *et al.* 2008; Kustas and Anderson, 2009; Karnieli *et al.* 2010). Land surface temperature play a significant role in most of the land-surface processes (Sellers *et al.* 1988; Mannstein, 1987).

Land surface temperature is linked to heat transport between the atmospheric boundary layer and land surface and makes estimation of latent heat and evapotranspiration, or sensible heat fluxes. LST constitute a significant input with regards to the modeling of the ecosystem, which can be performed at the global, regional and local scales. Land surface temperature varies in terms of surface energy balance as it controls the temperature of air at the lower layers of built-up atmosphere. LST is important to the balance of energy on earth surface and affects exchanges of energy and these together affect people's comfort especially those in urban areas (Voogt and Oke, 2003). In-depth knowledge on LST hence provide details on spatial and temporal differences of equilibrium state of the surface –this is important in several applications such as monitoring the climate, urban environment and climate studies, hydrological, evapotranspiration and the monitoring of vegetation (Bastiaanssen *et al.* 1998; Su, 2002; Arnfield, 2003; Voogt and Oke, 2003; Weng *et al.*, 2004; Kalma *et al.*, 2008; Weng, 2009; Hansen *et al.*, 2010). Land surface temperature has been extensively used in meteorological, climatological, ecological, and hydrological studies (Duan *et al.*, 2017; Weng and Fu, 2014; Anderson *et al.*, 2008; Sandholt *et al.*, 2002). It continues to be used for various scientific studies and it is a significant factor in assessing heat related risks, for estimation of building energy consumption, and for measuring surface urban heat islands (Mattew *et al.*, 2016; Weng and Fu, 2014; Deng and Wu, 2013; Hu and Brunsell, 2013).

Land surface temperature is very sensitive to several features on land surface and thus can be engaged in the extraction of information from the various LULC types. Due to the fact that strong heterogeneity of features of land surface like topography, soil, and vegetation (Neteler, 2010), land surface temperature changes are rapid in time and space (Prata *et al.*, 1995) and enough description of the distribution of land surface temperature as well as temporal evolution.
LST thus entails measurements with in-depth temporal and spatial sampling.

2.2 Urban Heat Island (UHI)

The UHI effect is among the best expressions of anthropogenic activities impact on local climate. UHI has been a concern since the last four decades. Voogt (2004) suggests that urban heat island is the distinctive warmth of the lithosphere and atmosphere in the built-up areas as against their rural regions. Cities have comparatively adequate thermal capacity and higher absorption of solar radiation (Weng, 2001). The effect of UHI constitute a phenomenon that produce higher temperatures in built-up regions than that of the non-urban surroundings (Jensen, 2000). The effect of urban heat island constitutes a significant climatic phenomenon to research because microclimate gets affected by local temperatures through process like vegetation growth, moisture retention, levels of plant, and atmosphere evaporation.

Comparison of the general warming of cities to that of the hinterlands is just one of the facet of the impacts of urbanization on local climate. A significant impact of UHI phenomenon is the local climatic variability and changes. UHI result as a mammoth division of land-cover within a particular region get replaced with built-ups that absorbs radiation from the sun during the day and later releases this radiation at night (Quattrochi *et al.* 2000; Oke, 1982). There are some factors linked to micro climatic warming and urban heat rise, LST is one of these factors. The phenomenon is basically affected by the amount of water and vegetation on pervious surfaces. The causes of UHI include change of land surfaces like urban expansion which uses materials capable of retaining heat. Also, population growth linked to rapid expansion of urban areas contribute to UHI development in these areas with concurrent upsurge in both maximum and minimum temperatures at similar rates. Economic output per capital and rapid population growth has been an exceptional character of this modern age (Sieferie, 2001; Cohen, 1995), affecting concerns on global environment (Rosa *et al.*, 2004). Rapid urbanization is a contributor to changes in LULC and affect UHI (Streutker, 2003; Gallo and Owen, 2002). Like most built-up areas in Africa, the Accra and Kumasi metropolises keep experiencing a quick urban expansion with a linkage to growth in human population.

Several research point to the fact that human activities strongly impact the atmosphere of the urbans through UHI establishment (Magee *et al.*, 1999; Oke, 1997). The sources of anthropogenic heat are factories, cars and homes. The most significant is heat absorbed and released by layers like

stones, black asphalt, concrete and bricks. These impervious layers have high capacity to capture, store and radiate heat.

2.3 Remote Sensing (RS) Approach to LST Estimation

Traditionally, ground measurement of Land Surface Temperature has always provided point values at the monitoring station usually sited in tree park-like surroundings (Nichol and To, 2012). This is plagued with the challenge of the discrete nature of the data recorded. Other challenges include the rising cost of purchase, installation as well as maintenance of climate equipment. This makes it hard to measure adequate LST at point locations in order to achieve a full coverage of an area. As local modeling depends on field data, RS constitute the primary source of estimation of LSTs at the global and regional scales (Li *et al.*, 2013).

Development of RS technology has improved the possibility of measuring LST over wide areas and even the entire globe. The RS methods make use of the thermal inertia of materials on the land surface and physical models are applied to generate LST (Jensen, 2000; Sobrino *et al.*, 2004). Satellite data have availed sufficient high temporal resolution which is key as a vital tool for monitoring the LST and UHIs of the Earth over long period of time. Thermal band from different satellite data has been used by several researchers (Yuan and Bauer, 2007; Weng *et al.*, 2004; Small, 2006; Gluch *et al.*, 2006; Weng, 2009; Kato and Yamaguchi, 2005) to evaluate LST.

Land surface temperature has always been retrieved successfully from satellite-infrared sensors like the Moderate Resolution Imaging Spectral-diometer (MODIS) and Advanced Very Highresolution Radiometer (AVHRR) aboard satellites. The best method of approach for a sinusoidal model over the quotidian product is most used to smoothen the sequential mean of land surface temperature (Tedesco, 2015). Hachem *et al.* (2009) posits that, choosing the best method enhanced the investigations of permafrost of mountains, particularly for uneven and sparsely observed remote regions.

Dash *et al.* (2002) indicates that the satellite thermal infrared sensors is responsible for measuring the top of the atmosphere (TOA) radiances, where brightness temperatures are derived using the Plank‘s law. The top of the atmosphere radiances constitutes the result of the upwelling radiance from space, the emitted radiances from earth‘s surface, and the down-welling radiance from the sky, which is the three fractions of energy. The difference between land surface brightness and top

of the atmosphere radiances generally ranges from 1K to 5K in the 10 to 12μm spectral area, and these are affected by atmospheric conditions (Prata *et al.* 1995). Thus, conditions of the atmosphere like the downward irradiance reflected, upward emission, and absorption from the surface (Franca and Cracknell, 1994) ought to be rectified before the land surface temperature is generated. The brightness temperatures must be corrected further with values of spectral emissivity before the computation of land surface temperature to explain the roughness properties of the nature and amount of the land surface, vegetation cover, and the moisture content and thermal properties of the soil (Friedl, 2002).

Several algorithms have been suggested and have been adopted for the estimation of LST for treating the various sensors aboard distinct satellites and making use of various assumptions and approximations for LSEs and RTE. Schmugge *et al.* (1998), considered two approaches to stem LST from multi-spectral thermal infrared images. The first approach makes use of a radiative transfer equation to render corrections to at-sensor radiance to the surface radiance, then by emissivity model to cause separation to the surface radiance into emissivity and temperature. The second approach uses the technique of split-window for land and sea surfaces, suppose the emissivity in the channels are similar (Dash *et al.* 2002). LST are thus worked out as the two channels are combined.

One particular challenge of this algorithm is that the coefficients are only effective for the set of data used in deriving them. That is to say, thermal responses datasets for a particular landscape process or phenomenon measured by means of specific thermal infrared sensor will fail to be inferred for the prediction of similar measurement of thermal infrared –either from both recorded images and sensors at separate periods making use of similar sensor (Quattrochi and Goel, 1995).

The upsurge in usage of Landsat data in recent times for the retrieval of LST has been the cause of creation of models that center on thermal band (TM6) only for Landsat sensors. Models like the radiative transfer equation was advanced for Landsat LST retrieval, however, the foremost challenge of this model is its inability to launch concurrently with satellite movements without in-situ radio-sounding. In finding solution to this challenge, a mono-window algorithm was created Qin *et al.* (2001). Land surface temperature is acquired by this algorithm from the TM6 of the sensor of thematic mapper which aboard Landsat 5 satellite. Factors used for the algorithm are the total atmospheric transmittance, the at-sensor brightness temperature, the effective mean

atmospheric temperature, and the land surface emissivity (i.e. all temperatures in Kelvin). This algorithm is regarded more robust as it includes other factors aside brightness temperature. The benefit of the mono-window is after surface emissivity values as well as the solar angel values have been combined to the model, there exist a higher correlation between the retrieved land surface temperature and the brightness temperature (BT) (Alsultan, 2005). In the estimation land surface temperature making use of the mono-window algorithm, the BT is calculated first, while incoming solar radiation and surface emissivity are given as the parameters for the algorithm. The values of the surface emissivity are extracted from the values of NDVI. Regression and correlation test by Lim *et al.* (2012), confirmed a more positive relationship between anticipated LST and the values computed using the mono-window algorithm. Jung *et al.* (2011) used the same algorithm in their study to establish the relationship between LST, land covers and spectral emissivity making use of Landsat ETM+ and ASTER imagery of Kuju volcano from 2000 to 2006. This study identified a negative correlation for the retrieved values of LST and values for the NDVI.

In the application of the split window algorithms and the mono-window algorithm on MODIS data, Zheng (2006) posits that one major challenge of using the retrieval algorithms is their requirement for surface emissivity values and atmospheric profile parameters, which are absent in the imagery from Landsat TM thermal channel. Additional computation must be done to have the parameters which render the land surface temperature retrieval process strenuous. Various studies have made use of the various algorithms and techniques to the retrieval of land surface temperature, using the thermal band in Landsat.

2.4 Land Use/Land Cover Classification

Geographic Information System (GIS) and Remote Sensing (RS) constitute important tools for the assessment and monitoring of changes in the environment as a result of its repetitive and synoptic coverage of space borne imagery thus useful for urban growth detection projects (Weng, 2001). Satellite remote sensing can collect multi-temporal data and as well turn it into usable information for observing changes in urban land processes.

The integration of GIS and RS constitute a useful tool for studying interactions in human environment, like changes in LULC. LULC mapping to generate information on the changing nature of the earth is therefore one of the key and typical RS applications.

Currently, there has been near real time availability and improvement of multi spatio-temporal data with upgraded techniques for making monitoring LUCC cost-effective and timely.

Many have used various algorithms or methods in LULC studies. The Supervised Maximum Likelihood Classification method has been widely used (Appiah, 2014; Basommi *et al.*, 2016; Kumi-boateng and Stemn, 2015; Amamo and Amenu, 2017; Yeboah *et al.*, 2017; Mensah, 2017) due to the need to make selection of the classes on the basis of pixel spectral properties and as well user friendliness of the classifier for images of low resolution (Appiah, 2014). Notwithstanding, development in technology have resulted in machine learning algorithms like the Random Forest (RF) algorithm.

2.4.1 Random Forest Classifiers

In the past twenty years, the random forest classifier as Breiman (2001) posits has attracted increased consideration as a result of its excellent results for classification and the speed in processing it (Rodriquez-Galiano *et al.* 2012). This algorithm constitutes an ensemble classifier that gives multiple decision trees, with the use of randomly selected subclass of training variables and samples. The RF classifier has gained popularity in the RS application as a result of its accuracy in classifications. Breiman (2001) avers that RF classifier uses set of CARTs for prediction. The trees are created through drawing subsets of training samples by means of replacement, implying that, similar samples can be selected on many occasions, whereas others may not at all get selected. That is, approximately two thirds of the in-bag samples are used in the internal cross-validation technique for the estimation on how well RF result model would perform (Breiman, 2001). Stumpf and Kerle (2001) indicates that the size of the sets of training samples have been identified to affect performance of RF classifier. According to Colditz (2015) investigation to date on RF classifier shows that the training samples sizes ought to represent about 0.25 percent of the entire study area. Deng and Wu (2013) adopted RF classifier in their quest of classifying large-scale urban impermeable regions and they observed that the method performs better when there is availability of a large number of samples.

Mellor *et al.* (2015) when investigating forest classification from Landsat data identified that random forest classification was comparatively insensitive to mislabeled training data. The researchers further identified that imbalanced training data can get introduced to take out errors in the classes posing greater challenge to the classification. On the other hand, investigations carried

out by Dalponte *et al.* (2013) and Millard and Richardson (2015) shows that random forest classifier is sensitive to the proportions of the different classes inside the training samples and to spatial autocorrelation of the training classes. Dalponte *et al.* (2013) continued that random forest classifier fails to withstand the excessive training data and thus tend to favour those in the representative classes.

2.4.2 Random Forests and RS Satellite Imagery

The random forest classifier has been used positively for the mapping of classes of LULC (Stefanski *et al.*, 2013; Tsutsumida and Comber, 2015; Haas and Ban, 2014; Colditz, 2015) as well as buildings in built-up regions (Belgiu and Drăgut, 2014); for classifying insect defoliation levels by the use of the red-edge band (Adelabu *et al.*, 2014); for mapping habitats of boreal forest using WorldView-2 imagery (Räsänen *et al.*, 2013); for mapping biomass with the use of temporal data of Landsat; for classifying built-up areas' impervious surfaces from data of the single date MODIS (Deng and Wu, 2013); for identifying tree health using IKONOS data; and for mapping the canopy of vegetation as well as the biomass using multi-temporal and unitemporal Landsat 8 imagery (Karlson *et al.*, 2015). Random forest classifier has been successful as well in using it for LULC classifications from both data of Polarimetric SAR (Uhlmann and Kiranyaz, 2014), multi-temporal SAR (Waske and Braun, 2009) and for oil spill mapping from data of SAR (Topouzelis and Psyllos, 2012).

Several researchers have investigated the potency of RF classifier for mapping reforested landslide with the use of calculated variables either for image objects or pixel defined by segmentation; or for improving urban object classification from the data of airborne LiDAR (Niemeyer *et al.*, 2014; Chehata *et al.*, 2009). However, few researchers have explored the usage of RFs in the classification of UAV data and in thermal RS as Sun and Schulz (2015) avers.

2.5 Driving Factors of Land Use/Cover Change

LUCC constitute a complex interaction between humans and the environment. In built-up areas in Ghana, predominantly Kumasi, Accra, the term urbanization basically refers to the expression of the external expansion of cities including converting prime vegetation or agricultural land cover into industrial and residential uses.

The main factors or forces contributing to LUCC is generally accepted to be two factors namely anthropogenic or socioeconomic factors and biophysical forces. According to Geist and Lambin (2002) the factors causing LUCC are referred to as the precise and subtle forces. There are several factors leading to LULC changes in other parts of the globe (Campbell *et al.*, 2005; Semeels and Lambin, 2001). These specific drivers include global market forces (Beilin *et al.*, 2014), pasturing (Calvas *et al.*, 2013), population growth (Bewket, 2002), urbanization (Dewan *et al.*, 2012), but may at times include other complex human interactions due to cultural and institutional influences.

Not long ago, climate change in the form of fire, changing patterns of rainfall, and drought, have all being considered as the upshot of land use/land cover changes (Kicklighter *et al.*, 2014; Roman-Cuesta *et al.*, 2014).

Attention on land use/land cover changes has increase on global scale, however, other causes have been identified in other regions of the world (Beilin *et al.*, 2014; Dessie and Kleman, 2007; Bewket, 2002). In Africa, Ethiopia to be precise, a study conducted by Tekle and Hedlund (2000) observed that settlement expansion is the main force contributing to land use/land cover changes as forest in the South Wello gets deforested. Also, according to Tegene (2002), charcoal making and collection of fuelwood constitute the main forces contributing to LULC processes.

A study along the Kokrobite and Bortianor shoreline discloses the changing pattern of increasing conversion of traditional and nature-based land use patterns to tourism-based establishments. This was found to culminate into rapid loss of vegetative cover making it highly susceptible to the high influence of coastal erosion and wetland ecological resource degradation (Boafo *et al.*, 2014).

2.6 LST Trend and LULC Change

Land Surface Temperature has been studied by several researchers across many parts of the globe from Middle East, Asia, Africa, South America among others. Description of the temperature trends and how they are attributed to natural factors and socioeconomic forces have been significant in understanding the role of human activities in altering climate system. The altering effect of climate change facing the world in recent decades have extensive impact on natural as well as human systems (IPCC, 2014). As has been widely discussed, the implication of human induced factor to warming of the atmosphere is extensive and it may demand substantial economic,

societal, and technological changes in trends (Van Den Bergh and Botzen, 2014; IPCC, 2014; Stern, 2007).

Various studies have demonstrated the connection between LUCC and corresponding LST dynamics. In Malang, spatio-temporal analysis of temperature shows widening of geographic space experiencing increasing temperature trends while establishing the link between the spatial pattern of temperature distribution and land cover change.

Higher level of anthropogenic activities has been attributed to higher Land Surface Temperature. Makinde and Agbor, (2019) identifies with this trend and alludes to the notion that high level of anthropogenic activities is a driving force of significant UHI effect in Akure, a central business district in Nigeria. Though change in land surface temperature does not give substantial evidence to explain the phenomenon of urban heat islands, which is considered as one of the significant LS factors contributing to urban surface heat (Ishola *et al.*, 2016).

Ishola *et al.* (2016) concludes that surface temperature is a major indicator of the presence of surface urban heat island in the city of Abeokuta. Areas in and around the city center experience increase surface temperature. Its distribution however altered being mixed pattern to UH as the impermeable regions increased drastically from about 13 percent of the entire region of the city after it was changed to high land surface temperature of 33℃ and above. It was however identified that higher surface temperatures were infrequently experienced in regions of cities, but also in city outskirts, particularly areas with advanced built-ups or developing sites due to fewer green/trees lands and other impervious areas like pavements (Makinde and Agbor, 2019).

Carlson and Sanches-Azofeifa (1999) investigated and concluded on a strong positive correlation between change in urbanization and land surface temperature. In other words, changes in land use especially in the cities led to pixels migrating from cool surface condition to hotter one. A five years study also supported assertions that increasing urbanization affected and converted dense green lands which come with low temperatures to sparse green lands which come with high temperatures as Jiang and Tian (2010) indicates.

Further study by Buyadi *et al.* (2018) on LULC changes and LST indicated increase in land surface temperature including the thermal signal of cities and bare land and established the ability of green land regions to positively influence the high temperature in the built-up areas. Xiao and Weng

(2007) showed that change in land surface temperature is directly linked to changes in the materials use for construction in the built-up regions and abundant vegetation in both rural and urban regions.

Similar research into Rural Cool Troughs (RuCT) and Peri-Urban Heat (PuHT) in the Bosomtwe district by Appiah *et al.* (2017) suggested that the district, was on a rural to peri-urban trajectory characterized by values of land surface temperature that range between 24℃ to 53℃. Their observation supported the conditions of the Peri-Urban Heat and the Rural Cool Troughs which resulted from changes in the landscape of the peri-urban and rural areas.

Domaley *et al.* (2018) further confirm this link between surface temperature and vegetation with their study that documented general negative correlation between vegetation and LST throughout Ghana with the northern sector demonstrating the strongest negative correlation of approximately -0.8 and the southwestern part of Ghana depicting a weak negative correlation.

Urban areas and bare soil recorded higher LSTs than vegetated areas buttressing the conclusion arrived in a study in Tarkwa that higher impervious and non-evaporative surfaces experience high LSTs due to absence of vegetation associated with lower temperatures (Aduah *et al.* 2012) According to Kumi-boateng and Stemn (2015), within a period of seventeen (17) years, urban development in the urban zones of Sekondi-Takoradi Metropolis also increased surface radiant temperature by 4.3℃ depicting the increasing yearly rate of change in the land use of built-up regions of 4.65% within the same period.

Carlson and Arthur (2000); Weng *et al.*, (2004); Jiang and Tian (2010); Chen *et al.*, (2006); Pal and Ziaul (2016); Rasul and Ibrahim (2017); Azhdari *et al.*, (2018); Fathizad *et al.*, (2017); Shiferaw (2011) have all studied the effect of LULC change on LST. Some of these have specifically investigated specific LULC categories including vegetation indices and their relationship with Land Surface Temperature changes.

3 Chapter Three: Approach and Methodology

3.1 Study Area

3.1.1 Physical Characteristics and Administrative Structure

The Greater Accra region is among one of Ghana‘s sixteen (16) administrative regions. The Greater Accra region shares boundaries with the Volta Region to the east, Eastern Region to the north,

Central Region to the west, and the Gulf of Guinea to the south. Its coastline is about 225 kilometers, stretching from Kokrobite in the west to Ada in the east. The region is the smallest among the sixteen (16) regions of Ghana occupying an area of 3,245 square kilometers, representing 1.4% of Ghana‘s entire land mass. The Greater Accra region is located in the southcentral part of Ghana and lies approximately within geographic coordinates of latitude (0º 13′ 55″E; 6º 6′ 28″N to the North, 0º 24′ 19″ W; 5º 28′ 23″ N to the South) and longitude (0º 30′

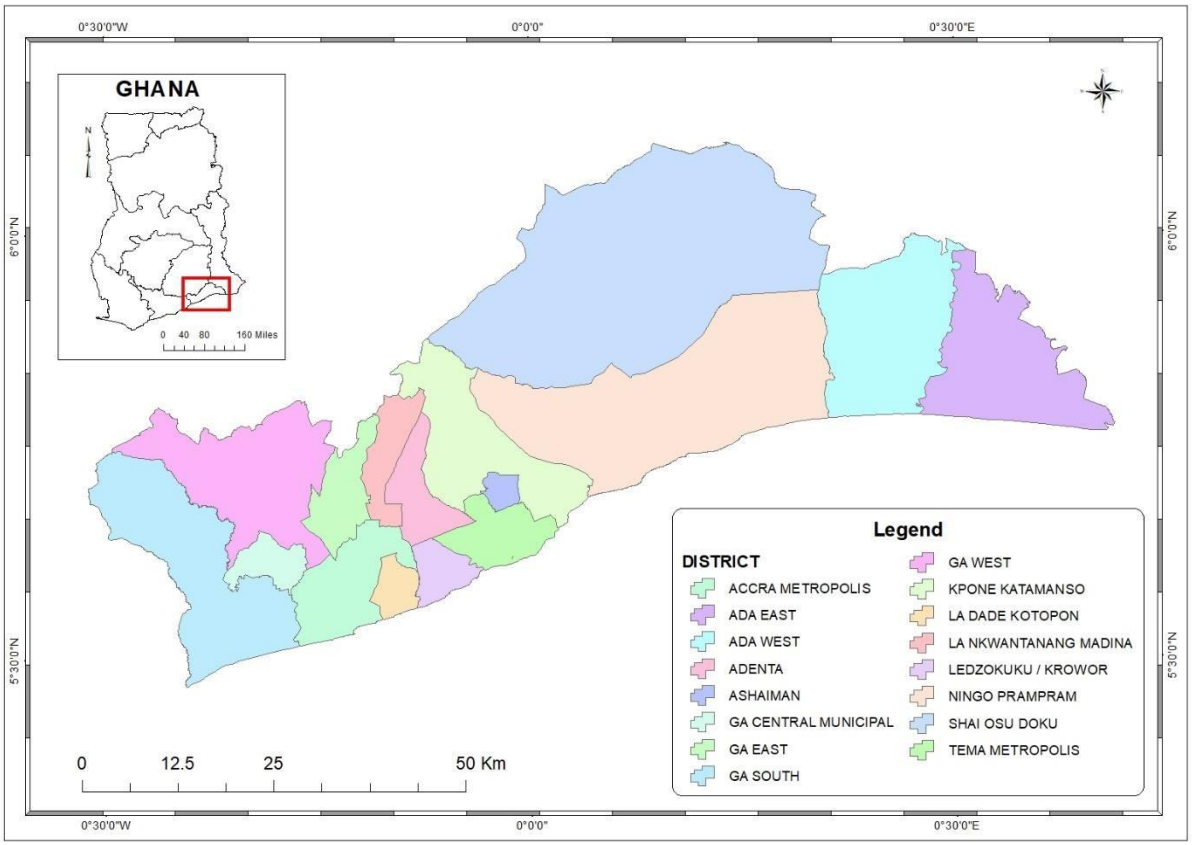

53″W; 5º 41′ 19″N to the West, 0º 41′ 29″E; 5º 46′ 4″N to the East).

Figure 3-1 Map of Greater Accra Region

The region comprises of sixteen (16) Metropolitan, Municipal and District Assemblies (MMDAs). Among these are five (5) District Assemblies, two (2) Metropolitans and nine (9) Municipal. The MMDAs are Accra Metropolitan Assembly (AMA), Adentan, Ga South, Ga East, Ga Central, Ada West, Ada East, Ashiaman, La Dade Kotopon, Kpone Katamanso, LedzokukuKrowor, Tema Metropolitan Assembly (TMA), Ningo Prampram, Madina, and La Nkwantanang.

The Greater Accra region is drained by notable rivers like Volta and the Densu. The region is also characterized by seasonal streams that flow from the Akwapim Ridge through numerous lagoons into the sea. Some of these wetlands and lagoons in the Accra metropolis, Dangme East and Tema are of high ecological importance but are extremely polluted largely through human activities. The prominent Volta River flows into the sea at Ada in the Dangme East District of the region.

3.1.2 Climate

The study region is in the dry, coastal, equatorial climatic zone. This zone experiences bi-modal rainfall season with an annual average rainfall ranging between 635 millimeters along the coast to 1,140 millimeters in the northern parts. The first begins in April and ends in June whereas the second is between September and mid-November. Major agricultural activities in the region are undertaken during this season. Both rainfall seasons peak, notably in June and October. Temperatures largely range from 20°C and 30°C (GSS, 2012). Close proximity to the equator ensures minimal variation in both annual and daily temperature throughout the year.

3.1.3 Vegetation Cover

Vegetation cover in the region is mainly coastal savannah shrubs scattered with thickets. Grasses in this area barely grow and so they are short and are even less than 1 meter with the maximum tree height of about 5 meters. Loss of dense forest in the region has been attributed to climate change and human activities (MLG, 1992).

3.1.4 Demographic and Economic Characteristics

According to the PHC (2010), the region has 4,010,054 inhabitants which account for 16.3% of the total population of Ghana. This makes it the most populated region. The Greater Accra region has the highest dense population in Ghana, and it is attributed to high population growth as well as in-migration. The age structure of the region is youthful, as it is characterized by high rate of fertility.

The region is the center of most economic activities in the country. Notable economic districts among the several distinct political and administrative areas that together form the Greater Accra region is the AMA and Tema. The Accra Metropolitan area is an economic center of the region. It provides key political, economic and administrative functions with several financial and government institutions concentration. The Tema metropolis is also not only a port city but also the industrial hub of Ghana.

The Ga districts absorb much of the urban expansion occurring within the urban core of Accra and Tema. Agricultural activities of the region on the other hand are predominantly found in the Ga and Dangme districts where farmers are mainly engaged in the old system of farming.

3.2 Research Approach

The research adopted both GIS and remote sensing methods as shown in the methodological flowchart in Figure 3-2 and used both raster and vector geospatial data. The various techniques as shown in Table 3-1 are broadly categorized into four major procedures namely;

- Satellite Image Pre-processing
- LULC Classification and Accuracy Assessment
- Change Detection Analysis
- Correlation Analysis

Software suite used in this research were ArcGIS Pro 2.2, ENVI 5.5 and SNAP to analyze satellite images and LST data. Outputs were presented in charts, maps, bar and line graphs.

Table 3-1: Research Approach

Objective	Research Question	Methodology
1. To identify the changing pattern of LULC over the past thirty-two (32) years.	What is the changing trend of LULC in the region?	Satellite Image Pre-processing (Radiometric correction, Image enhancement etc.) Land cover/Land use Classification (Random Forest Classification Algorithm) Accuracy Assessment (Overall accuracy & Kappa Coefficient). Change Detection Analysis
		(identify and quantify differences)
2. To understand LST variability in the Greater Accra region.	Is there spatial variation in Land Surface Temperature?	LST estimation using the mono window algorithm Spatial Autocorrelation

3. To analyze LST variations associated with LU/LC changes.	□ What is the relationship between LULC and LST? □ Can LST changes be explained by the changing nature of LULC in the region over the years?	□ Correlation Analysis □ Zonal Statistical Analysis □ LULC Indicator Analysis

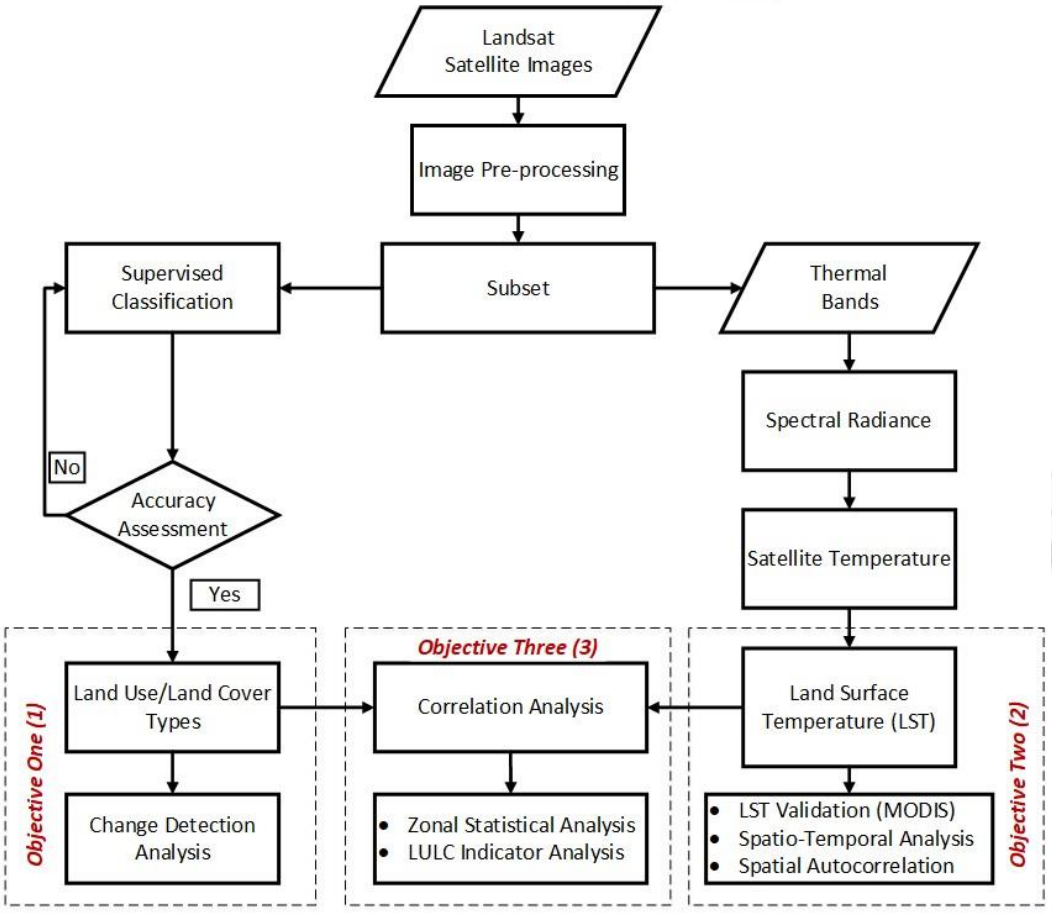

Figure 3-2 Methodology Flowchart

3.2 Data Type and Source

The study was based on the use of a time series of Landsat satellite images, MODIS Land Surface Temperature data and vector dataset.

3.2.1 Landsat Satellite Images

Remote Sensing data from Landsat missions was obtained from the US Geological Survey Department online resource website. Landsat was the first civilian earth observation satellite in the

world and have created the longest continuously acquired space-based, moderate-resolution data archive.

In an attempt to reduce errors that may result from cloud cover interference during analysis, only images between the months of December and February (dry season) were acquired while ensuring that ―cloud cover‖ for each scene of satellite image was restricted to 10 percent. These satellite images were used for LULC classification. Details of specific satellite images acquired are shown in Table 3-2.

Table 3-2 Details of Landsat Satellite Images

SATELLITE	SENSOR	ACQUISITION DATE	RESOLUTION	NUMBER OF BANDS
LANDSAT 5	TM	22-12-1986	Multispectral Band- 30m Thermal Band – 120(30)m	7
LANDSAT 7	ETM +	26-12-2002	Multispectral Band- 30m Thermal Band – 60(30)m	8
LANDSAT 7	ETM +	04-01-2018	Multispectral Band- 30m Thermal Band – 60(30)M	8

Source: United States Geological Survey

3.2.2 MODIS Land Surface Temperature Data

MODIS land surface temperature products is among the globally available sources of LST. It has been created as a sequence of products beginning with a swath (scene) and progressing, through spatial and temporal transformations, to daily, eight-day and monthly global gridded products.

The MOD11C1 granule consists of 16 layers at a pixel size of 5600 meters. This include five observation layers, six emissivity layers including their quality indicator (QC) layers, and day and night land surface temperature layers and QC layers. Corroboration at the second stage has succeeded for all products of MODIS land surface temperature or emissivity.

MODIS was launched onboard Terra and Aqua NASA satellites in 1999 and 2002 respectively. Each satellite captures daily images of the entire earth‘s surface, making available two images of a specific location per day. In this study, due to data availability challenge for the year 1986, MODIS LST data with same acquisition date for only 2002 and 2018 were used in the validation of Landsat satellite derived LST.

3.2.3 Vector Datasets

GIS vector data of study area boundary representing the administrative region of Greater Accra region together with road network dataset was collected from the Centre for Remote Sensing and Geographic Information Services (CERSGIS). This data assisted to define the various administrative regions that make up Greater Accra and help identify major road networks in the region.

3.3 Methods

This sub-section enumerates analytical geospatial techniques and methods utilized in generating results outputs.

3.3.1 Satellite Image Pre-processing

Image pre-processing is a fundamental technique in ensuring error free and accurate classification. Image pre-processing involves geometric/radiometric corrections, image enhancement, stacking and subset. Images acquired from USGS were already georeferenced into the WGS 84 UTM zone 30. Radiometric correction processed the images for the imperfectly transparent atmosphere, imperfections in scanning instruments, seasonal and daily variations for received solar radiations, flaws as a result of curved shape of the earth among others. These preprocessing techniques which are aimed at preparing images for better analysis were executed with ENVI 5.5 software suite.

Image Stacking was performed to ensure that all multispectral bands were combined into a single layer of multiple bands. The single layer of multiple bands ensures easy and relevant band combinations to focus on specific features during image classification. In supervised classification, band combination is very useful and suitable (Saleh, 2011; Lillesand *et al.* 2008). This was followed by image subset using regional boundary shapefile of the Greater Accra Region. It is a procedure through which an area of interest is masked out from the entire scene of the image.

3.3.2 Land use/Land cover Classification

Image classification is adopted to assign corresponding groups with homogeneous characteristics to discriminate multiple objects from each other in imagery. Pixel based classification could be supervised or unsupervised (Levin, 1999). This research used supervised classification which is the most widely used approach since it makes provision for more accurate classes definition and

enhance classification precision. Supervised classification uses samples of known spectral characteristics to classify pixels.

3.3.2.1 Classification Scheme

The Landsat satellite images were classified into four land cover classes; built-up, waterbody, bare land and vegetation for the assessment of changing land use trend. The selection of the land cover classification scheme was a modified USGS Land use/land cover classification system as conceptualized by Anderson *et al.* (1976). Based on the main objective of this study which was to investigate how LULC change is affecting LST, the following modification were made to the classification scheme (see Table 3-3)

Table 3-3 Description of LULC types

Land use/ Land cover Class	Description
Urban/Built up Land	Residential, Commercial, Industrial, Transportation, Mixed Urban or Built-up
Bare Land	Dry Salt Flats, Beaches, Sandy Areas other than Beaches, Bare Exposed Rock, Strip Mines, Quarries, and Gravel Pits, Transitional Areas, Mixed Barren Land.
Vegetation	Cropland and Pasture, Orchards, Groves, Vine yards, Nurseries, and Ornamental Horticultural Areas, Confined Feeding Operations, Other Agricultural Land. Deciduous Forest Land, Evergreen Forest Land, Mixed Forest Land Herbaceous Rangeland, Shrub and Brush Rangeland, Mixed Rangeland.
Waterbody	Streams and Canals, Lakes, Reservoirs, Bays and Estuaries. Forested Wetland and Non-forested Wetland.

Source: Modified Classification Scheme from Anderson *et al.* (1976)

Supervised classification algorithms group pixels into different classes based on the training samples or spectral signatures for every predefined land cover class. In sampling training data prior to supervised classification, the eight elements of image interpretation were considered to aid in the identification of land cover classes. These factors are colour, shadow, size, texture, shape,

association, and pattern relationship. Campbell and Wynne (2011) suggest factors such as sample size, class heterogeneity, placement, data collection method and supervised classification algorithm. Again, when selecting the training strategy, a number of factors were considered and they include size of the training data, difference in the image, number of pixels used, time and cost, and the impact of spatial autocorrelation (Foody and Mathur, 2002; Saha *et al.* 2005). For each image, training data was gathered at a minimum of 50 samples sites for each land cover class. The training data were collected with the aid of the knowledge of study area from ground truthing field visit.

3.3.2.2 Random Forest Algorithm for Land use/Land cover Classification

This algorithm constitutes one of the most effective machine learning models use for predictive analysis. The random forest algorithm predicts using various decisions from series of individual base models. Model ensembling refers to the technique of using various models to achieve an enhanced predictive performance. In the random forests, every base model is constructed individually with the use of various subsample of dataset. The Random Forest model is conceptualized in Figure 3-3.

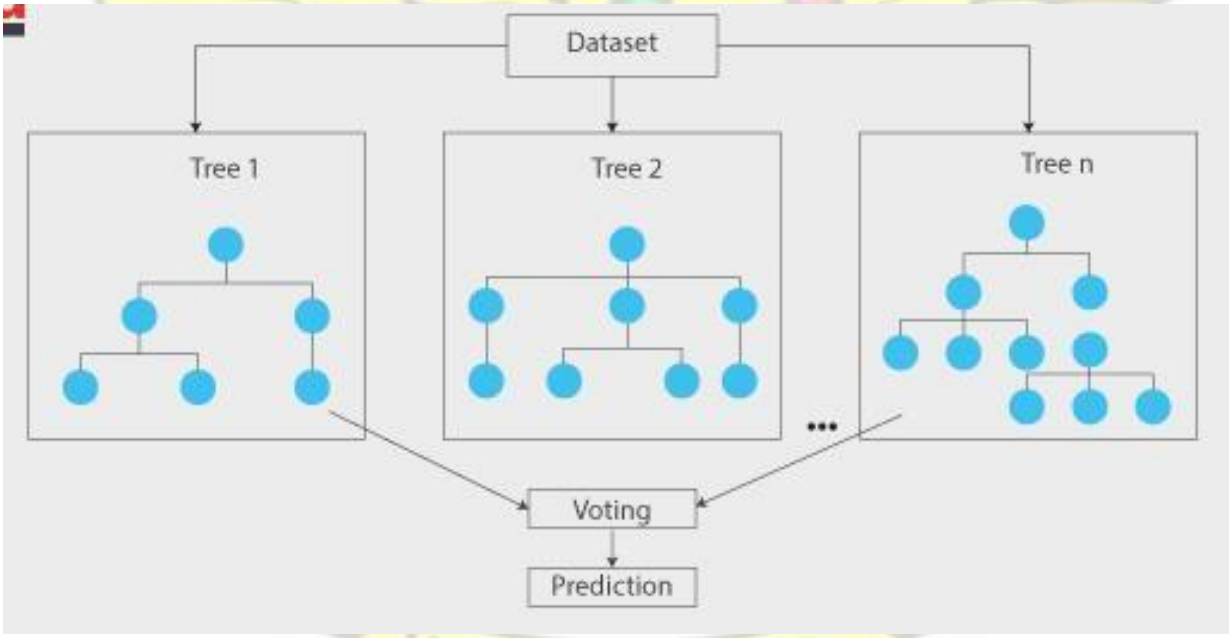

Figure 3-3 Random Forest Model

Random Forest (RF) algorithm was implemented in SNAP to classify satellite images based on gathered training datasets. Random Forest algorithm grows many classification _trees‘ premised

on the assertion that a set of classifiers (trees) do perform better classifications than an individual classifier.

3.3.2.3 Accuracy Assessment

Accuracy assessment is aimed at determining the accuracy of a classification outcome and it is basically used for RS data processing and analysis (Hashemian and Fatemi, 2004). This was undertaken using stratified random sampling method for ground truthing field survey. The study used error matrix approach which compared classified images and referenced data through the selection of points at random for the purpose of testing the accuracy of classification. Error matrix defines a square combination of numbers organized in rows and columns representing the number of pixels assigned to a particular land cover class relative to the real category verified from referenced data (Congalton, 1991).

Accuracy assessment for land cover classification was based on reference data generated from several sources including unused training datasets, GIS layers, Google Earth and other higher resolution satellite images. In this study, for each land cover class, 25 percent random points from unutilized training dataset were selected and used for accuracy assessment in ENVI 5.5.

Quantitatively, the measure of accuracy of classified images was calculated in the form of overall accuracy (total number of correctly classified pixels divided by the total number of pixels sampled) and kappa coefficient. Kappa values are characterized as <0 as indicative of no agreements and 0–0.2 as slight, 0.2–0.41 as fair, 0.41–0.60 as moderate, 0.60–0.80 as substantial and 0.81–1.0 as almost perfect agreement (Chander and Markham, 2003; Kepner *et al.* 2000). A kappa value of 1 indicates perfect agreement whiles a value of 0 indicates no agreement.

$$k = \frac{N\sum_{i=1}^{n} m_{i,i} - \sum_{i=1}^{n}(G_i C_i)}{N^2 - \sum_{i=1}^{n}(G_i C_i)} \qquad (3.1)$$

Kappa coefficient was calculated using equation 3.1;

Where:

i : is the class number n **:** is the total number of classified pixels compared to the reference pixels **mi,i** is the number of values belonging to the reference class **i** that have also been classified as

class **i** (pixels found in both the reference and classified maps) **Ci :** is the total number of predicted pixels belonging to class **i**

Gi : is the total number of reference pixels belonging to class **i**

3.3.3 Change Detection Analysis

Change Detection Analysis involved techniques to quantify and identify the differences in classification outputs of the images between 1986 and 2018. This measured changes between paired images representing an initial state and final state. Change detection statistics and change detection difference map tools are key in the interpretation and statistical analysis of the changing trend of LULC in the study region.

Various tools from post classification toolbox in ENVI 5.5 were adopted for the analysis of change detection. The thematic change tool was also used to generate maps depicting land cover class transitions.

3.3.4 Land Surface Temperature (LST) Estimation Algorithm

A mono-window algorithm adopted from Qin *et al.* (2001) was used to estimate LST. This algorithm is regarded more robust as it explains other factors instead of brightness temperature. One advantage of the mono-window according to Alsultan (2005) is that after surface emissivity values as well as the solar angel values have been combined to the model, there exist a higher correlation between the brightness temperature and the retrieved land surface temperature.

In this study, this LST estimation algorithm used the single Landsat thermal band of the atmospheric window between 10.40 and 12.50 μm. The mono-window algorithm for Landsat TM requires three significant factors to estimate land surface temperature. These are the effective mean atmospheric temperature, atmospheric transmittance, and ground emissivity (Qin *et al.*, 2001).
The flow chart shown in Figure 3-4 identifies the major steps in LST retrieval from Landsat satellite images.

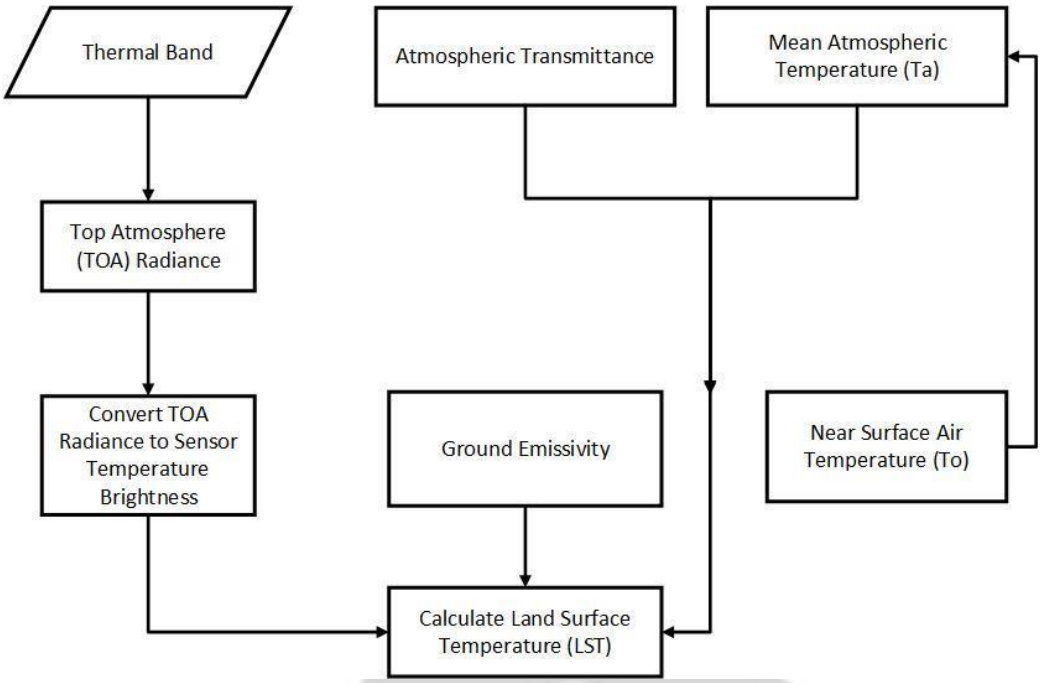

Figure 3-4 Major Steps in Estimating LST

3.3.4.1 Conversion to Top of Atmosphere Radiance

Acquired TM band data was converted from Digital Numbers (DN) to Top of Atmosphere (TOA) spectral radiance using the radiance rescaling factors in the metadata of the various images with the formula shown in equation 3.2:

$$L\lambda = ML \times Qcal + AL \qquad (3.2)$$

where:

Lλ: TOA spectral radiance (Watts/ (m2 * srad * μm))
ML: Band-specific multiplicative rescaling factor
AL: Band-specific additive rescaling factor
Qcal: Quantized and calibrated standard product pixel values (DN)

3.3.4.2 Conversion to Top of Atmosphere Brightness Temperature

TOA spectral radiance calculated above was input for the formula below to convert data from spectral radiance to top of the atmosphere brightness temperature in kelvin with the aid of

$$T = \frac{K_2}{\ln\left(\frac{K_1}{L_\lambda + 1}\right)} \qquad (3.3)$$

thermal constants documented in the metadata of satellite images (see Table 3-4).

where:

T: Top of atmosphere brightness temperature (K)

$\mathbf{L_\lambda}$: TOA spectral radiance (Watts/(m2 * srad * μm))

$\mathbf{K_1}$/ $\mathbf{K_2}$: Band-specific thermal conversion constant

Table 3-4: Thermal Conversion Constants used for LST Estimation

Constant Variable	Landsat 5 TM	Landsat 7 ETM+
K_1	607.76	666.09
K_2	1260.56	1282.71

3.3.4.3 Deriving Land Surface Temperature

3.3.4.3.1 Calculation of Mean Atmospheric Temperature

A key component of LST estimation using the mono-window algorithm is the mean atmospheric temperature. This is related to the air temperature and dependent on the climatic zone of the region. In other words, under clear sky without great turbulence (standard atmospheric distributions), the mean atmospheric temperature (T_a) is a linear function of near-surface air temperature (T_0). This is attributed to the assumption that the impact of distributed water vapour as well as the distribution of atmospheric temperature T_a is constant for the standard distributions (Qin *et al.*, 2001).

The Greater Accra region lies within the tropics, thus the formula;

$$\mathbf{T_a=17.9769+0.91715*T_o} \quad (3.4)$$

Where T_a and T_0 are in Kelvin.

3.3.4.3.2 Atmospheric Transmittance

An accurate estimation of transmittance (t) is very significant in the retrieval of Land Surface Temperature. A principal influencing factor however is water vapour content. It has been established to have strong influence on atmospheric transmittance (Coll *et al.* 1994; Cracknell, 1997; Sobrino *et al.* 1991).

Qin *et al.* (2001) posits that simulation of atmospheric conditions by the use of atmospheric simulation programs are mostly used in calculating atmospheric transmittance for Landsat TM band.

High temperature profiles (refer to Table 3-5) was used in this study.

Profiles	Water vapour (w) (g cm^{-2})	Transmittance estimation equation	Squared correlation R^2	Standard error
High air temperature	0.4–1.6	$\tau_6 = 0.974290 - 0.08007w$	0.99611	0.002368
	1.6–3.0	$\tau_6 = 1.031412 - 0.11536w$	0.99827	0.002539
Low air temperature	0.4–1.6	$\tau_6 = 0.982007 - 0.09611w$	0.99463	0.003340
	1.6–3.0	$\tau_6 = 1.053710 - 0.14142w$	0.99899	0.002375

Table 3-5 Estimation of Atmospheric Transmittance

Source: Qin *et al.*, (2001).

3.3.4.3.3 Calculation of Land Surface Emissivity

Emissivity (e) of a surface is a function of different parameters such as texture of surfaces, chemical composition, properties, physical structure, and water content and has the ability to influences the total radiation of the surface (Prata, 1993; Snyder *et al.*, 1998). Emissivity (e) values for this study were adopted from the Digital Imaging and Remote Sensing (DIRS) Laboratory of the Chester F. Carlson Center for Imaging Science at Rochester Institute of Technology (RIT).

3.3.4.3.4 Calculation of Land Surface Temperature

Upon successful calculation of surface emissivity, Land Surface Temperature was finally derived as:

$$\mathbf{LST} = \frac{\alpha(1-c-d)+(\beta(1-c-d)+c+d)T_{Brightness}-d*T_a}{c} \quad (3.5)$$

Where: α = -67.355351, β = 0.458606 are coefficients approximated for temperature range of 0–70°C **c = emissivity (e) * transmittance (t)** d = (1-t) *(1+(1-e) *t) (3.6)

Land Surface Temperature in kelvin is converted to degrees Celsius by subtracting 273.15.

3.3.5 Land Surface Temperature Validation

Evaluating and ascertaining the certainty of satellite retrieved LST can facilitate its use for various applications. It is important for one to assess accuracy to provide users of land surface temperature a reliable source of information on the quality of data and imminent improvement. Even though a number of algorithms exist in this modern time for retrieval of land surface temperature from TIR

satellite data, not enough studies have been carried out for the validation of LSTs derived from satellite. It is difficult in taking ground measurements of the land surface temperature and the large spatiotemporal variations in the LST itself makes study difficult. However, one key advantage of this validation is that even without ground measurement, LST can be validated anywhere with well documented and validated LST data coverage. MODIS LST data was analyzed against LST estimates computed from Landsat satellite images as a validation procedure.

3.3.6 Correlation Analysis

Establishing the nature of relationship between Land use/land cover types and Land Surface Temperature is key to the understanding of the contribution of anthropogenic factors to LST changes. Correlation analysis between LST and LULC was used to understand how LST dynamics are influenced by LULC changes. Correlation analysis assesses the linear relationship between two variables and provides a measure of both the strength and direction of the relationship. Correlation makes no assumption on causality in the relationship. To help identify the type of relationship between variables, visual inspection of a scatterplot is invaluable and thus was employed in this analysis. As a measure of the strength of the relationship between LST and LULC, the Pearson Coefficient (Pearson r) of correlation was determined. The formula

$$r_{xy} = \frac{\sum_i ((x_i - \bar{x})(y_i - \bar{y}))}{\sqrt{\sum_i (x_i - \bar{x})^2 \sum (y_i - \bar{y})^2}} \quad (3.7)$$

for r is: where x is the sample mean of variable x and y is the sample mean of variable y.

4 Chapter Four: Results and Discussions

This chapter is one of the most important sections of this research study. The section reported results from the analysis of data for Land use Land cover change, spatial variability of Land Surface Temperature and the relationship between the two. It also presents arguments on insights gathered using techniques and methods describe in the previous chapter. Results are presented as maps, tables, charts and graphs.

4.1 Land Use/Land Cover Patterns

This subsection presented the coverage extent and changing pattern of LULC within the Greater Accra region for the three-year stamps under study.

4.1.1 Land use/Land cover Mapping and Analysis

Similar in many studies (Appiah, 2014; Basommi *et al.*, 2015, 2016; Kumi-boateng and Stemn, 2015; Amamo and Amenu, 2017; Yeboah *et al.*, 2017; Mensah, 2017; Bewket 2002; Dessie and Kleman 2007; Beilin *et al.*, 2014), the application of Remote Sensing again proved to be key in land use/land cover mapping especially over large geographic areas.

Satellite image classification using the random forest algorithm, identified four major LULC types in the Greater Accra region. The LULC types were Vegetation, Bare land, Built-up and Waterbody. LULC maps were generated from acquired Landsat satellite imagery for the year 1986, 2002 and 2018.

4.1.1.1 Spatial Pattern of 1986 LULC Classification

The total area of the study region is about 3,668 square kilometers. Figure 4-1 shows the Land use/Land cover map of 1986. In this year, results indicate 46.5% representing 1,706.1 km^2 of the total land mass was bare land, while vegetation covered 48.5%. Built-up land represented the least of the LULC categories of 67 km^2. Table 4-1 shows each LULC category and coverage extent.

Table 4-1 LULC Types and Coverage Extent of 1986

LULC Type	Area (Square Kilometer)	Percentage
Bare land	1,706.1	46.5
Vegetation	1,779.8	48.5
Water	116.3	3.2
Built-up	67.0	1.8

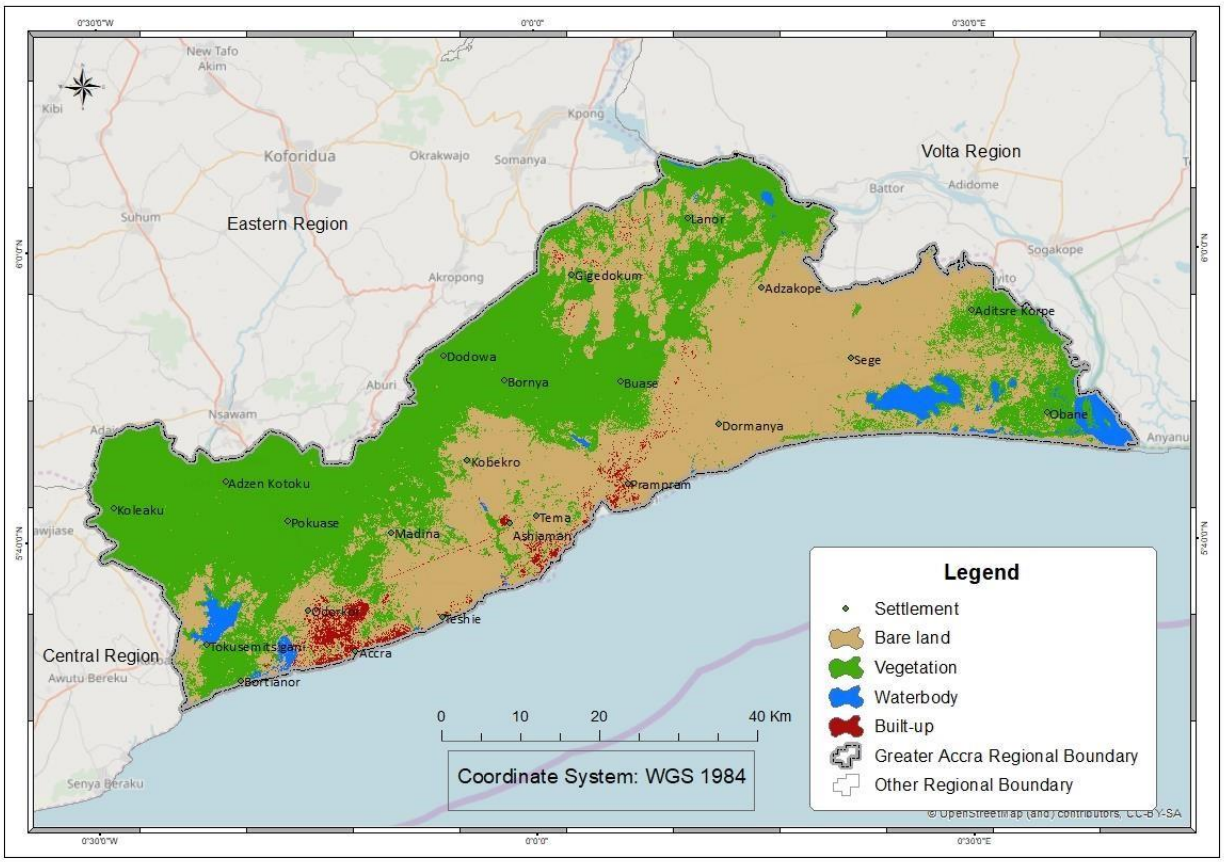

Figure 4-1 LULC Classification Map of 1986

4.1.1.2 Spatial Pattern of 2002 LULC Classification

Observation and examination of the classified imaged revealed that in the year 2002 the study area was dominated by two LULC types namely vegetation and bare land representing 56.4% and 32.8% of total land mass of the Greater Accra region respectively. The geographic representation of the extent of individual land cover types is seen in Figure 4-2. The same extent of the individual LULC types in square kilometers together with their respective percentage of land size covered is shown in Table 4-2.

Table 4-2 LULC Types and Coverage Extent of 2002

LULC Type	Area (Square Kilometer)	Percentage
Bare land	1,202.0	32.8
Vegetation	2,068.2	56.4
Water	88.7	2.4
Built-up	310.3	8.5

Land use and land cover classification for 2002 from ETM+ sensor of Landsat 7 mission in Figure 4-2 showed that majority of the study area during the period was under vegetation cover and bare land accounting for 2,068.2 square kilometers and 1,202.0 square kilometers respectively. While, built up area and water body accounted for 310.3 square kilometers (8.5%) and 88.79 square kilometers (2.4 %) respectively.

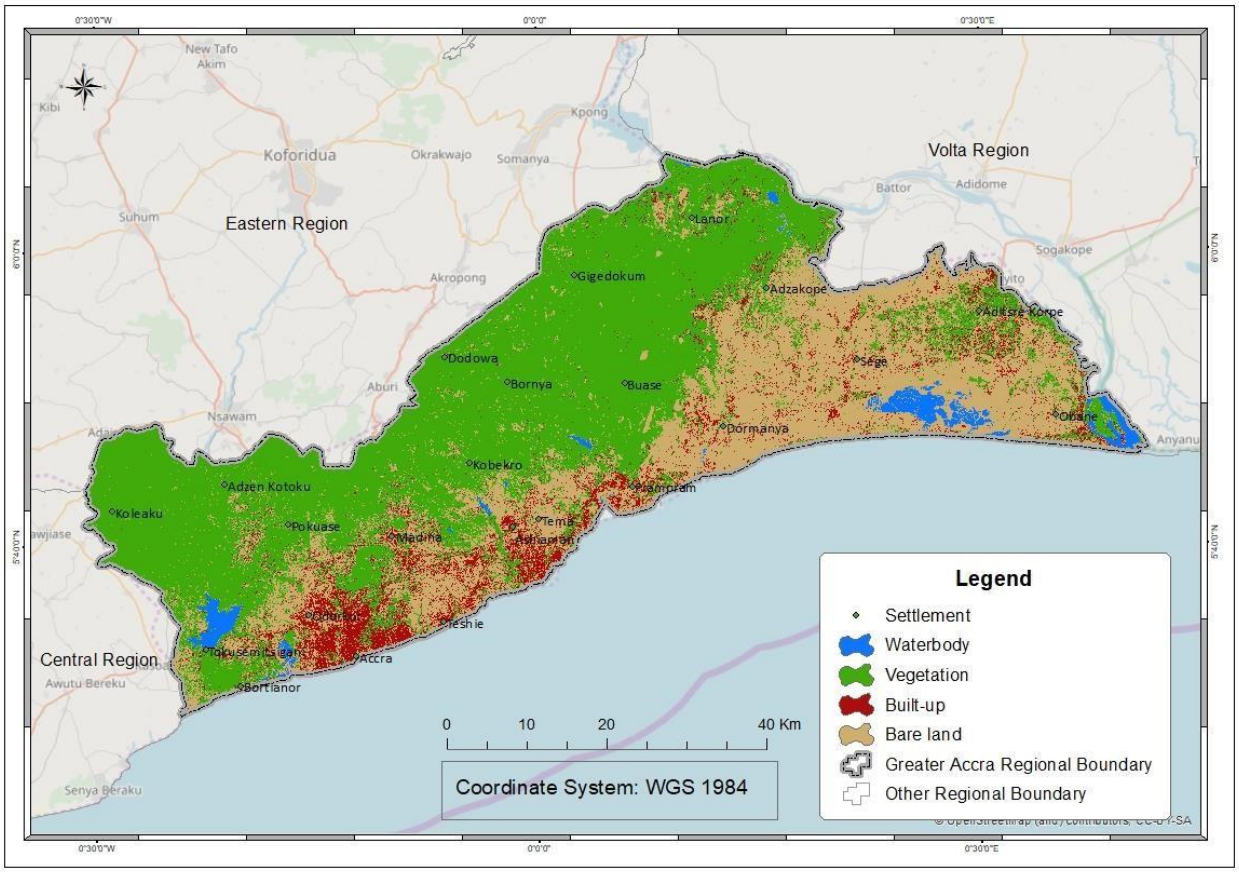

Figure 4-2 LULC Classification Map of 2002

4.1.1.3 Spatial Pattern of 2018 LULC Classification

It was evident from the analysis of the 2018 image that, spatial distribution of LULC types suggest the fast pace increase of urban expansion at the peri-urban surroundings of most developed areas like the Tema, Ada, Amasaman among many other towns. Figure 4-3 depicts the extent to which the urban expansion is creeping on other LULC categories. Vegetation however still appeared to be the largest LULC type covering about 1,750.2 Km^2 (47.7%). This is to a large extent accounted for by the protected areas in and around Shai Hills in the north-eastern parts of the region.

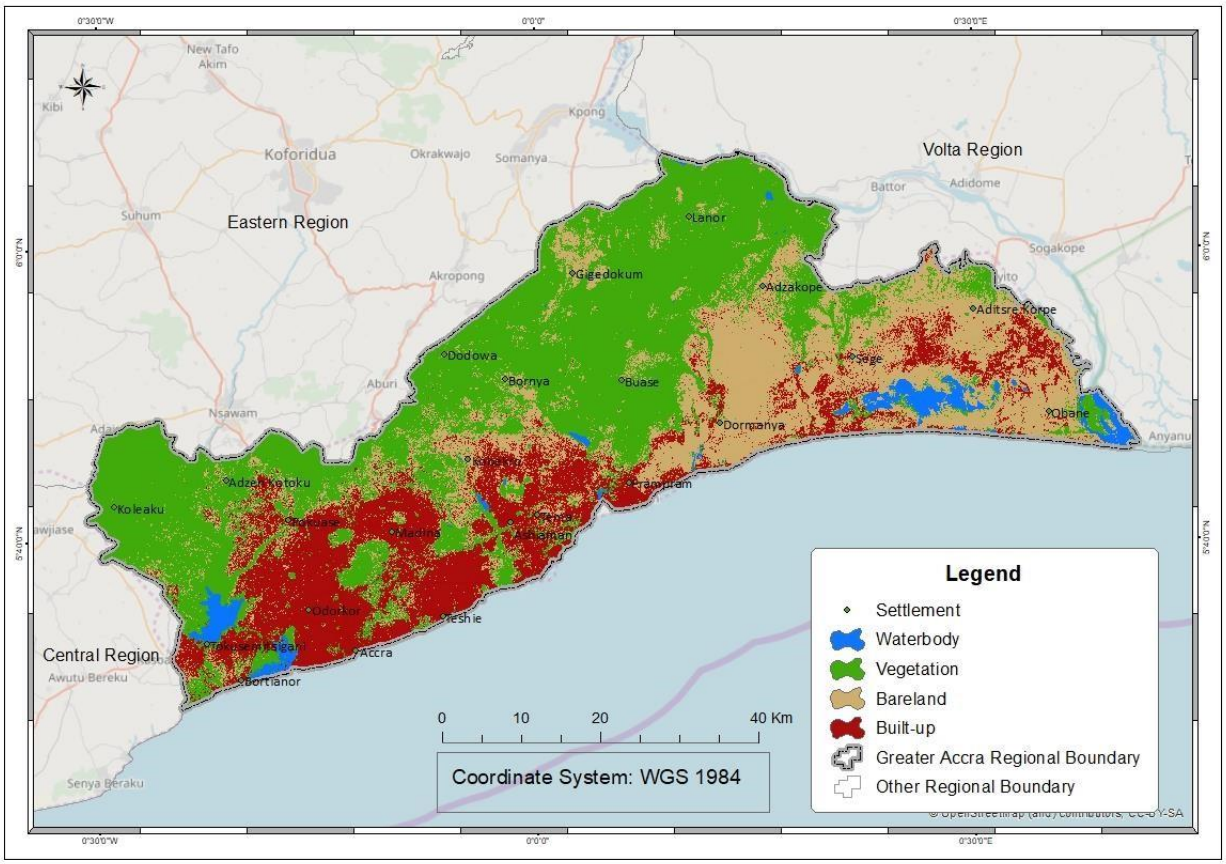

Figure 4-3 LULC Classification Map of 2018

Table 4-3 LULC Types and Coverage Extent of 2018

LULC Type	Area (Square Kilometer)	Percentage
Bare land	1,020.5	27.8
Vegetation	1,750.2	47.7
Water	107.1	2.9
Built-up	791.3	21.6

It can be observed from Table 4-3 that in 2018, following the largest cover of vegetation, bare land and built up together accounted for 49.4% of the study area, while water had a coverage of the remaining 2.9% covering an area of 107.1 Km^2.

4.2 Results of LULC Accuracy Assessment

Notwithstanding the limitations of Kappa statistics, it is a widely used measure of classification accuracy. Accuracy of classifications are influenced by range factors including quality of classified images and lack or inadequate local knowledge of the study area resulting in

misclassifications. Shao (2006) classified change detection errors as error from reference data, post-processing, pre-processing and classification. Accuracy assessment is said to be a process of validating the insight and statistics derived from change detection, spatial analysis and prediction (Campbell and Wynne, 2011). The _confusion matrix‘ approach was used in assessing the accuracy of classification and results are shown in Table 4-4

Table 4-4 Accuracy Assessment of LULC Maps

LULC Classification	Overall Accuracy	Kappa Coefficient
1986	88.7892%	0.8029
2002	90.3571%	0.7818
2018	99.8154%	0.9968

Classification accuracy assessment was performed for all three LULC maps. As it is shown in Table 4-4, the overall accuracy and Kappa coefficient values derived indicate high accuracy of the classification procedures adopted. The overall accuracy for the three LULC maps were higher than 85% with 2018 having the highest accuracy.

A kappa value of 1 indicates perfect agreement whiles a value of 0 indicates no agreement. The values that lie 0.60–0.80 are however characterized as substantial and 0.81–1.0 as almost perfect agreement (Kepner *et al.*, 2000; Chander and Markham, 2003). Accuracy assessment of LULC maps show kappa coefficients that indicate that classification for 1986 and 2018 had almost perfect agreement while 2002 recorded substantial agreement.

Table 4-5 Producer Accuracy

LULC Type	1986	2002	2018
Vegetation	100	100	100
Bare land	64.29	100	96.77
Built-up	79.17	88.10	99.83
Waterbody	100	87.82	99.69

Producer's Accuracy is the map accuracy from the point of view of the map maker (the producer). This indicates the extent to which real features on the ground correctly shown on the classified map or the probability that a certain land cover of an area on the ground is classified as such. In other words, it is the number of reference sites classified accurately divided by the total number of reference sites for that class. The Producer's accuracy complements Error of Omission accuracy metric, which is mathematically represented as; Producer's Accuracy equals one hundred percent minus Omission Error (100% - Omission Error).

From

Table 4-5 producer accuracy assessment of all LULC types are shown. Among the four LULC categories, vegetation had the highest with perfect producer accuracy for the entire period. This could be explained by the ability to clearly distinguish vegetation from other LULC types especially in the near-infrared spectrum. The two lowest accuracy values were recorded in 1986 for Bare land and Built-up, 64.29% and 79.17% respectively. The low accuracies are largely due to the identical spectral properties of both Bare-land and Built-up areas in some parts of the Landsat satellite images particularly in 1986. Water bodies recorded the second highest total producer accuracy among the three LULC maps due to the spectral uniqueness and defined boundaries of water bodies.

4.3 Land Use/Land Cover Change (LUCC) Dynamics in the Greater Accra Region

In this study, post-classification change detection was used in the analysis of Land use/Land cover changes. The post classification change detection approach offers thorough and in-depth insight into the extend of change in LULC types.

The LULCC classification results over the thirty-two-year period from 1986 to 2018 are summarized in Table 4-6. This table shows the pattern of change in land use/land cover between 1986 and 2018. Bare land cover type indicates steady decline from 1986 with a coverage of 1,706.1 Km^2 to 1020.5 Km^2 in 2018. On the contrary, Built-up displays an increase trend of 724.3 Km^2 during the same period.

Table 4-6 Extent of Change in LULC Types

Extent of Change in Km^2			
	1986	**2002**	**2018**
Bare land	1,706.12	1,202.00	1,020.54
Vegetation	1,779.80	2,068.20	1,750.15
Waterbody	116.25	88.70	107.14
Built-up	67.00	310.30	791.33

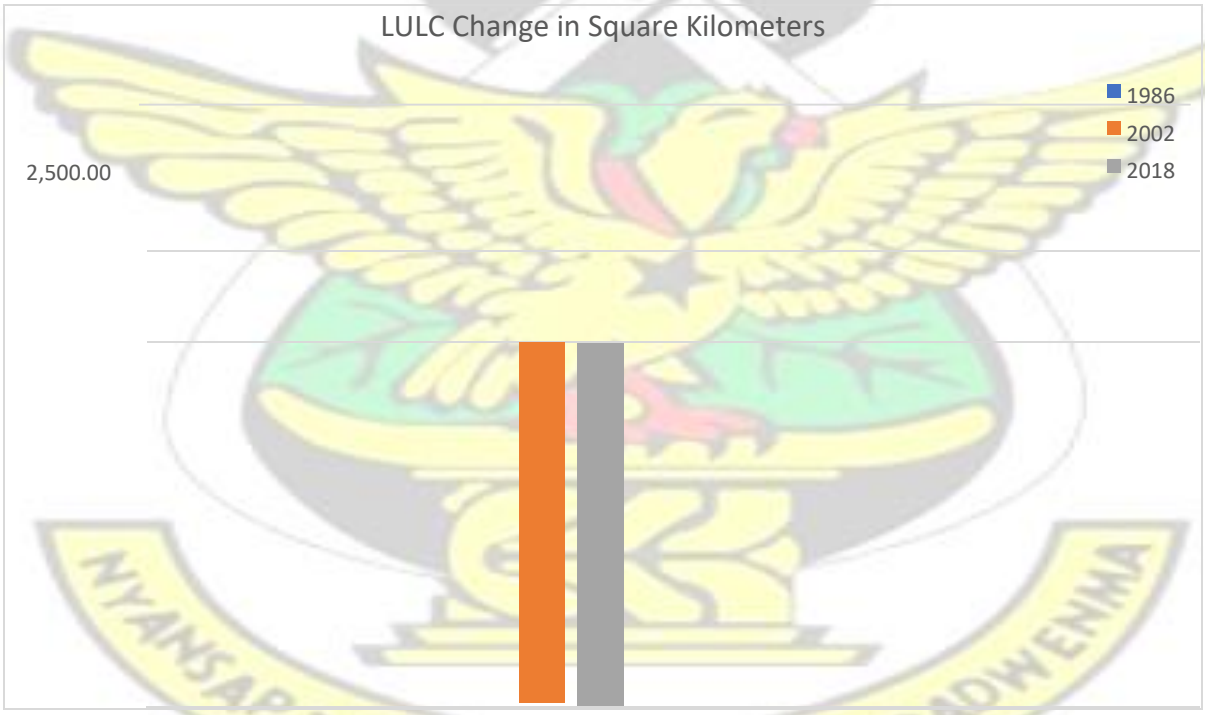

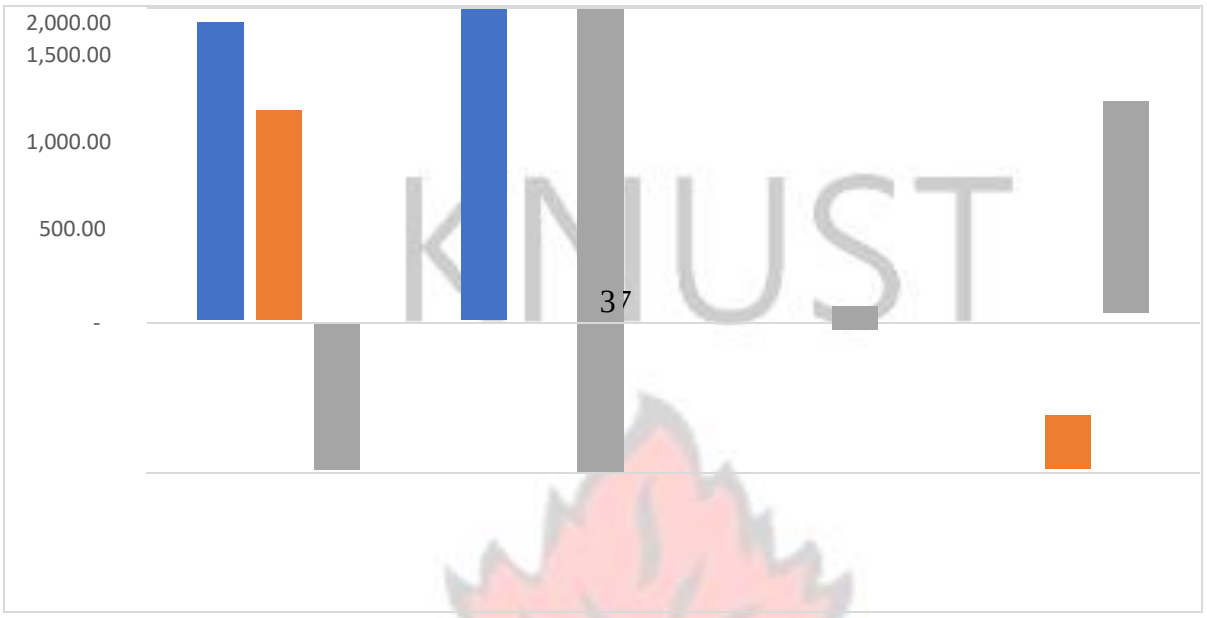

Statistical analysis of all three classified images disclosed that waterbody was the least overall LULC type (see Table 4-6) over the period. Water bodies in the study region experienced undulating trend with a decrease in 2002 and an increase in 2018 respectively amounting to a total decrease of 7.84% as depicted by Figure 4-4.

Analysis further showed that vegetation cover increased by 16.2% from 1,779.8 Km^2 to 2,068.2 Km^2 between 1986 and 2002. It however decreased by 15.38% amounting to a total coverage of

Bareland Vegetation Water Builtup

318.05 Km^2.

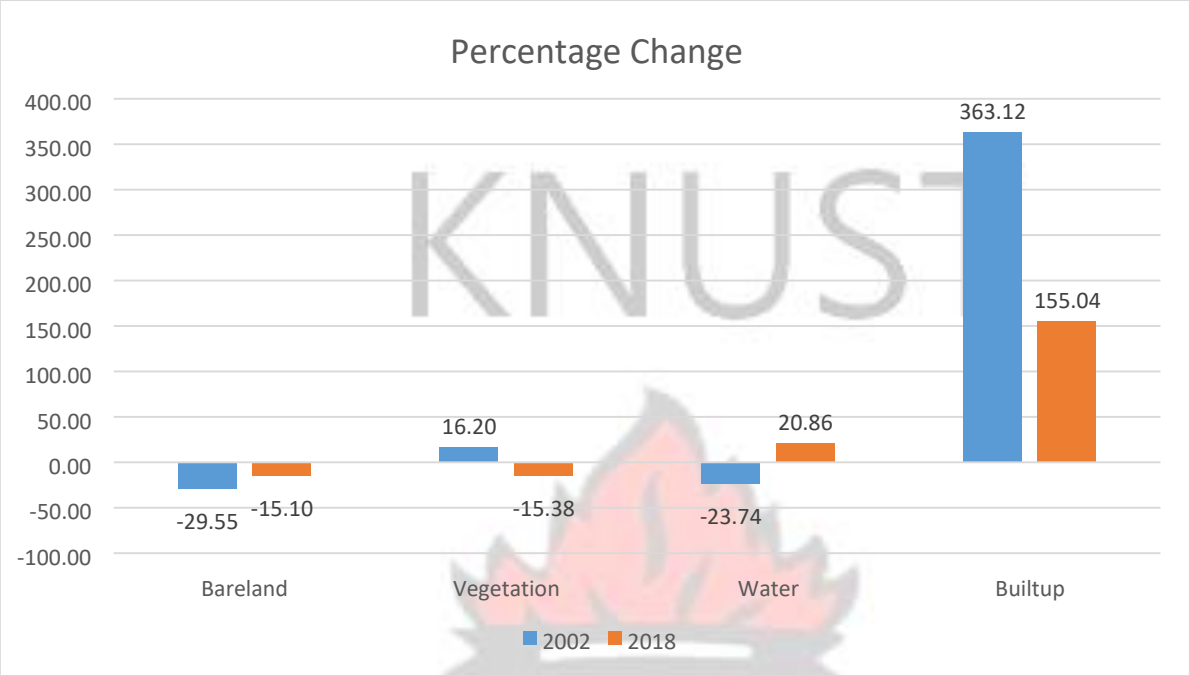

Figure 4-5 Graphical Representation of LULC Change

Figure 4-4 Percentage Change in LULC Types

4.3.1 Vegetation Cover

LULC type classified as vegetation was one of the major LULC categories in the Greater Accra. Beginning 1986, vegetation cover increased from 1,779.80 Km^2 to 2,068.20 Km^2 in 2002 representing 16.20% increase as shown in Figure 4-6.

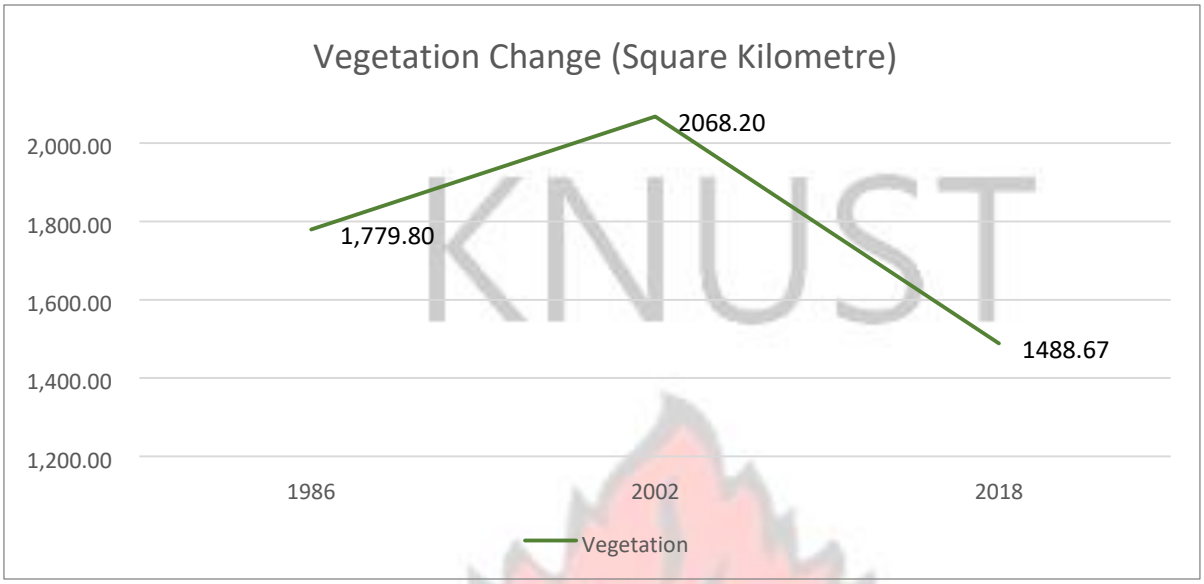

Figure 4-6 Vegetation Cover Trend

The increase in vegetation cover was indicative of the region‘s recovery from extreme adverse impact of drought experienced during the 1980s in most parts of Ghana (Ofori-Sarpong, 1986). This implies that areas that were supposedly dry bare land began to fallow and farmers began to grow crops post drought season under favourable weather conditions. Vegetation cover statistics show 13.04% of Bare land transitioned into Vegetation cover between 1986 and 2002 (see Figure 4-1 in appendix) . The vegetation increase in 2002 was in areas like the Kpone Kantamanso district, around Weija lake in Ga South, Ningo Prampram and Shai Osu Doku. Amidst the vegetation increase however, Ada East district experienced decrease in vegetation cover while northern parts of Ada West district had a slight increase in vegetation

On the other hand, for the period between 2002 and 2018 vegetation decreased from 2,068.20 Km^2 to 1,488.67 Km^2. Percentage decrease is shown in Figure 4-7. This is corroborated by Yeboah *et al.*, (2017) which emphasized the transition of vegetation (forest and agricultural land) to built-up environment in Accra between 1985 and 2010.

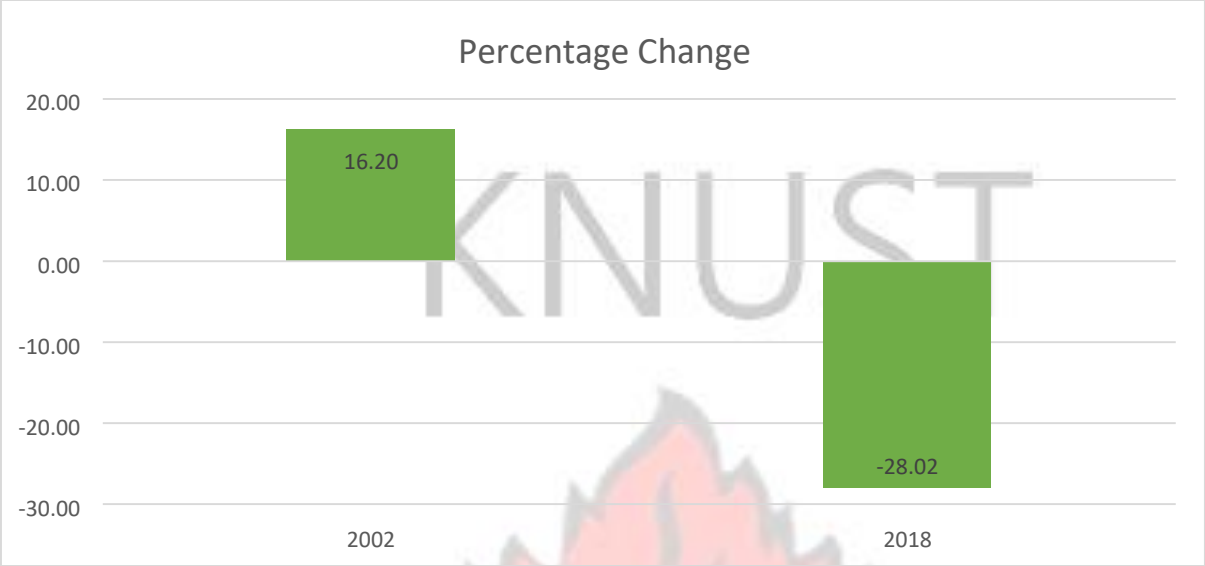

Figure 4-7 Percentage Change in Vegetation Cover

Change analysis of LULC map of 2002 and 2018 gives the indication that, decrease vegetation could be explained by the increasing nature of deforestation for developing settlements and builtup environment largely attributed to population increase especially in peri-urban areas like, Pokuasi, Odokor, Madina, Ashiaman, Ga East district and southern parts of Ga South district. This explains the 16.33% and 10.38% vegetation cover loss to Bare land and Built-up respectively within the period see Figure 4-1 and Figure 4-2 in appendix). Urban expansion, agricultural activities and firewood harvesting have also been identified by Stow *et al.* (2013) and Yankson and Gough (1999) as contributing factors to loss of vegetation cover in Accra. The Ghana Energy Commission (2014) identifies firewood and charcoal to be of high preference among many households in the country. Statistics indicate that amidst the urban population, a total of 75% of households depend on these sources of energy for cooking leading to decreasing forests and woodland cover (Addae and Oppelt, 2019).

4.3.2 Bare and Open Land Cover Change

Analysis suggested that bare land covered the second largest land mass of 1,706.12 Km^2 in the Greater Accra region in the year 1986. This represented 46.50% of the total area of the region. Bare land was extensive in districts like the Shai Osu Doku, Ningo Prampram, Ada including areas around the Songor Lagoon protected area. These areas are vastly covered by large tracts of open land with isolated outcrop of rocks and in some cases very sparse vegetation cover. The dominant

spread of bare land LULC type in the region, could also be equally be attributed to the drought of the 1980s. The drought was characterized by dryness with related inevitable rampant bushfires. Bushfires were one of the leading causes of deforestation in West Africa (Korem 1985). According to the Environmental Protection Council (1986), 847 bushfires were recorded in the country in 1982 resulting in about 50% loss of vegetation cover.

Over the duration of this study bare land experienced the highest change of 60.22% decrease between 1986 and 2018 representing consistent decrease from 1706.12 to 833.31 Km^2. The trend of Bare land over the period is depicted in Figure 4-8. The highest rate of change of 30.67% decrease in Bare land LULC type was recorded between 2002 and 2018 while 29.55% was noted between 1986 and 2002.

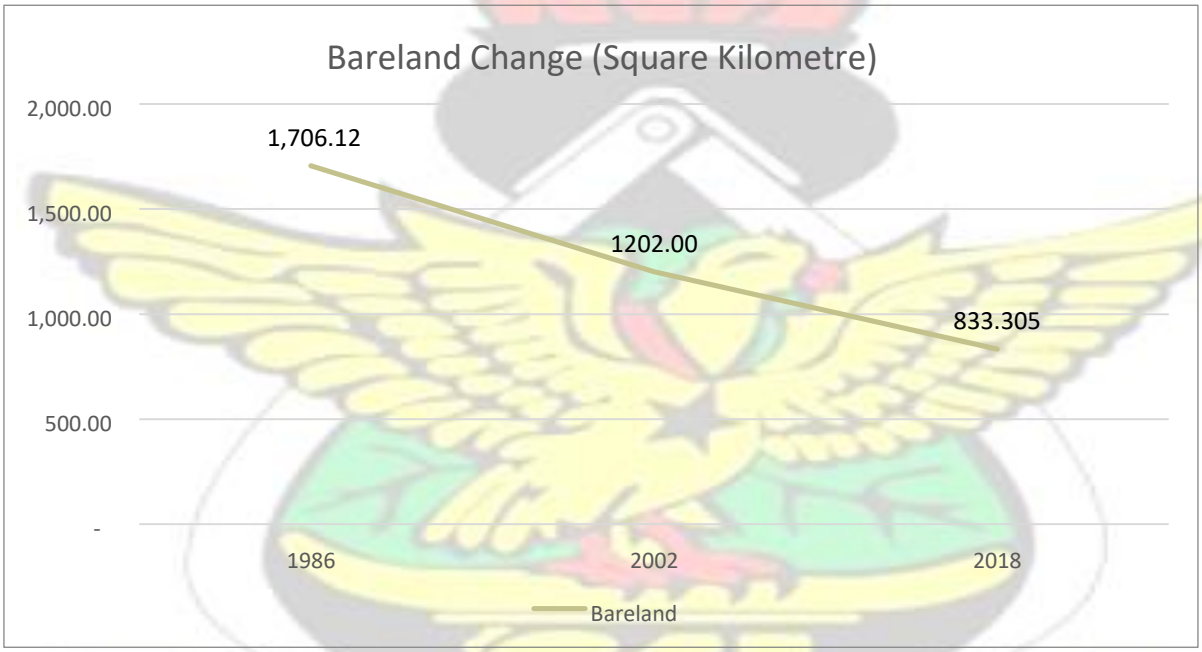

Figure 4-8 Bare land Cover Trend

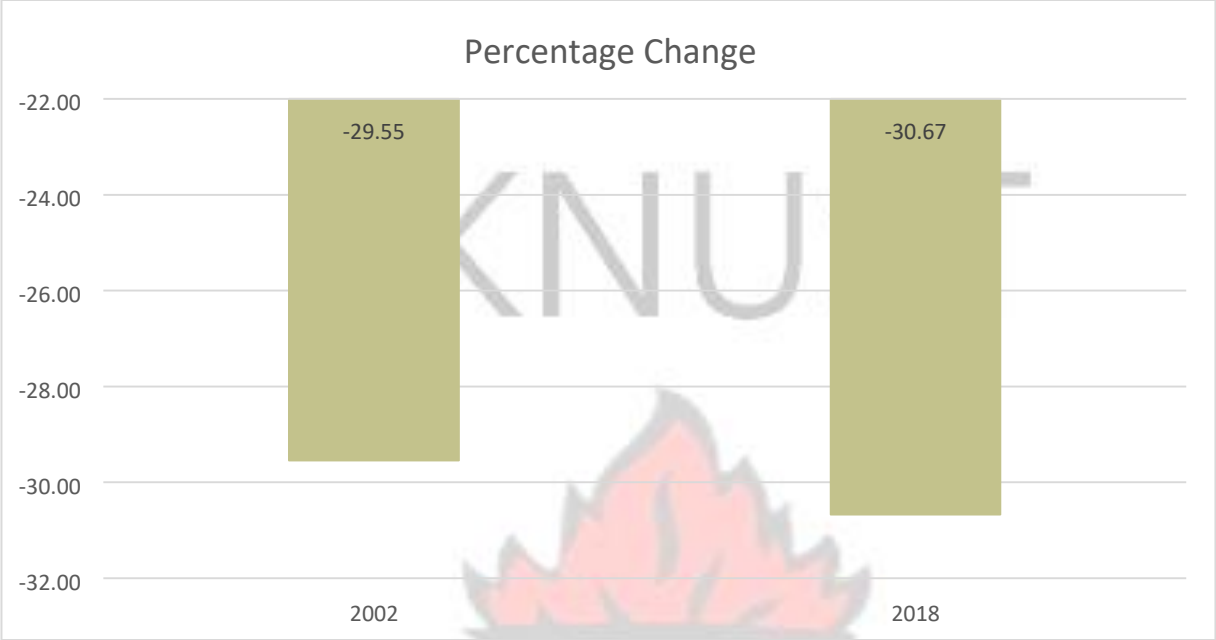

Figure 4-9 Percentage change in Bare land

The spatial distribution of bare land in the region has mainly been seen to be a transition land cover type between built-up along the coast and vegetation cover largely in the northern parts of the region. Bare land spread around the urban core can be suggested as an indication of the early stages of urban development mainly around Adenta, Abokobi, Madina, Ashaiman and Ledzokuku Krowor in GAMA. Large tract of bare land transitioned throughout the years to two main LULC types namely, built-up and vegetation. Many open spaces in and around the urban core of Accra were developed into various retail, industrial, and residential purposes causing the reduction of barren land surrounding the urban developments. This is seen in the increased rate of ―bare land to built-up‖ conversion rate from 12.01% (204.98 Km^2) between 1986 and 2002 to 33.23% (399.59 Km^2) between 2002 and 2018.

While in districts like the Shai Osu Doku, Ningo Prampram and Ada West and East, decreased bare land trends were predominantly associated with increased urban expansion, the reduction was higher compared to districts in the Greater Accra Metropolitan Area(GAMA) like AMA, TMA, Ashaiman, Adenta, Ledzokuku Krowor, La Dade Kotopon, Ga East and Central. This could be explained by the fact that most areas outside GAMA were covered with large tracts of bare land and open barren land with sparse vegetation cover in some cases.

As alluded to earlier, Bare lands appear to also have a relationship with vegetation in the region. From the year 1986 to 2002, about 33.28% of Bare land was rehabilitated to Vegetation while 15.13% was also transformed to same between 2002 and 2018. It is suggested that the phenomenon could be explained by increasing large farmlands and fallow land in peri-urban areas of the region. Notwithstanding the changes, consistent bare land coverage was maintained along the banks of the Songor Lagoon protected area with isolated patches of vegetation.

4.3.3 Urban and Built Environment Expansion

In 1986, total area of built-up area in the study area was estimated to be 67.0 Km^2 stretching out through central urban core of Accra with a spatial extent of 1.83%. Notwithstanding the comparatively small extent of built-up, it had the highest expansion rate in the region between 1986 and 2018 (See Table 4 6). From Figure 4 10, Built-up increased from covering 1.83% (67.0 Km^2) of the study area in 1986 to 33.06% (1,212.90 Km^2) in 2018. Analysis revealed that growth rate of urban development was astronomically high but higher for the period between 1986 and 2002 than between 2002 and 2018. Built-up expanded by 363.15% between 1986 and 2002, and 290.88% between 2002 and 2018 as shown in Figure 4-10.

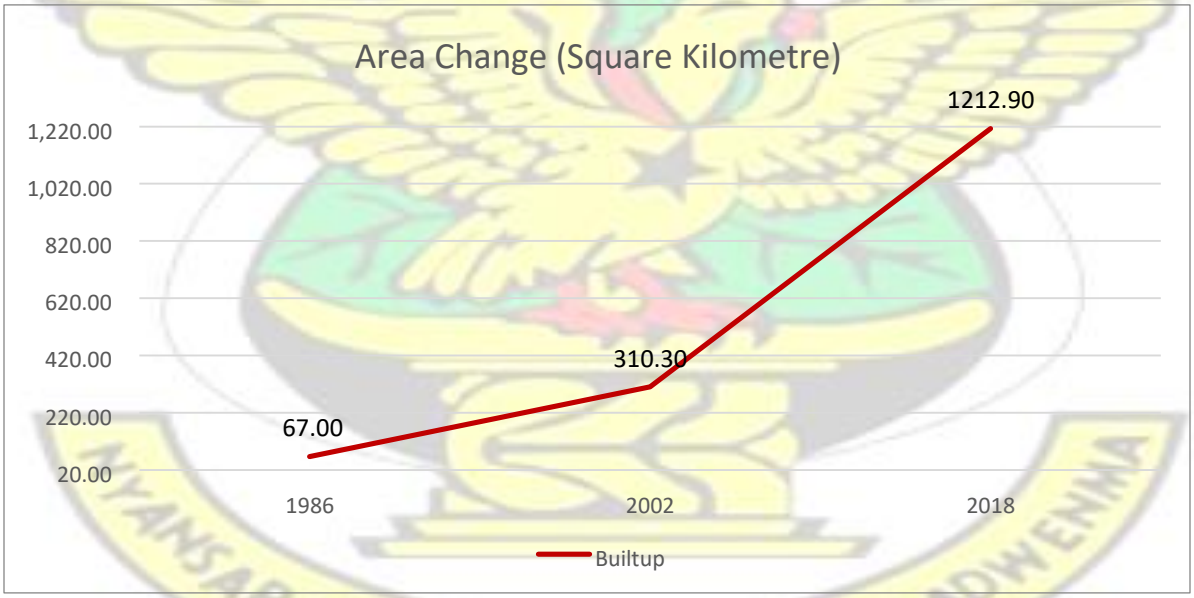

Figure 4-10 Percentage Change in Built-up

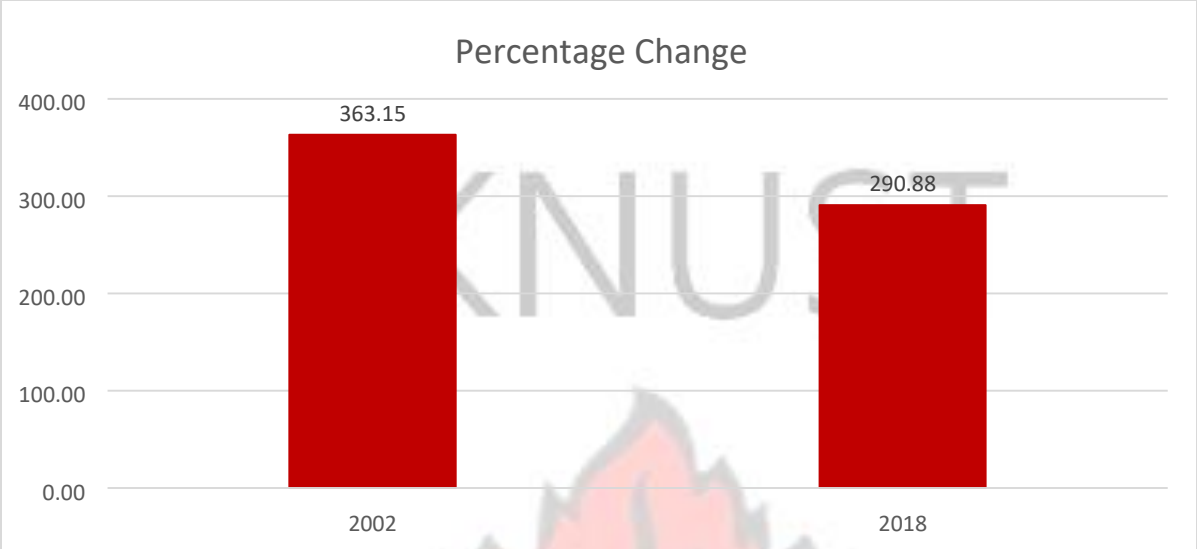

Figure 4-11 Percentage Change in Built-up

This shows the increasing exponential rate of built-up environment. The rate of change however decreased by 72.27% for the period between 2002 and 2018. This largely agrees with Osei et al (2015) acknowledgement that the urban extent of the Greater Accra region increased by 226.33% between 1985 and 2014.

Urbanization driven by population growth can be associated with the drastic positive change in built-up area. Braimoh (2004) suggest that the extensive expansion of built-up areas in Ghana is partly caused by population increase. According to the Ghana Statistical Service (2012), the population of Greater Accra region has almost tripled between 1984 and 2010 with population of the region increasing from 1,431,099 to 4,010,054. This is a consistent annual population growth rate of 3.3%, 4.4% and 3.1% in 1984, 2000 and 2010 respectively. The growth pattern supports the trend of built-up increase for the duration of this research such that higher population growth rate is recorded between 1984 and 2000 corresponding a higher expansion in Built-up LULC type between 1986 and 2002 of 363.15% Similar to decreased population growth rate for the region between 2000 and 2010, urban expansion also increased at a reduced rate of 290.88% between 2002 and 2018.

Notwithstanding the trend exhibited by the annual population growth rate, statistics from the same 2010 census report indicated a consistent increase in proportion of urban population in the region. It shows a continuous rise from 83.0%, 87.7% and 90.5% progressively from 1984 through 2000 to 2010. The urbanization of Accra has been mainly due to the rapid increase in population as a result of the urban biased development strategies adopted by policy makers since the colonial era:

centralized city for industry, manufacturing, commerce, administrative functions socioeconomic amenities and infrastructure development (Addae and Oppelt, 2019).

4.3.4 Waterbodies

Water bodies in the region experienced the least change among all four LULC categories. This change was undulating characterized with a decrease between 1986 and 2002 and an increase between 2002 and 2018. It underwent a total change of decrease of 7.84% for the entire duration from 1986 to 2018. The undulating nature of waterbody cover type shown in Figure 4-12 indicates a fall from 116.25 Km^2 in 1986 to 88.65Km^2 in 2002 and a subsequent increase to 107.14Km^2 in 2018 accounting for a total loss of 9.11 Km^2.

The changes are seen to be accounted largely by waterbodies drying into Bare land (20.05%) and other parts transitioning into Vegetation (12.81%) during the first 16-year period between 1986 and 2002. Expansion for the second time period was accounted for by 2.73% representing 32.85 Km^2 of Bare land transformed into waterbody between 2002 and 2018 (see Figure 4-1 and Figure 4-2 from appendix). This may be due to the expansion of water into bare land areas located along the banks of water bodies in the region.

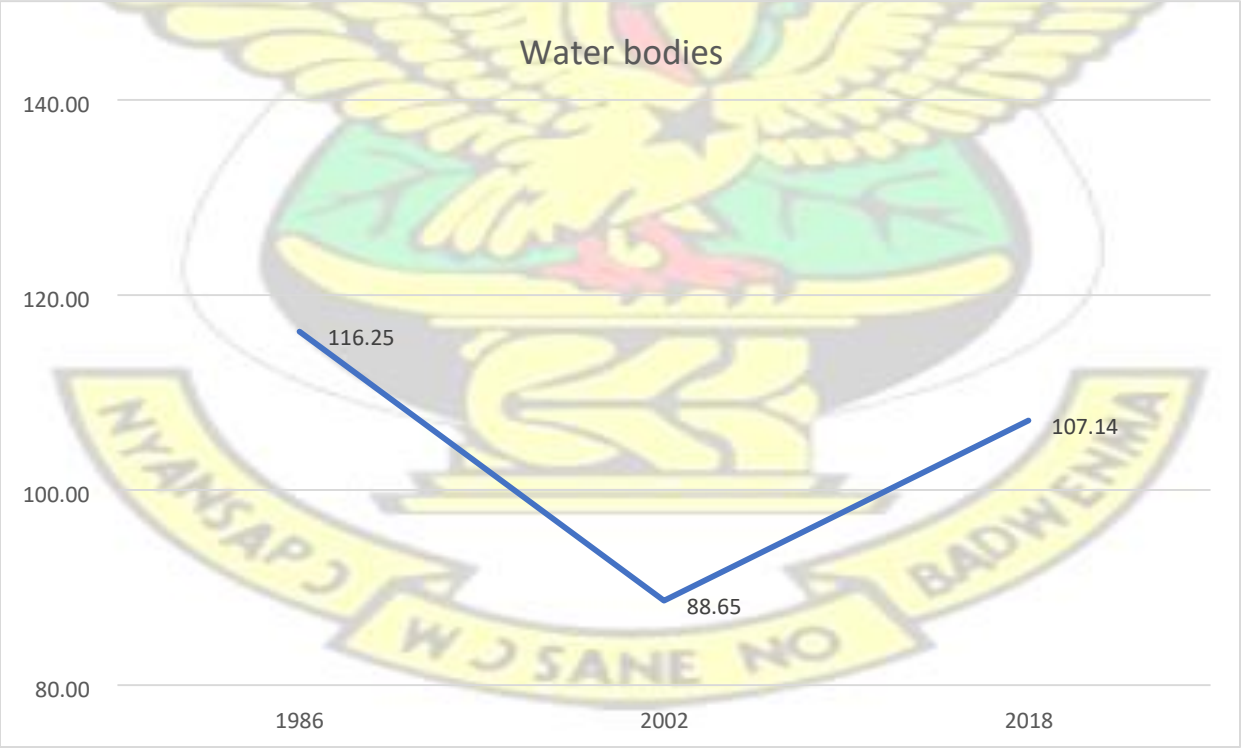

Figure 4-12 Waterbody LULC Trend

Water bodies covered 3.17% (116.25 Km^2) of the study area in 1986, reduced to 2.42% (88.65 Km^2) in 2002 and a subsequent increase coverage of 2.92% (107.14 Km^2) in 2018. In the 23.74 Km^2 loss of water bodies in the region between 1986 and 2002, highest contributor to this reduction was bare land with 25.05% representing 29.19 Km^2 of water resources changed into bare land. Out of the total change in the same period, 12.82% and 1.92% were also converted into vegetation and built-up respectively (see Figure 4-1 and Figure 4-2 from appendix). Contrary to the first time period, water resources increase from 88.73 Km^2 to 107.14 Km^2 between 2002 and 2018. This change could also be explained largely by the changes experienced in the Songor Lagoon, the Densu estuary and connected Pambros salt production site.

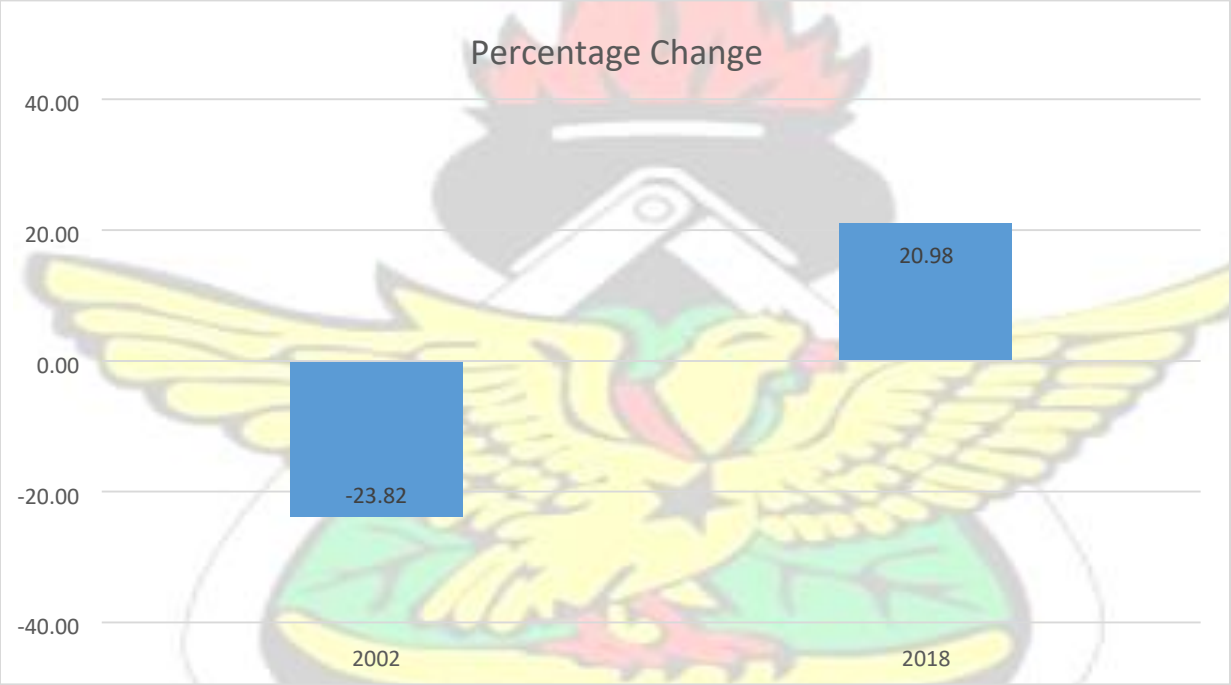

Figure 4-13 Percentage Change in Water bodies

The Songor lagoon decreased into visible minor lakes as asserted by United Nations Environment Programme (2006). Over the period between 1986 and 2002, both lagoons experienced decrease volumes of water content. According to the study, between 1990 and 2000 many African water resources have undergone dramatic changes mostly due to the impact of irrigation and other human activities. The Songor Lagoon was prominently featured to be drying up, and to be undergoing drastic transformation with surrounding lowlands exhibiting signs of becoming dryer and less habitable. Water resource management expert have also associated increasing temperatures associated with climate change with the decline of water bodies in the country.

On the contrary, the period between 2002 and 2018, the same lagoons experienced increase water volumes. This expansion around of Pambros and the Densu estuary could however be said to be limited by the rapid urbanization occurring in and around the estuary on several sides. The rapid urban expansion occurring in the area has resulted in massive pollution of the Densu lake from both domestic and commercial sources (Karikari and Ansa-Asare, 2006).

Increase between 2002 and 2018 could be linked to the increase damming of these two lakes for salt production purpose which causes water to be held behind the dam, thus causing the lake to expand backwards. In support of these plausibility, Václavík and Rogan (2009) noted that the construction of the Slezská Harta dam in the Olomouc region of Czech Republic resulted in a slight increase in the total area cover by water bodies in the region. Accumulation of sediments at the bottom of water bodies could also explain reduced depth of these water bodies but increases their submergence surface area. Braimoh & Vlek (2004) observed that the area of the Bontanga dam in northern Ghana had increased in size due to erosion.

4.4 Land Surface Temperature Analysis

This section presents the analyses of LST change, using derived LST from the Landsat satellite images. MODIS Land Surface Temperature data together with statistical techniques were further used as an authoritative data for the validation of LST estimates.

4.4.1 Land Surface Temperature Validation

In this study, MODIS Land Surface Temperature data (MOD11C1) made available by US Geological Survey was used for the validation of derived LST values. Due to launch date of MODIS, data for 1986 were nonexistent, thus validation was done for only 2002 and 2018. Both Daytime MODIS LST data and derived LST data were processed to ensure conformity and allow for comparative analysis.

Table 4-7 Cross-Table Validation of LST

	2002			2018		
Sample Site	**Derived LST**	**MODIS LST**	**Residual**	**Derived LST**	**MODIS LST**	**Residual**
	2002			**2018**		
1	31.08	31.21	0.13	29.78	27.87	-1.91
2	32.57	35.35	2.78	27.96	29.67	1.71
3	33.46	36.09	2.63	30.38	31.77	1.39

4	28.36	30.01	1.65	25.51	28.15	2.64
5	32.28	34.45	2.17	29.78	30.75	0.97
6	31.08	31.79	0.71	29.48	29.01	-0.47
7	32.87	34.85	1.98	30.67	31.85	1.18
8	30.18	32.03	1.85	28.87	30.01	1.14
9	28.97	32.85	3.88	29.78	29.37	-0.41
10	31.08	31.69	0.61	29.48	29.01	-0.47
11	29.88	29.19	-0.69	29.48	29.03	-0.45
12	28.67	30.87	2.20	28.57	29.45	0.88
13	27.75	30.01	2.26	27.96	28.19	0.23
14	32.87	34.85	1.98	30.67	31.85	1.18
15	27.14	29.63	2.49	28.27	29.85	1.58
16	26.83	28.27	1.44	26.43	26.71	0.28
17	27.75	30.43	2.68	27.96	28.19	0.23
18	32.87	35.11	2.24	30.67	31.85	1.18
19	28.36	30.01	1.65	25.51	28.15	2.64
20	30.78	31.25	0.47	29.78	29.47	-0.31

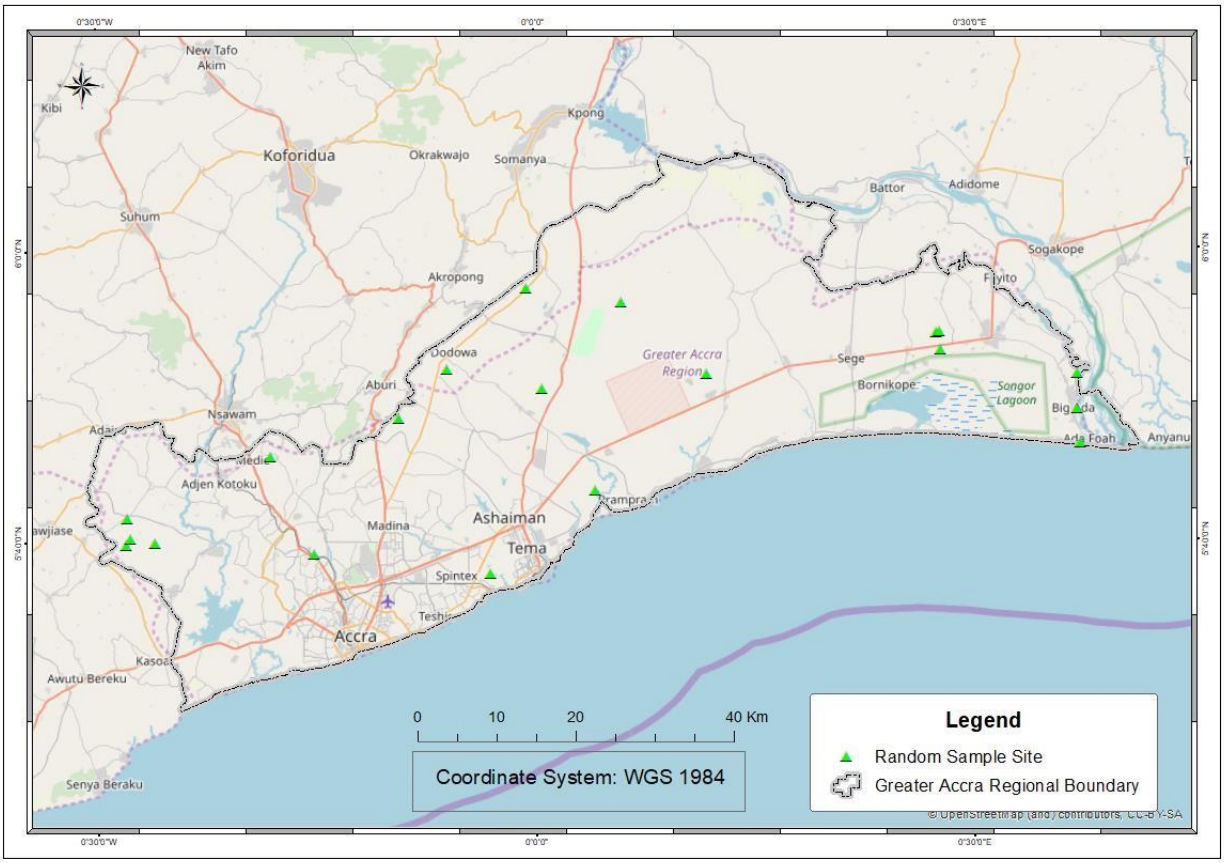

Figure 4-14 Spatial Distribution of LST Validation Sample Sites

The processing activities included data extraction, rescale, projection and resampling. LST values derived from Landsat satellite images by the mono-window algorithm method were validated against MODIS LST data. This approach involves the comparison of retrieved LST values with well documented and validated LST values retrieved from other satellite data (Trigo *et al.*, 2008). The validation method in this study used the LST MODIS data as an authoritative reference for validation. Table 4-7 shows LST values from twenty randomly selected sample locations (see Figure 4-14) and their corresponding MODIS LST values. From Table 4-7, residual or difference between derived LST and MODIS LST were between -0.69℃ and 3.88℃ for 2002 and between -1.91℃ and 2.64℃ for 2018.

MODIS LST data validated derived LST from Landsat satellite imagery from the correlation analysis shown in Figure 4-15 and Figure 4-16. Correlation Coefficient (R) of 0.892 and 0.730 for 2002 and 2018 respectively indicate high positive correlation between derived LST and MODIS LST.

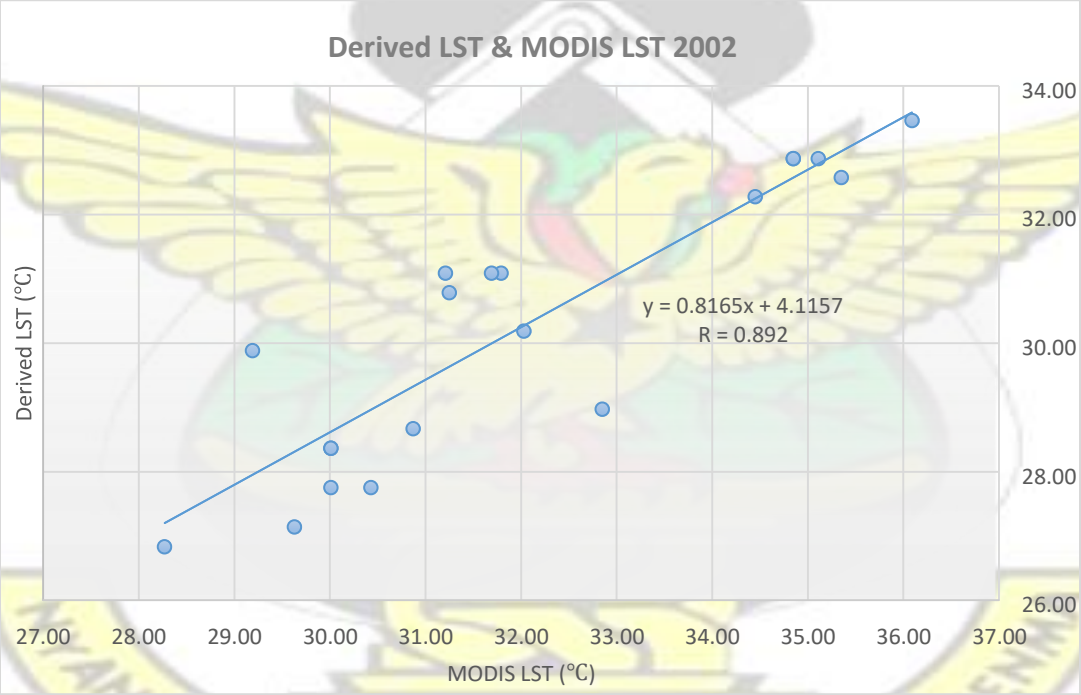

Figure 4-15 Correlation between Derived LST and MODIS LST for 2002

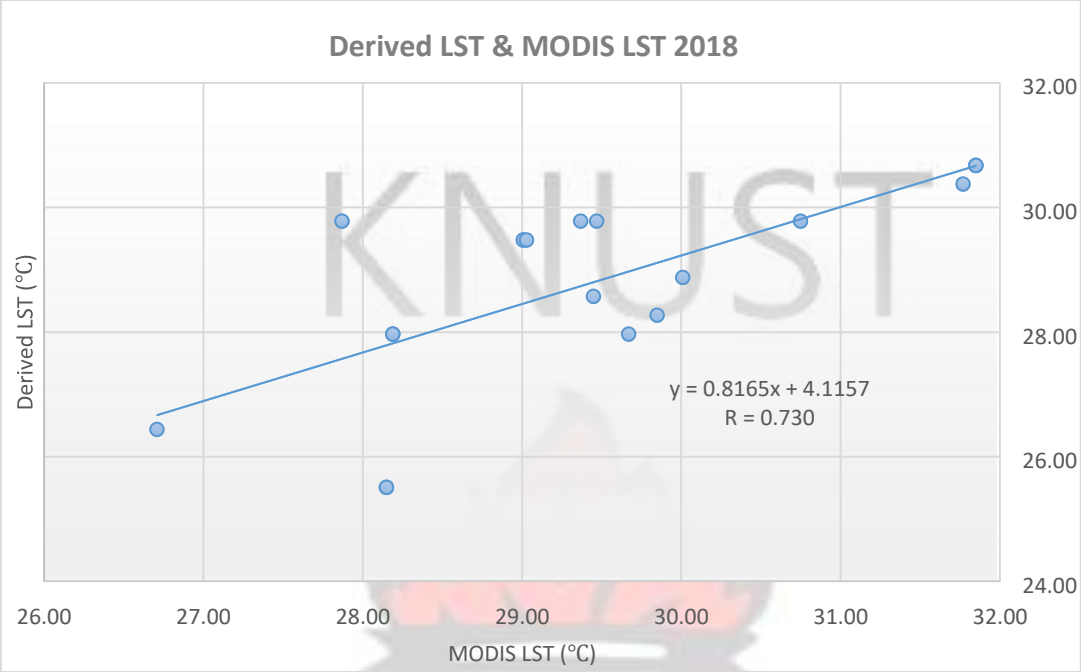

Figure 4-16 Correlation between Derived LST and MODIS LST for 2018

Table 4-8 shows the Root Mean Square Error (RMSE) and Coefficient of Variation (CV) of the validation results. It can be concluded from the table that MODIS LST generally validates derived LST with identical CV values.

Table 4-8 Accuracy Assessment of LST Validation

	Root Mean Square Error (RMSE)	Coefficient of Variation (CV)	
Year	***MODIS/Derived LST***	***MODIS***	***Derived LST***
2002	2.038	7.346%	7.116%
2018	1.289	5.034%	5.505%

Notwithstanding, derived LST values appear to have generally recorded relatively lower values than MODIS LST values across most the random sample locations. The disparity in values can be attributed to factors associated with differences in satellite specifications as shown in Table 4-9.

Table 4-9 Comparison of Landsat and MODIS Specifications

Specifications	Landsat	MODIS (MOD11C1)
Spectral	7 bands	36 bands
Pixel size	30 m	5600 m
Scene width	185 km	2,330 km
Image frequency	16 days	Daily
Corrections	None	Surface reflectance
Cost	Free	Free

Pixel size and LST spatiotemporal mismatches of Landsat and MODIS together with resultant propagation of error in processing these LST data to ensure pixel alignment for comparative analysis could be mainly cited for the differences between derived LST and MODIS LST values. This results in the two satellites to contain land surface information under different viewing angles at different pixel resolution or scale.

Qian *et al.*, (2013) and Trigo *et al.*, (2008) also emphasize the sensitive nature of accuracy of this validation method to spatial and temporal mismatches of the two LST measurements.

Cloud contamination could also be another factor accounting for some discrepancies. It has the potential to affect satellite temperature measurement (Jin and Dickinson, 2000). The potential contamination decreases the land surface temperature values. This might explain the relatively lower observed LST values.

4.4.2 Spatio-Temporal Dynamics of Land Surface Temperature Distribution

Thermal band from different Landsat satellite mission 5 and 7 were used to estimate Land Surface Temperature for the entire Greater Accra region. For easy comparison and analysis of estimates of the 32-year period, all three Land Surface Temperature maps were fitted to a scale of six classes of the same range. The scale ranges were; below 22℃, 22.0℃- 24.0℃, 24.1℃-26.0℃,

26.1℃-28.0℃, 28.1℃ -30.0℃ and above 30.0℃. The computed LST maps give an overview of the spatial distribution. LST values tabulated in

Table 4-10 indicates values as low as 20.19^{o} C and as high as 36.95 ^{o} C clearly showing mean LST increase in 2002 but a slight decrease in 2018.

Table 4-10 Land Surface Temperature Statistics

Summary Statistics of Temperature within Stu ly Area			
	Minimum	**Mean**	**Maximum**
1986	20.49	25.07	29.65
2002	20.19	28.57	36.95
2018	21.73	28.12	34.50

Analysis of the Landsat thermal imagery revealed yearly variation of LST over Greater Accra region (Figure 4-17 to Figure 4-19). There is a general increasing trend in LST over time, consistent with the observed urban expansion of the study area. The trend however indicates a significant increase between 1986 and 2002 but a decrease in LST from 2002 and 2018. The mean LST decrease between 2002 and 2018 was 0.45°C less than the average LST observed in 2002. The mean, maximum and LST range observed in 2002 buttresses the generally high spatial pattern of LST observed in the same year as shown in Figure 4-18.

Spatial variation of the LST displayed similar patterns for all the three timestamps studied. Higher LST was generally concentrated in the core of urban centers and bare land areas comprising sandy areas and dry salt, bare exposed rock, and quarries. High temperatures are also more apparent along the coastal belt of the region stretching northwards as development spread in the same direction. The pattern of low temperatures on the other hand was consistently identified around northern boarders spreading towards the north-western corner of the region.

4.4.2.1 Land Surface Temperature (LST) Variability in 1986

Analysis of estimates from 1986 shows LST range between 20.49℃ and 29.65℃ and an average of 25.52℃. The spatial patterns show LST variability in the region. Visual inspection of map clearly shows extensive high LST with range between 26℃ and 28℃ were mainly around areas like central Accra stretching towards the north and eastern part of the region, all the way to the immediate environs of the Songor lagoon protected area. Settlements lying within this zone included Ashaiman, Tema, Kobekro, Teshie and Prampram. There were also isolated and patches of hotspot areas that experienced between 28.1℃ and 30.0℃ but no area within the region experienced LST above 30.0℃.

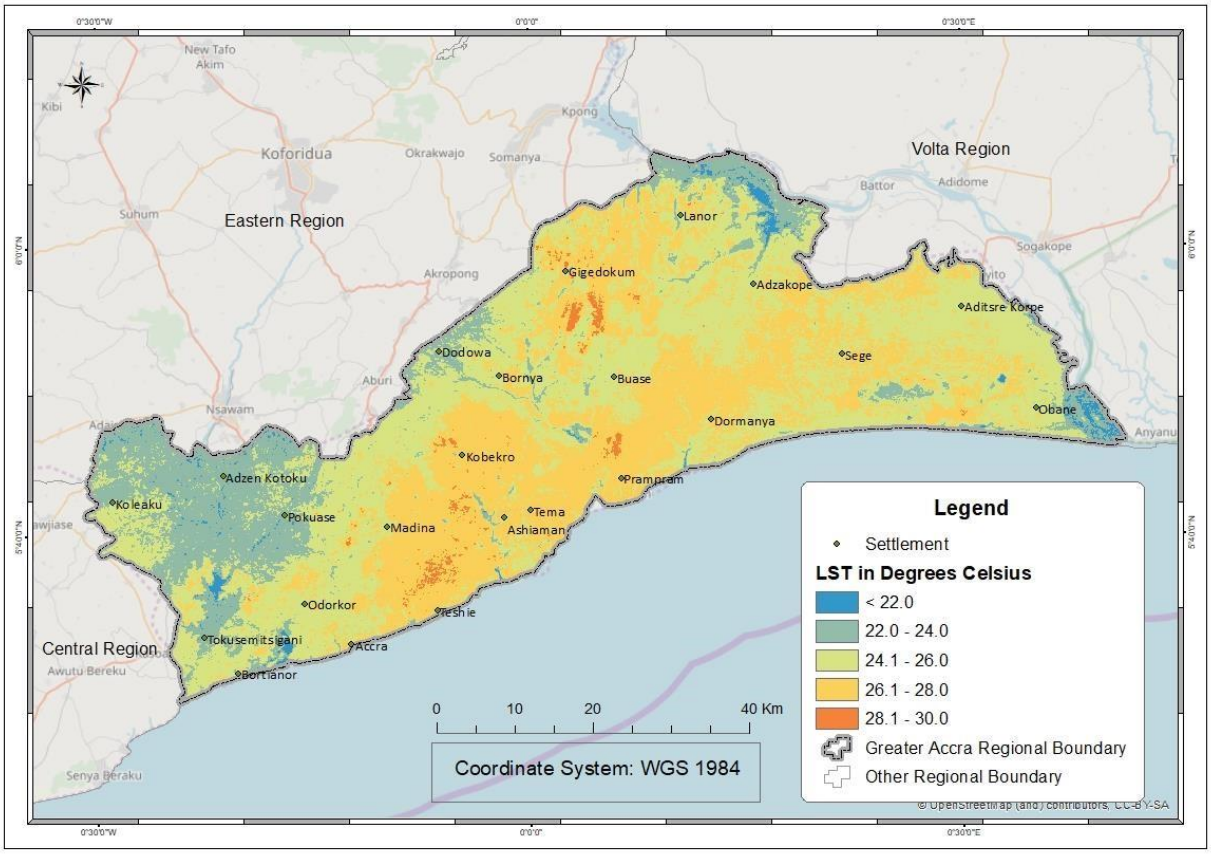

Figure 4-17 Spatial Distribution of Land Surface Temperature in 1986

Low LST values of less than 22℃ and between 22-24℃ were as expected found to be closely associated with water bodies and vegetation in the region. These cold spots were mostly in the north-western corner of the region where then rural areas like Amasaman, Pokuase, Adzen Kotoku and Koleaku are located. Furthermore, LST values between 24℃ and 26℃ were observed to be covering the banks of water bodies and exhibited a transitional zone between areas of ranges 26.1 ℃ -28.0℃ and 22.0℃ – 24.0℃.

4.4.2.2 Land Surface Temperature (LST) Variability in 2002

In the year 2002 as depicted by Figure 4-18, the entire region experienced abrupt increase in LST of above 30℃ in areas stretching from the Lake Volta estuary at the eastern boarders of the region to northern parts of the Shai Osu Doku district. The middle belt of the region extending through developed areas like Tema and most residential developments of AMA to Weija and its environs were all portions of the region that also experienced LST above 30℃.

The same high temperature could be observed along the entire coastline spreading in-land. Relatively low LST values remain associated with waterbodies and some known vegetated areas. Songor Lagoon area however exhibited the most number pixels that experienced low

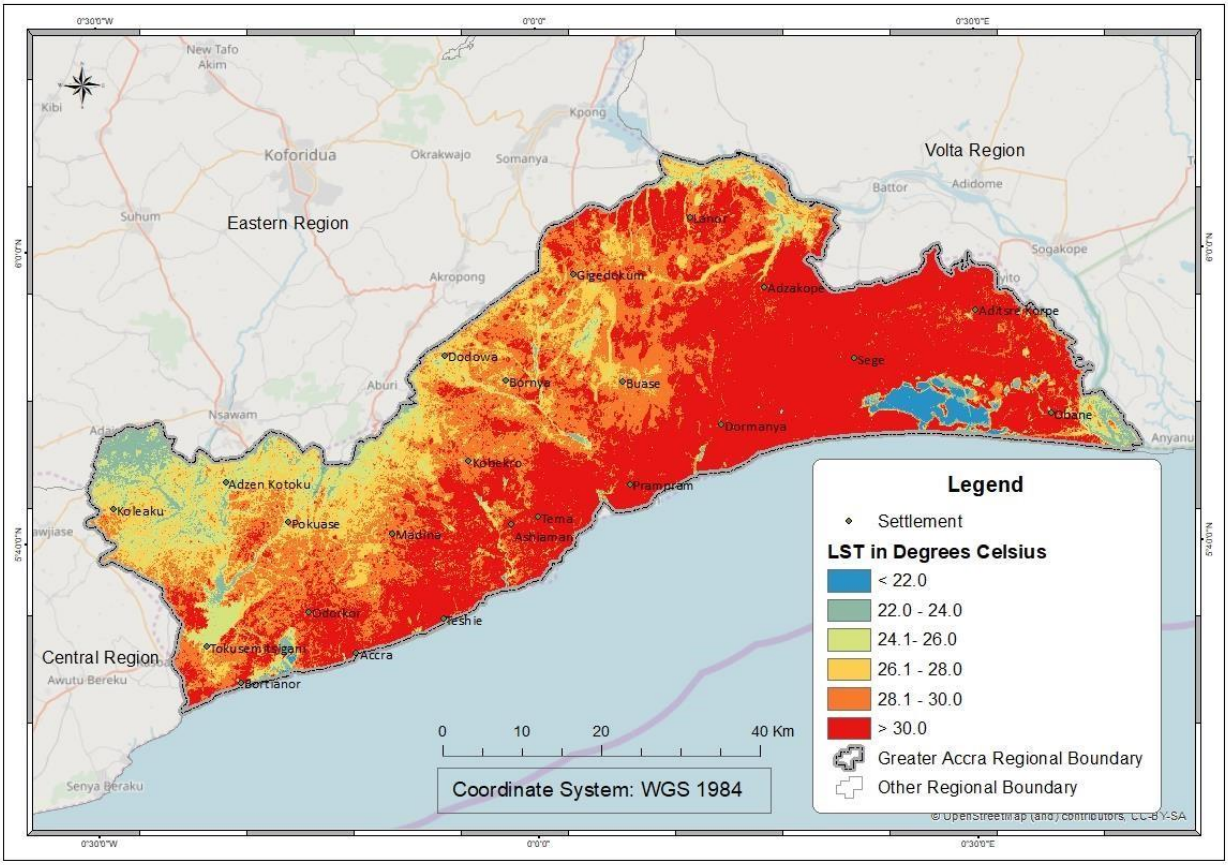

temperatures below 22°C.

Figure 4-18 Spatial Distribution of Land Surface Temperature in 2002

Most of the land mass in the region experienced temperature above 30ºC. These included areas of vegetation cover which indicated a rise compared to 1986. Parts of Central Accra and Ningo Prampram district and Kobeko, extending to some parts of Shai hills were all areas identified to have recorded temperatures between 28 C and 30°C. Statistical analysis of all the three LST maps estimated, the year 2002 presented the highest range of LST values with minimum temperature of 20.19 C and maximum of 36.95°Cand the highest mean of 28.57°C. Temperature readings above 30 C were observed extensively covering over 70% of the total area of the region. This high LST extended continuously from the shores of the estuary of the Volta river westward towards north-eastern corner of AMA stretching up to Madina and its environs as shown in Figure 4-18.

According to Asante and Amuakwa-Mensah (2014), Ghana experienced increased greenhouse gases emission of 107% between 1990 and 2006. In the year 2006, carbon dioxide became the lead GHG accounting for 46%, followed by Methane (34%) and Nitrous oxide (20%). This can be associated with decreasing vegetation cover during this period leading to increase release of Carbon dioxide into the atmosphere. Land use change is linked to approximately 70% of anthropogenic emissions of carbon dioxide (CO_2) in Africa (Andrew, 2018). Van Leeuwen *et al.* (2011), observed that deforestation activities is a factor behind increasing land surface temperature because aridification and land surface degradation causes the radiative properties of the surface to change. This is due to the lowest and highest emissivity of urbanized and vegetated environments.

4.4.2.3 Land Surface Temperature (LST) Variability in 2018

Figure 4-19 showing LST trend for 2018 indicate high temperatures above 30℃ largely transition into the 28.1℃ – 30.0℃ range in most parts of AMA, towards Pambros, Weija lake and northwards into Ga West district and northern part of Ga South district. This range of LST was not as extensive as in 2002 and were largely located within the Ada districts, Ningo Prampram, Shai Osu Doku and some parts of Ashaiman. The outskirts of Ga West, South and Madina ranged from 26℃ to 28℃ with isolated occurrences of 24℃ to 26℃ within the same outskirts. Generally, temperatures for the year were high such that no area experienced LST below 22℃. Some parts of Weija lake, Pambros, Songor lagoon nevertheless also experienced low LST between 22℃ and 24℃.

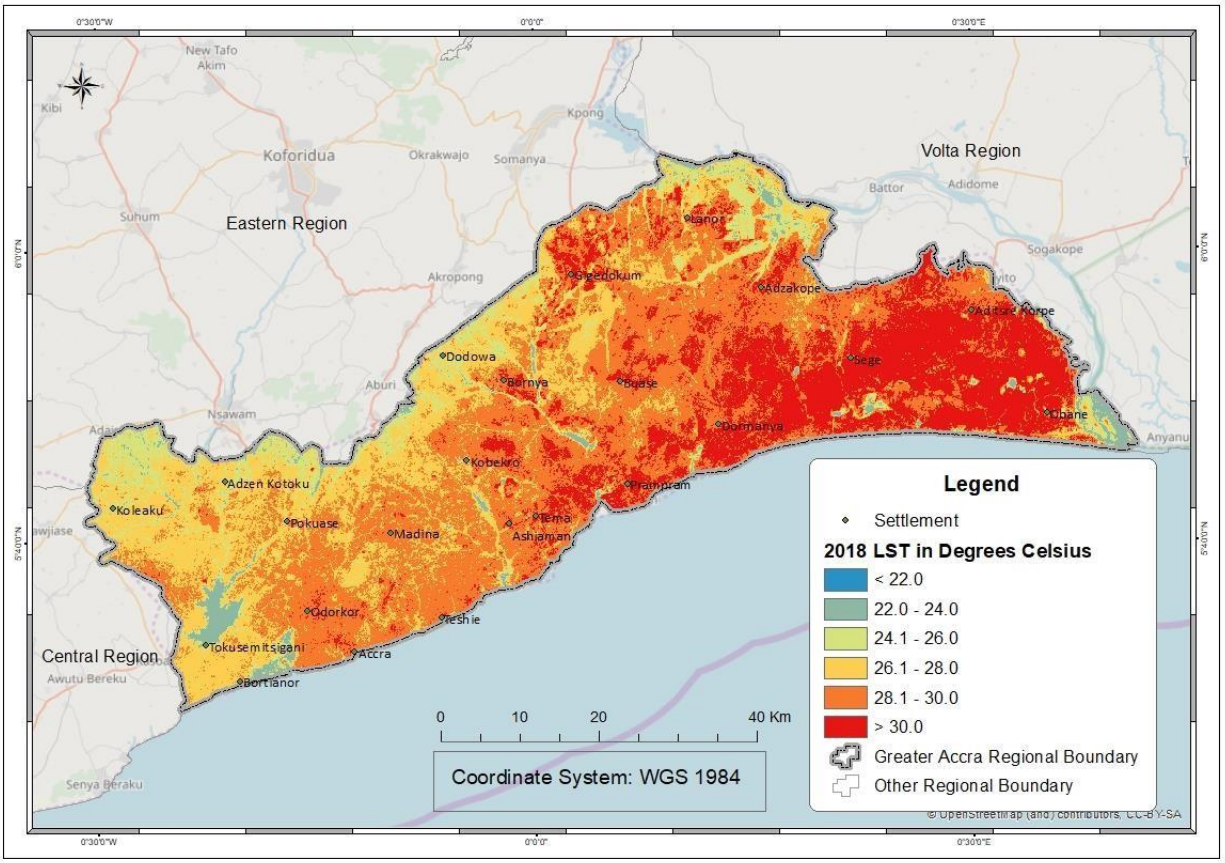

Figure 4-19 Spatial Distribution of Land Surface Temperature in 2018

4.4.3 Measure of Association in the Spatial Pattern of LST

Spatial autocorrelation is a measure of correlation of phenomenon across a geographic space. It indicates the significance of spatial characteristics affecting a given phenomenon in space and the dependency of objects with spatial properties. Strongly positive or negative results indicate that a clear spatial property is found in the object with a high correlation. From Figure 4-20, Figure 4-21 and Figure 4-22, spatial autocorrelation (Global Moran's I) analysis indicates the pattern of Land Surface Temperature in Greater Accra is clustered for all three timestamps. The z-score of 3.002 and 2.617 for 1986 and 2002 respectively demonstrate cluttering with less than 1% likelihood that the observed clustered pattern is a result of random chance. Z-score for 2018, 2.401 though also indicate clustering, it has less than 5% likelihood that the observed clustered pattern is a result of random chance.

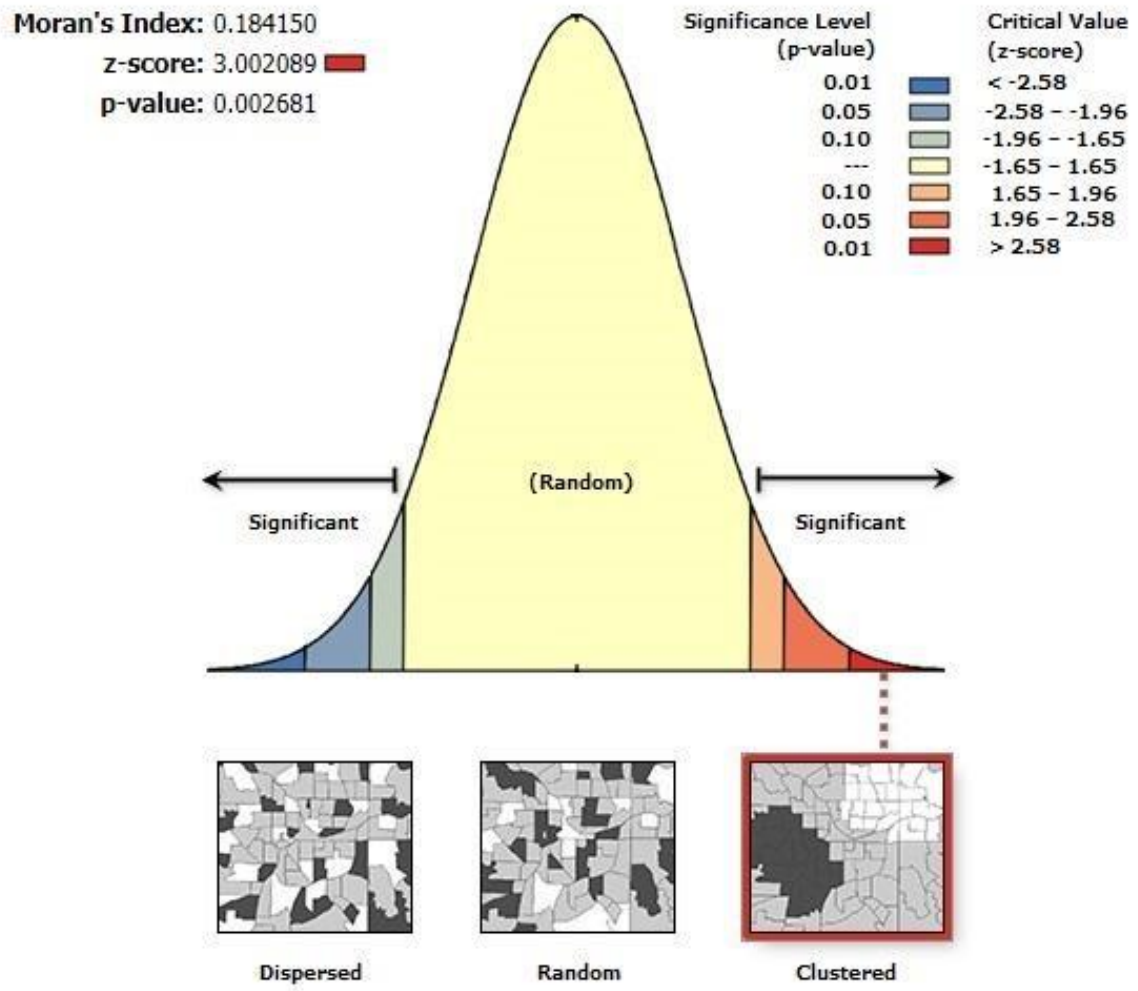

Given the z-score of 3.00208901821, there is a less than 1% likelihood that this clustered pattern could be the result of random chance.

Figure 4-20 Spatial Autocorrelation for 1986

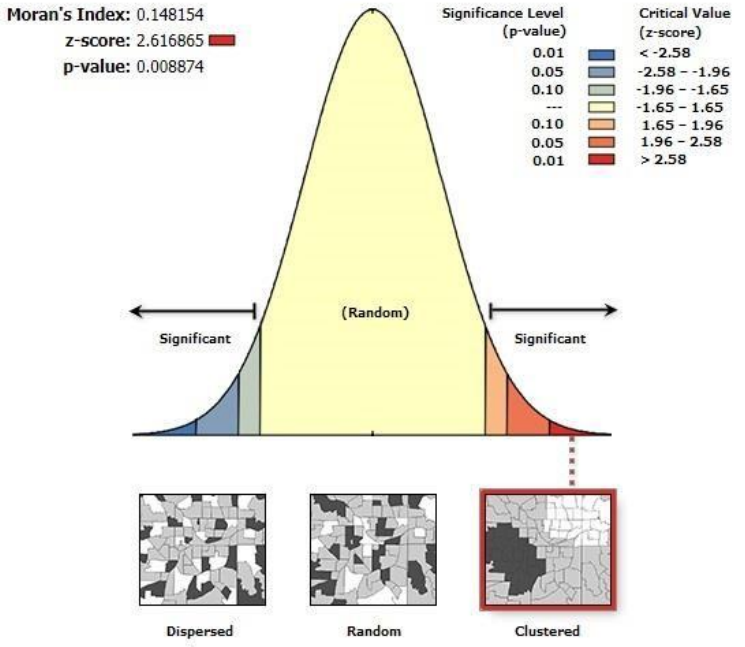

Given the z-score of 2.61686537646, there is a less than 1% likelihood that this clustered pattern could be the result of random chance.

Figure 4-21 Spatial Autocorrelation for 2002

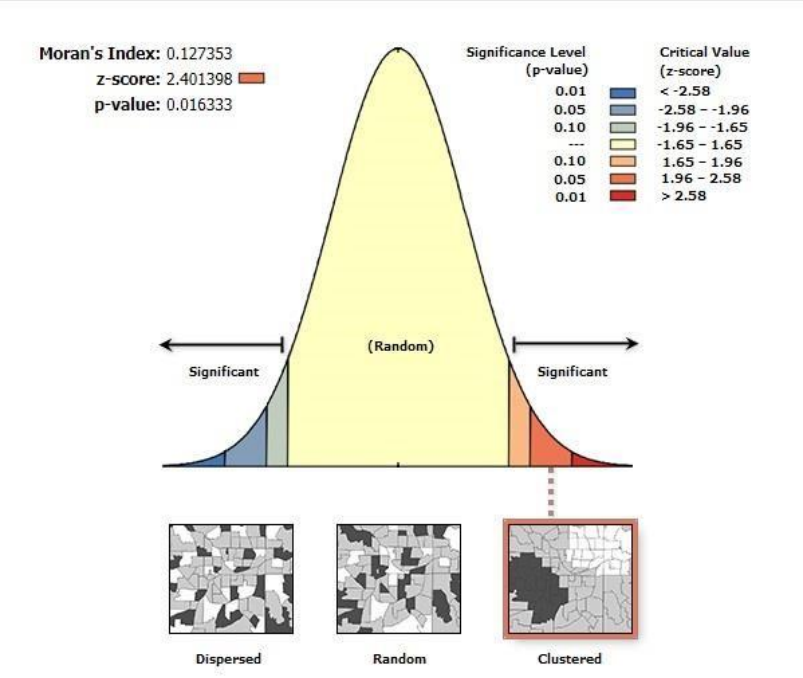

Given the z-score of 2.40139831864, there is a less than 5% likelihood that this clustered pattern could be the result of random chance.

Figure 4-22 Spatial Autocorrelation for 2018

4.5 Relationship between LST and LULC Types

The relationship between LULC and LST were analyzed. This subsection relates the results of the LULC and LST changes presented in the previous sections of this chapter. Zonal statistical and correlation analysis were applied in comparing LULC types and indices with LST estimates.

4.5.1 Zonal Statistical Analysis between LULC Types and LST

To analyze land surface temperature variations associated with the four different land use/cover categories identified in the study area, statistics (minimum, maximum and mean) on LST for these LULC patterns were extracted by zonal statistical analysis. Table 4-11 shows the results from the analysis.

Table 4-11 Land Surface Temperature categorized by Land use/Land cover type

LULC Type	Minimum LST			Maximum LST			Average LST		
	1986	2002	2018	1986	2002	2018	1986	2002	2018
Vegetation	20.99	21.16	21.73	29.18	35.79	34.5	25.08	28.47	28.12
Bare land	20.49	20.19	22.69	29.65	36.66	34.5	25.07	28.42	28.59
Built up	21.98	21.8	22.69	29.65	36.08	34.5	25.81	28.94	28.59
Waterbody	20.49	20.19	22.05	28.71	29.28	32.45	24.60	24.73	27.25

Table 4-11, shows that LST has generally increased from 1986 to 2018 in the Greater Accra region. The mean LST estimates as shown in Figure 4-23 shows identical trend for built-up and vegetation land use/land cover types.

Vegetation experienced equally high temperatures with a 3.39℃ increase in LST between 1986 and 2002. Though built-up experienced similar trend, there was an increase of 3.13℃ from average LST of 25.81℃ in 1986 to 28.94℃ in 2002. From 2002 to 2018 however both vegetation and built-up experienced a decrease in LST of 0.35℃. Average land surface temperature values for bare land increased from 25.07℃ to 28.42℃ and 28.59℃ in 2002 and 2018 respectively. This indicate 3.35 ℃ and 0.17℃ increase for 2002 and 2018 amounting to a total increase of 3.52℃ over the 32-year period. Waterbody land use/land cover category also experienced increase temperatures throughout the duration of 0.13℃ and 2.52℃ increase in 2002 and 2018 respectively (see Figure 4-23). These LST increase are significantly high compared to IPCC global temperature increase values.

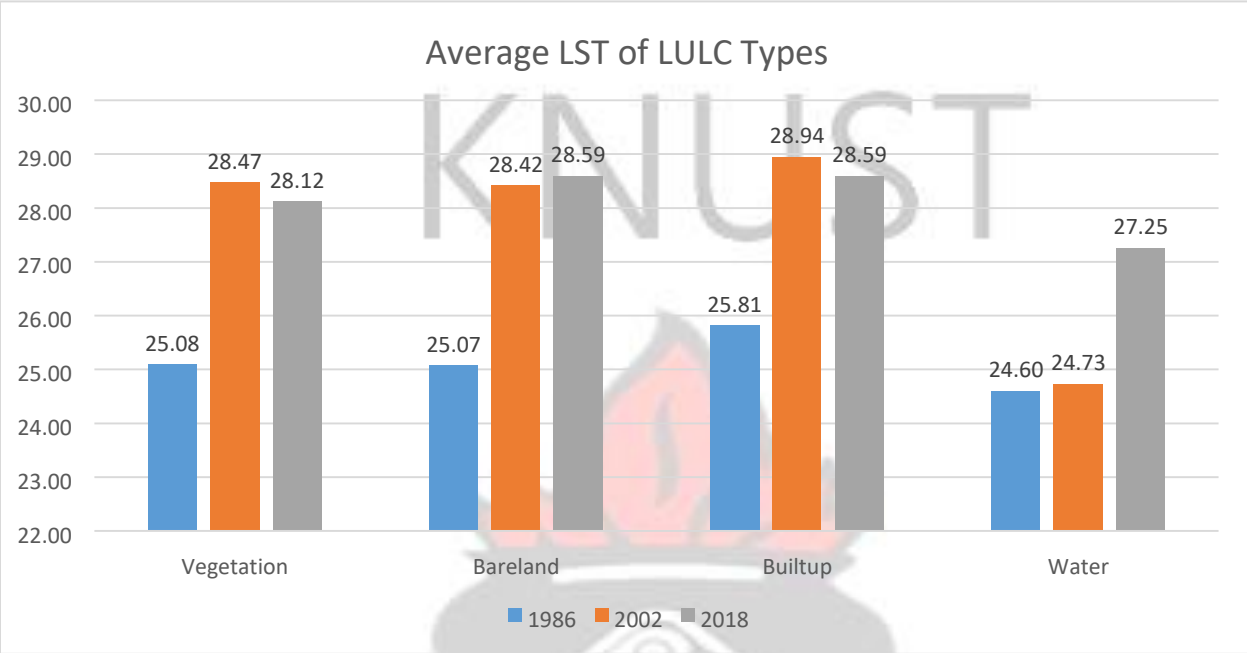

Figure 4-23 LULC type and Average LST

Among all four LULC categories, built-up areas have the highest average LST for all three time periods except for 2018 which it recorded same as bare land. This is followed by Vegetation, Bare land and Water bodies, in descending order. From Table 4-12, bare land experienced the highest negative change of 685.58Km^2 decrease and this corresponded to the highest increase in LST of 3.53℃ over the period the study. This could be explained by the large extent of bare land in the region especially in the eastern parts of the region as asserted by Price (1990), that bare soil locations experienced a wider variation in surface radiant temperature.

Table 4-12 Comparison between LULC Change and LST Change between 1986 and 2018

	LULC Change in Km^2	LST Change in ℃
Bare land	- 685.58	+ 3.53
Vegetation	- 29.65	+ 3.04
Built-up	+ 724.34	+ 2.78
Water bodies	- 9.11	+ 2.65

Vegetation cover between 1986 and 2018 decrease by a total of 11.82 percent (29.65Km^2) and this accounted for the second highest LST increase of 3.04℃. This is explained by the generally negative correlation between vegetation and temperature as concluded by Domaley *et al.*, (2018).

Built-up and waterbody LULC categories recorded a positive change of 724.3 Km^2 (654.03%) and a negative change of 9.11 Km^2 (7.84%) respectively (refer to Table 4-12). It was however surprising that built-up which experienced astronomical increase mostly in the form of urban development recorded the third highest LST increase of 2.78℃ between 1986 and 2018. Though this supports conclusions from other studies on the role of urban expansion on urban microclimate specifically land surface temperature, comparison between built-up LULC change and LST increase clearly shows that in Greater Accra region, the influence of urban expansion influence on LST increase is average. Inferential statistics from the analysis indicate that for the 32 years of this study, built-up environment could be said to be increasing at an average of 20.44% per annum while LST increased by an average of 0.09℃ every year. This is however not conclusive as changing trend for both LULC and LST for the period of 1986 to 2002 was higher than between 2002 and 2018.

Average land surface temperature increase level of 2.65℃ was observed for LULC type classified as waterbody. This was the least among all the LULC types but considered higher compared to corresponding temperature of built-up. It could however be explained by two major salt production lagoons sites within the region namely Pambros at the west south of the Weija lake and the Songor lagoon. These are major salt production sites and relatively high increasing temperature recorded for waterbodies within the region may be attributed to the ability of salt to absorb heat very effectively because of its physical and chemical properties. Salt's heat absorption properties influence the freezing temperature of liquid, particularly water. This has implication on global warming as LST rises.

4.5.2 Correlation Analysis between LST and LULC Types

In understanding the relationship between LST and land cover, investigation of the thermal characteristics of each LULC type is essential. Many indices have been used as a metric in LULC analysis. Prominent among these is the Normalized Difference Bareness Index (NDBAI), Normalized Difference Water Index (NDWI), Normalized Difference Built-up Index (NDBI) and Normalized Difference Vegetation Index (NDVI).

NDVI, NDBAI, NDWI and NDBI have been widely useful in the study of vegetation cover, bareness index, water state especially the water content within vegetation and for the evaluation built up respectively. These land coverage indices have a strong association with Land Surface Temperature (Sun *et al.*, 2012; Zhang *et al.*, 2009). Satellite images were converted from DN values to Surface Reflectance value and the four indices were computed as a measure for vegetation, built up, waterbody and bare land LULC types. The values of the results of all four indices vary between -1 and +1 (see Figure 4-3 to Figure 4-14 from appendix).

To analyze the relationship between each of these indices and LST, random sample points were generated for each LULC type. For each of LULC type, 100 random points were generated thus a total of 400 sample points were used in this correlation analysis. Values for each index and related LST values were plotted in a scatterplot to examine the relationship.

4.5.2.1 Normalized Difference Vegetation Index (NDVI) and LST

The Normalized Difference Vegetation Index (NDVI) is an index of plant ―greenness‖ or photosynthetic activity. It is the most commonly used vegetation indices. LST studies widely use the NDVI parameter because NDVI is less sensitive to the changes in atmospheric conditions than other indices; it has, therefore, become very popular for vegetation monitoring (Raynolds *et al.*, 2008)

Values of NDVI can range from -1.0 to +1.0, with values less than zero indicative of no ecological meaning, so the range of the index is truncated to 0.0 to +1.0. Higher values signify a condition associated with highly photosynthetically active vegetation. Low NDVI values on the

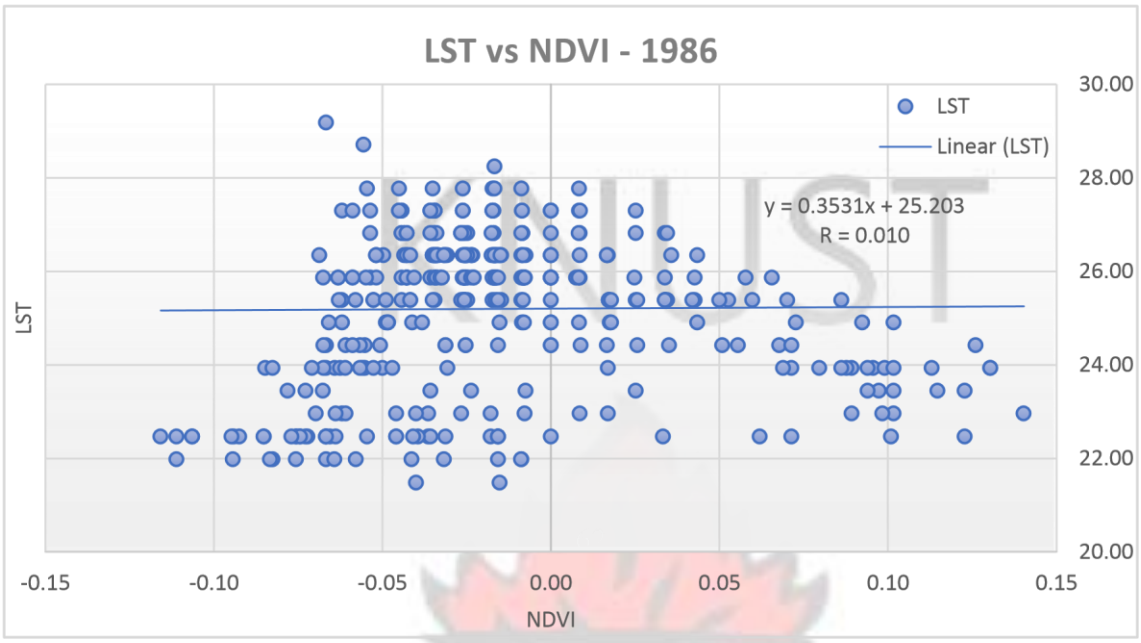

other hand mean little photosynthetic activity or greenness.

Figure 4-24 Relationship between LST and NDVI in 1986

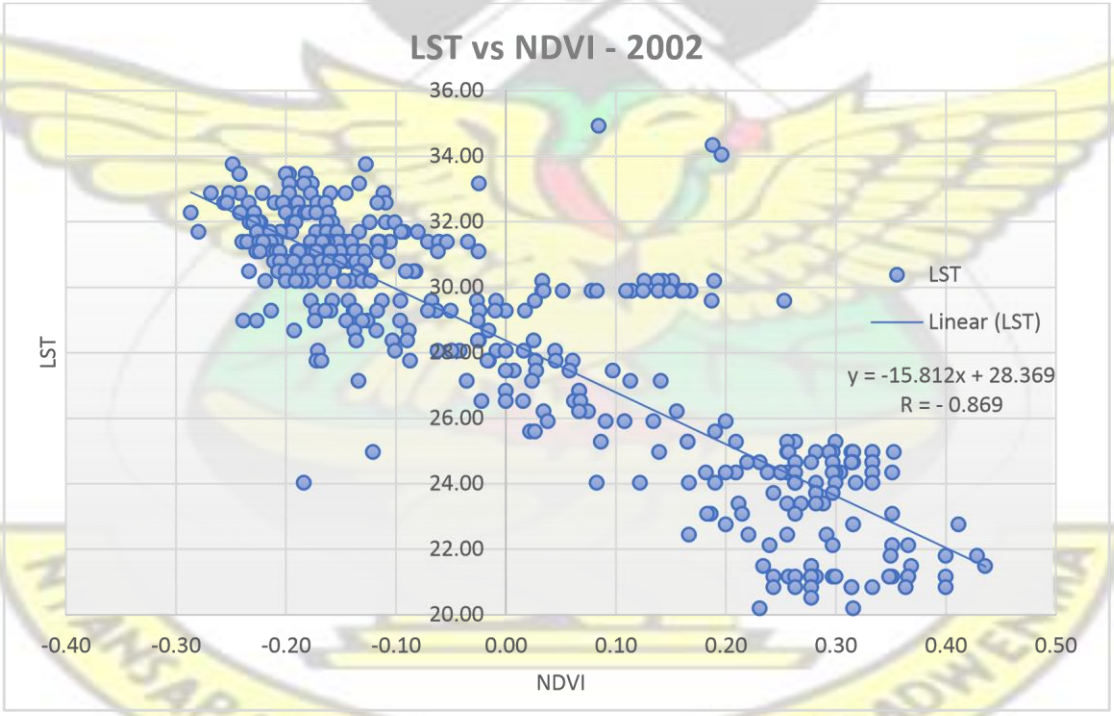

Figure 4-25 Relationship between LST and NDVI in 2002

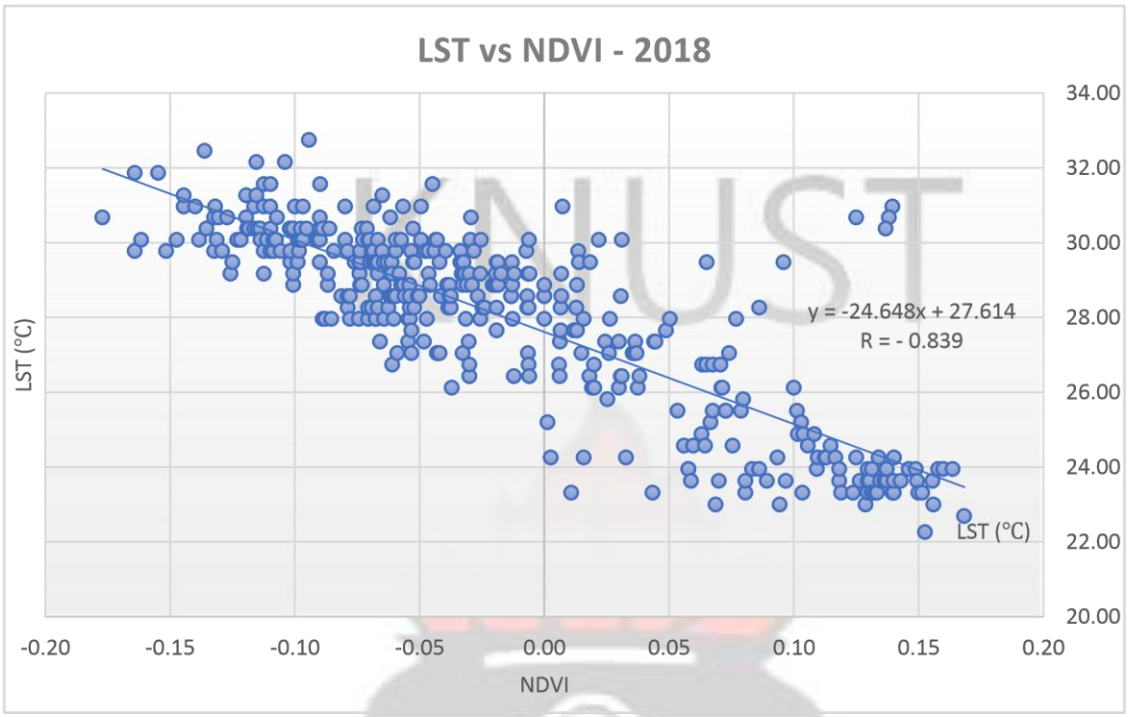

Figure 4-26 Relationship between LST and NDVI in 2018

Examination of relationship between NDVI and LST over the years shows generally negative relationship as indicative in the correlation coefficient (R) of 0.010,-0.869 and -0.839. This indicates an inverse relationship between vegetation cover and LST in the Greater Accra region suggesting high NDVI areas may be associated with lower LST as concluded in Aduah *et al.* (2012) and Kumi-boateng and Stemn (2015). It can however be seen from Figure 4-24 that the very weak correlation coefficient in 1986 was an exception to the general assertion that LST and NDVI are negatively correlated. Relationship in 1986 as indicated illustrates the weakest with almost no relationship between the two parameters. This affirms conclusion of Yuan and Bauer (2007) that the amount of vegetation cover is not the only factor affecting LST values.

4.5.2.2 Normalized Difference Bareness Index (NDBAI) and LST

Distribution and change of bare land play an important role in the ecosystem, which usually implies physiographical and anthropogenic impacts on ecologic environment. NDBAI is a derived index for mapping bare land areas from Landsat satellite images. NDBAI analysis the association between mid-infrared and thermal radiation.

Scatterplot shown in Figure 4-27 to Figure 4-29 all show positive association between LST and NDBAI. Correlation coefficient (R) of 0.628, 0.833 and 0.800 are recorded for 1986, 2002 and 2018 in Figure 4-27, Figure 4-28 and Figure 4-29 respectively.

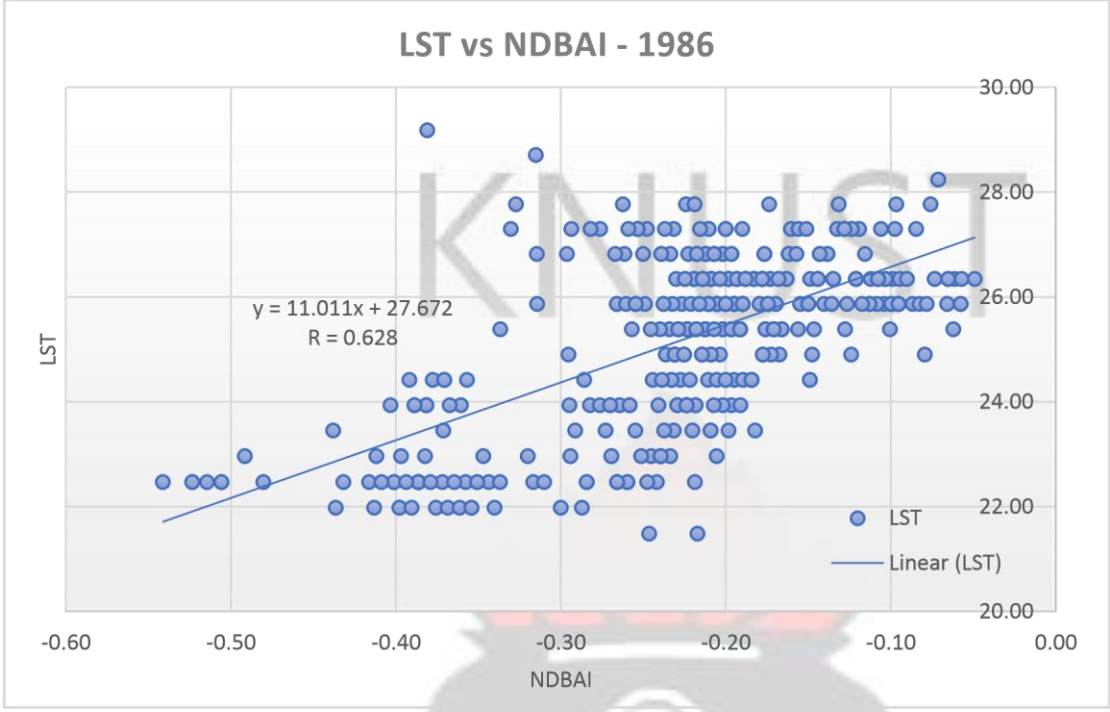

Figure 4-27 Relationship between LST and NDBAI in 1986

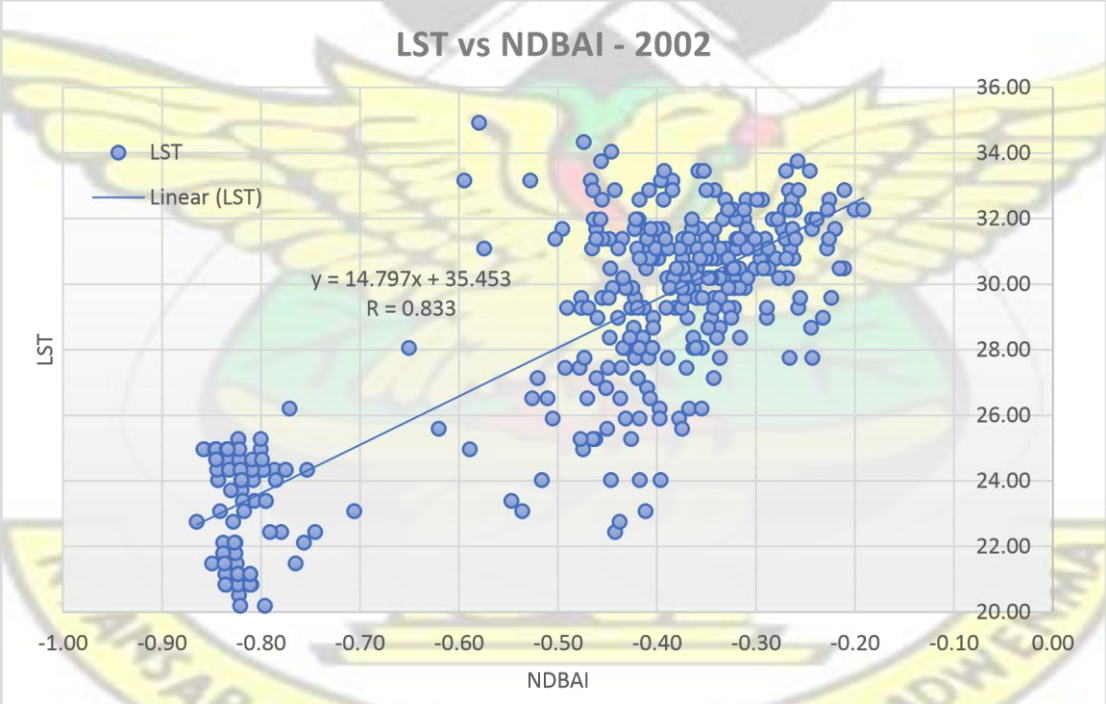

Figure 4-28 Relationship between LST and NDBAI in 2002

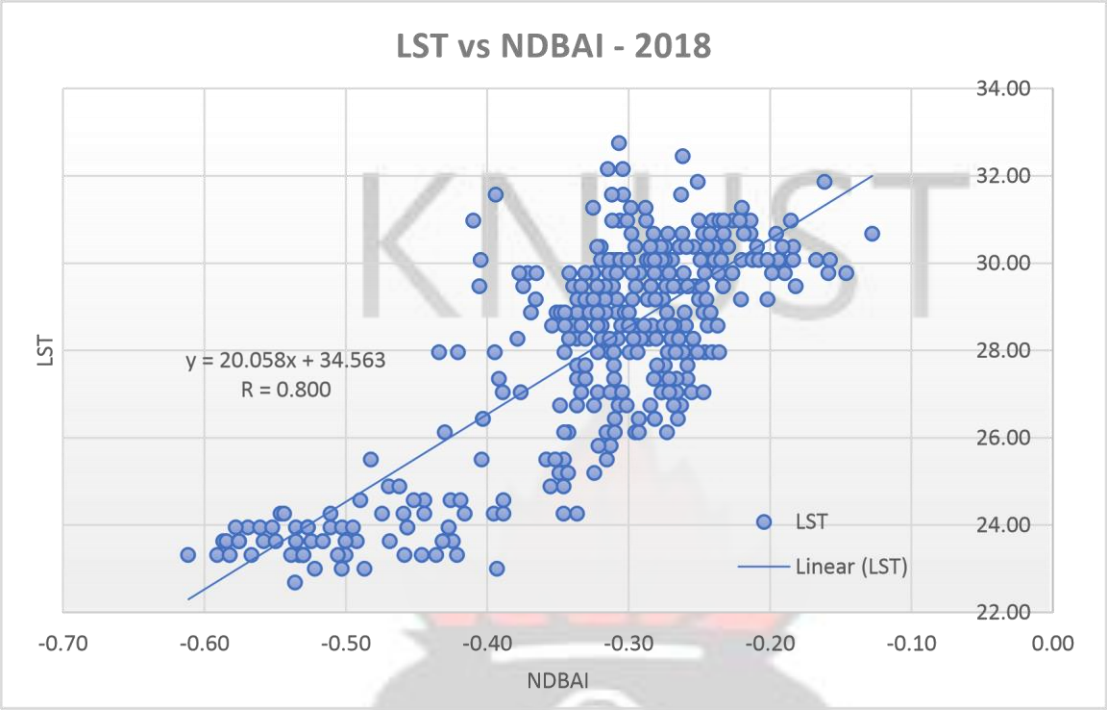

Figure 4-29 Relationship between LST and NDBAI in 2018

This represent a strong positive relationship between LST and bare land. Trend of R can clearly be associated with increase average LST for bare land from 25.07℃ to 28.42℃ and 28.59℃ as seen in Figure 4-23. This implies that LST would increase with an increase in the density of, bare land.

4.5.2.3 Normalized Difference Built up Index (NDBI) and LST

NDBI is useful in understanding urban landscape or in built-environment research. This index emphasizes urban development where there is typically a higher reflectance in the shortwaveinfrared (SWIR) region, compared to the near-infrared (NIR) region.

From Figure 4-30, Figure 4-31 and Figure 4-32, NDBI as an index of built-up shows the strongest positive correlation between urban development and LST in the Greater Accra region. This implies an increasing NDBI index (Built up LULC) results in related increase in Land Surface Temperature.

Observation made from scatterplots of 1986, 2002 and 2018 indicates linear correlation coefficient of 0.741, 0.918 and 0.893 respectively.

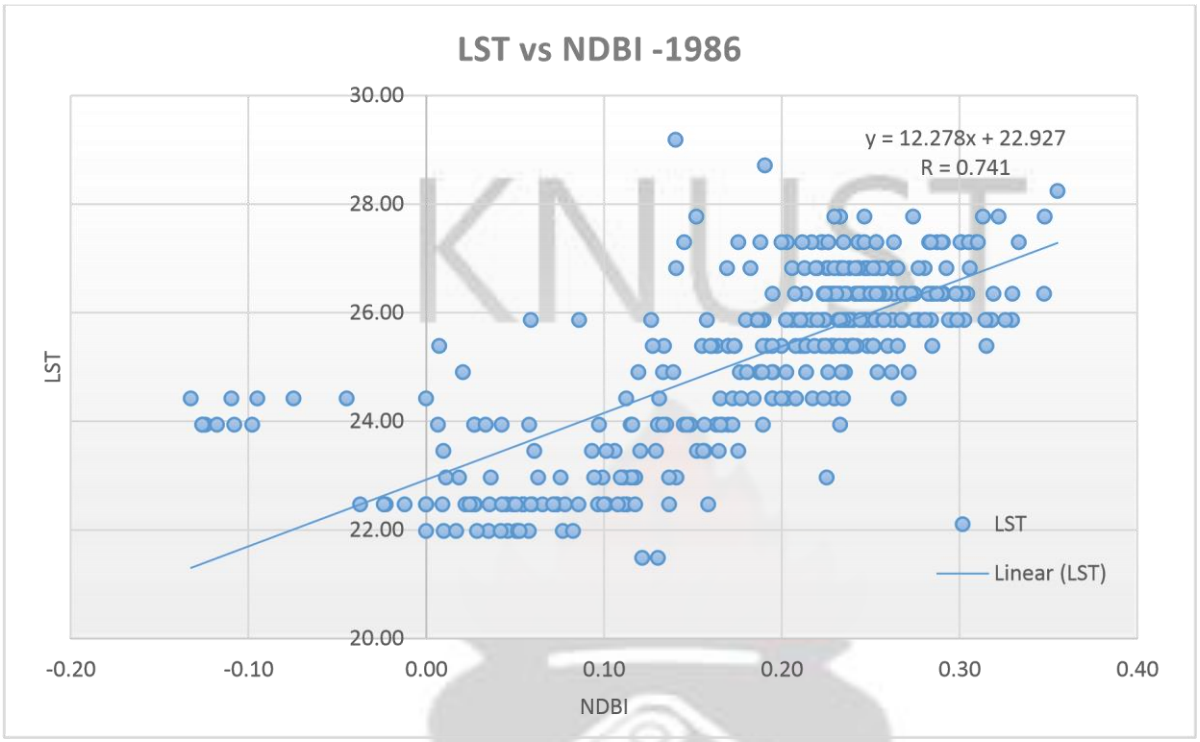

Figure 4-30 Relationship between LST and NDBI in 1986

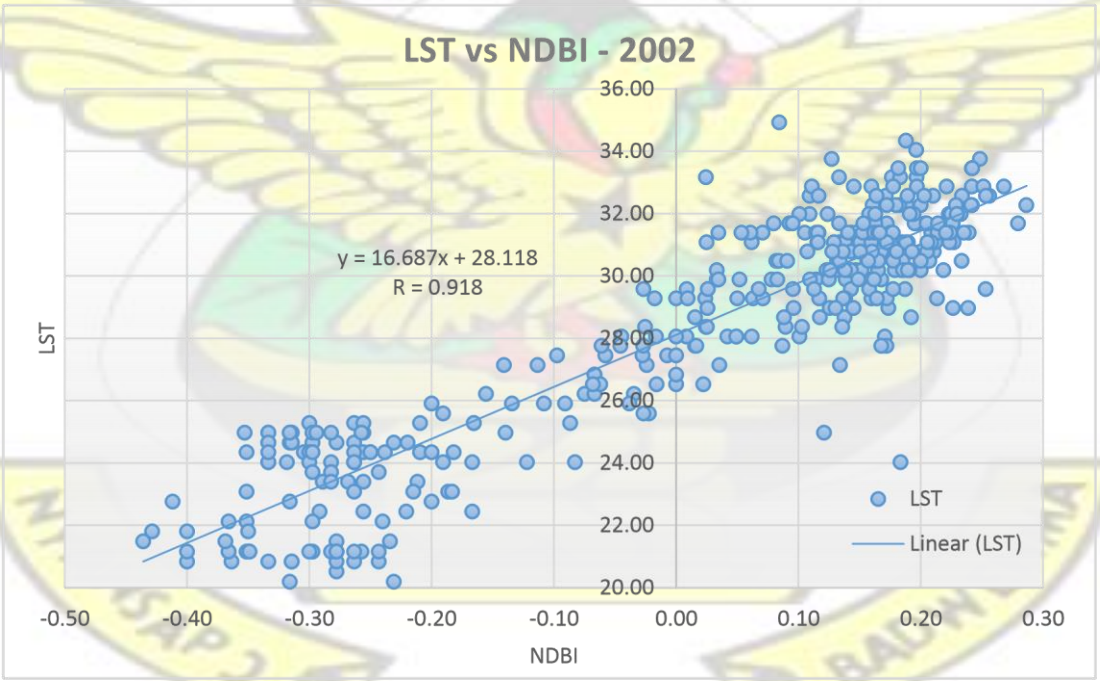

Figure 4-31 Relationship between LST and NDBI in 2002

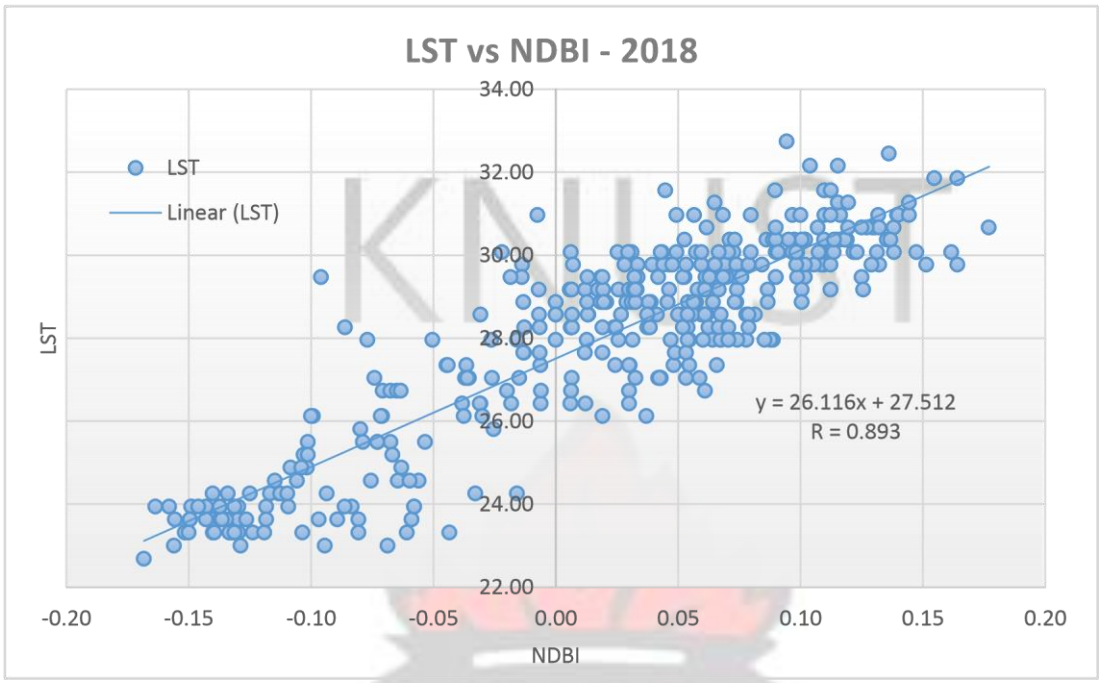

Figure 4-32 Relationship between LST and NDBI in 2018

4.5.2.4 Normalized Difference Water Index (NDWI) and LST

NDWI is known to be strongly related to the plant water content and therefore a very good proxy for plant water stress. According to Gao (1996), NDWI is a good indicator for vegetation liquid water content.

This was the only index that recorded all negative correlation among all four indices. As shown in Figure 4-33 to Figure 4-35, negative correlation coefficient of NDBI of -0.741, -0.918 and 0.893 for 1986, 2002 and 2018 were recorded respectively. This could be explained the low LST estimates association with water bodies and dense vegetated areas within the region.

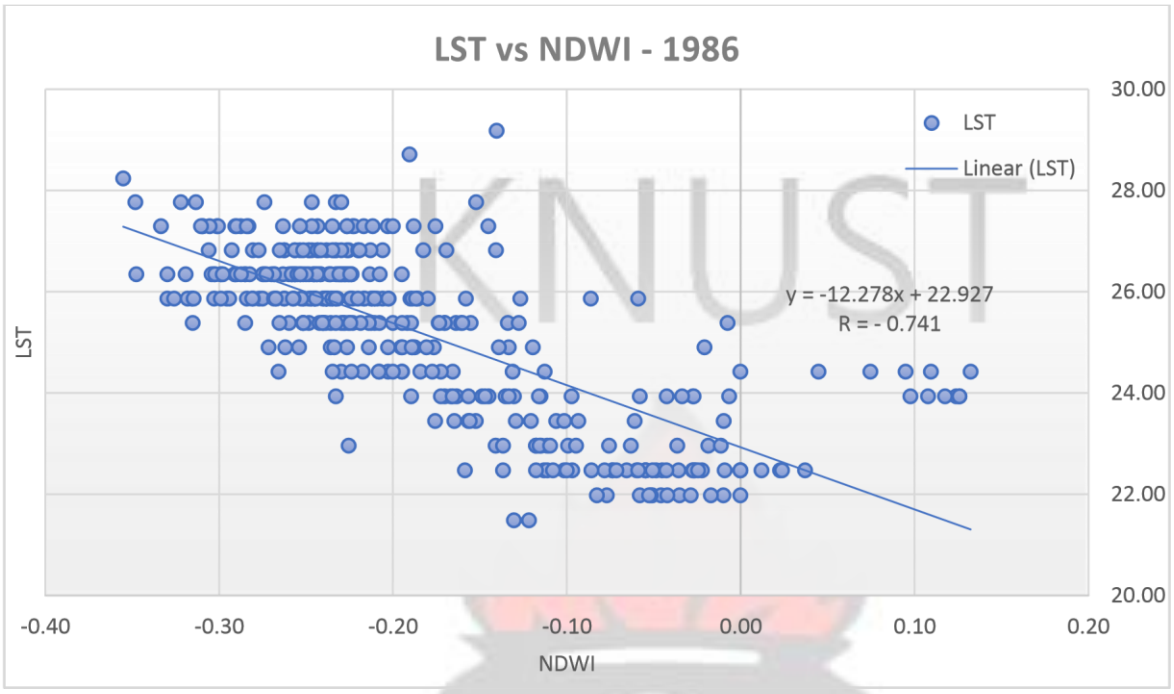

Figure 4-33 Relationship between LST and NDWI in 1986

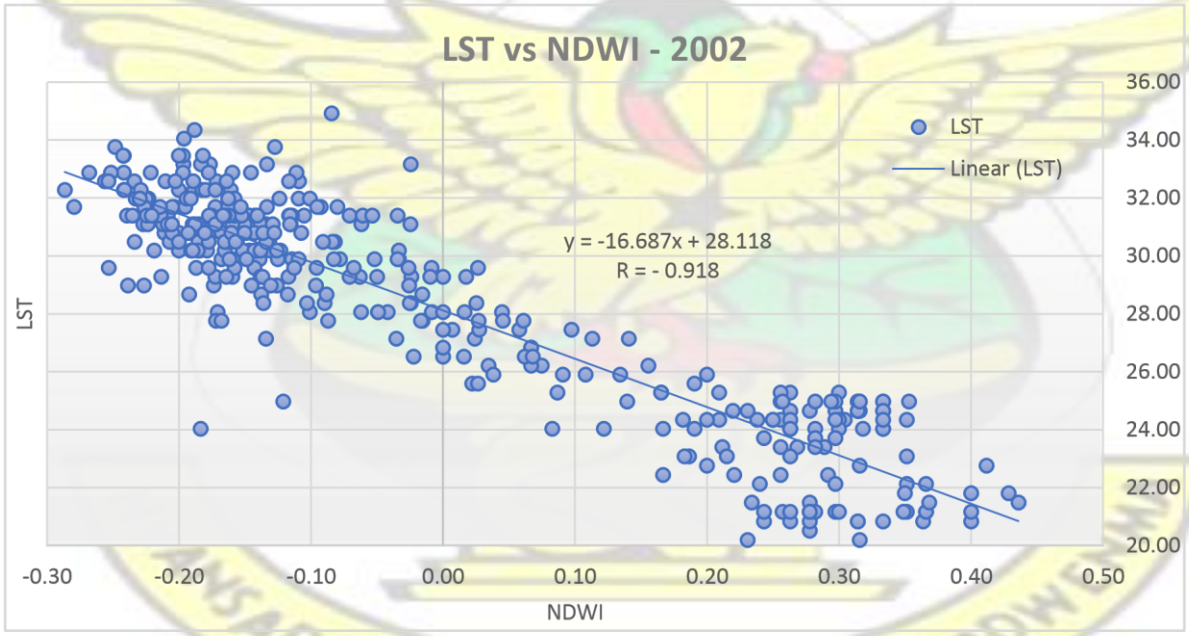

Figure 4-34 Relationship between LST and NDWI in 2002

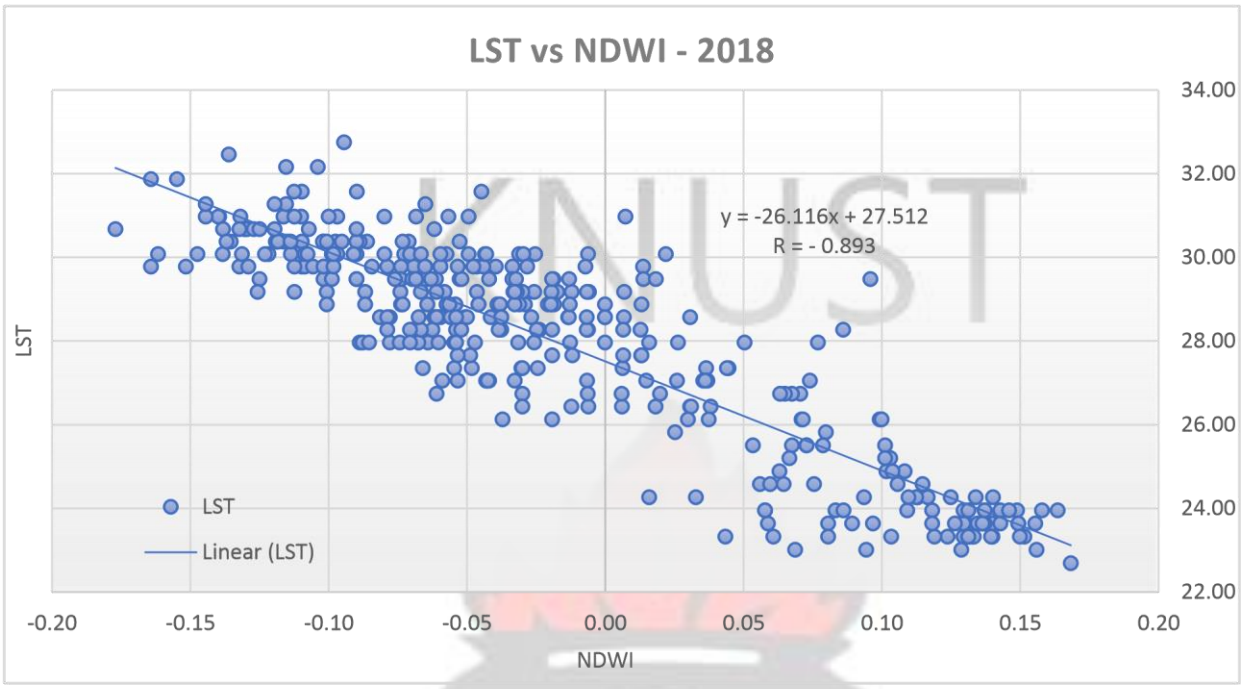

Figure 4-35 Relationship between LST and NDWI in 2018

This study employed geospatial and statistical techniques to address research objectives. All four LULC types identified experienced change over the duration of the study. Changing pattern indicate increasing built up and decreasing bare land, vegetation, and water bodies. Analysis show increased LST over the entire region over the past 32 years. Correlation analysis were also employed in arriving at results that indicated various relationship between LULC indicators (NDVI, NDWI, NDBI and NDBAI) and LST.

5 Chapter Five: Conclusions and Recommendations

5.1 Conclusions

This study explored LULC changes and investigated LST variations using remote sensing and GIS technology in the Greater Accra region between 1986 and 2018. Remote sensing and Geographic Information System application has proven to be useful in understanding changing pattern of LULC, variability of LST and insight from LST variations associated LUCC.

The results of the research revealed that LULC in Greater Accra region has changed significantly over the 32-year period. The four major LULC types identified were Vegetation, Built-up, Bare land and Waterbody. Bare land cover type indicated steady decline from 1986 to 2018 representing a total of 60.22% decrease. Water bodies experienced varying trend with a decrease in 2002 and an increase in 2018 amounting to a total decrease of 7.84% loss representing 9.11 Km^2. Analysis further showed that vegetation cover exhibited similar but opposite pattern of 16.20% increase in 2002 followed by a 28.02% decreased. This amounted to a total of 11.82% decrease in vegetation cover. On the contrary, built-up increased by 654.03% (724.3 Km^2) between 1986 and 2018.

Land Surface Temperature was observed to have increased by 3.05℃ over the 32-year period of this study across the Greater Accra region. The trend indicated a significant increase of 3.5℃ between 1986 and 2002 but a decrease of 0.45℃ to 28.12℃ from 2002 and 2018. The increasing trend in LST over time was found to be consistent with the observed urban expansion of the study area. Higher LST were generally concentrated in the core of urban centers and bare land areas comprising sandy areas and dry salt, bare exposed rock, and quarries. High temperatures are also more apparent along the coastal belt of the region stretching northwards as development spread in the same direction. The pattern of low temperatures on the other hand was consistently identified around northern boarders spreading towards the north-western corner of the region.

A relationship was established between LST and LULC. Total change in LST for the entire period of the study shows increase of 3.53℃, 3.04℃, 2.78℃ and 2.65℃ for bare land, vegetation, built-up and waterbody land use/land cover types respectively. Nevertheless, among all four LULC categories, Built-up areas have the highest average LST for all three time periods except for 2018 which it recorded same as Bare land. Analysis of the overall change in LULC in association with LST reveals that Bare land experienced the highest negative change of 60.22% decrease, and this corresponded to the highest increase in LST of 3.53℃ over the same period. Both NDBAI and

NDBI exhibited a positive correlation with LST. NDVI demonstrated a negative linear correlation while NDWI indicated the strongest negative linear correlation with LST. Land use/Land cover change can be linked to rising Land Surface Temperature Changes in the Greater Accra region of Ghana

5.2 Recommendations

The study recommends the following;

- Barren land and Open spaces should be utilized for afforestation projects.
- Relevant regulatory bodies should ensure the control of urban development through land use planning to prevent the creation of _Concrete Jungles‘.
- Appropriate authorities should ensure water bodies are protected as a mitigation measure against temperature changes.
- Local government authorities should ensure effective urban planning to curb the contribution of LULC change to LST change.
- Government should provide policy direction to address anthropogenic causes of surface temperature changes.

Limitations

1. The use of specific timestamp satellite imagery data. With the advent of platforms like the google earth engine, more data are readily made available for use. Notwithstanding, spatial autocorrelation (Global Moran's I) test undertaken indicate LST pattern is not a result of random chance.
2. Challenge with data availability.
3. Spatial distribution of random sampling site for LST validation is not entirely even.

References

Addae, B., & Oppelt, N. (2019). Land-Use/Land-Cover Change Analysis and Urban Growth Modelling in the Greater Accra Metropolitan Area (GAMA), Ghana. Urban Science, 3(1), 26.

Adedeji, O., Reuben, O. and Olatoye, O. (2014). _Global Climate Change‘, (April), pp. 114–122.

Adegoke, J. O., Pielke Sr, R. A., Eastman, J., Mahmood, R. and Hubbard, K. G. (2003). Impact of irrigation on midsummer surface fluxes and temperature under dry synoptic conditions: A regional atmospheric model study of the US High Plains. *Monthly Weather Review*, *131*(3), 556-564.

Adelabu, S., Mutanga, O. and Adam, E. (2014). Evaluating the impact of red-edge band from Rapideye image for classifying insect defoliation levels. *ISPRS Journal of Photogrammetry and Remote Sensing*, *95*, 34-41.

Aduah, M. S., Mantey, S. and Tagoe, N. D. (2012). Mapping land surface temperature and land cover to detect urban heat island effect: a case study of Tarkwa, South West Ghana. *Research Journal of Environmental and Earth Sciences*, *4*(1), 68-75.

Alsultan, S., Lim, H. S., MatJafri, M. Z. and Abdullah, K. (2005). An algorithm for land surface temperature analysis of remote sensing image coverage over AlQassim, Saudi Arabia. *From Pharaohs to Geoinformatics FIG Working Week*, 16-21.

Amamo, B. A. and Amenu, B. T. (2017). Analysis of Land use and Land Cover Change, Drivers and Impact on Agricultural Productivity in Esera Woreda, Dawro Zone, Southwest Ethiopia.

Anderson, J. R., Hardy, E. E., Roach, J. T. and Witmer, R. E. *A.* (1976). *A Land Use and Land Cover Classification System for Use with Remote Sensor Data*; US Geological Survey Professional Paper No. 964; USGS: Reston, WV, USA.

Anderson, M. C., Norman, J. M., Kustas, W. P., Houborg, R., Starks, P. J. and Agam, N. (2008). A thermal-based remote sensing technique for routine mapping of land-surface carbon, water and energy fluxes from field to regional scales. *Remote Sensing of Environment*, *112*(12), 4227-4241.

Anderson, M. C., Norman, J. M., Kustas, W. P., Houborg, R., Starks, P. J. and Agam, N. (2008). A thermal-based remote sensing technique for routine mapping of land-surface carbon, water and energy fluxes from field to regional scales. *Remote Sensing of Environment*, *112*(12), 4227-4241.

Andrew, R. M. (2018). Global CO 2 emissions from cement production. Earth System Science Data, 10(1), 195.

Appiah, D. O. (2014) ‗Geospatial Analysis of Land Use and Land Cover Transitions from 1986 – 2014 in a Peri-Urban Ghana', pp. 1–23.

Appiah, D. O., Forkuo, E. K. and Bugri, J. T. (2017). ‗Land Surface Temperature Extracts for Peri-Urban Heat and Rural Cool Troughs in Ghana', *International Journal of Advanced Remote Sensing and GIS*, 6(1), pp. 2204–2222.

Arnfield, A. J. (2003). Two decades of urban climate research: a review of turbulence, exchanges of energy and water, and the urban heat island. *International Journal of Climatology: a Journal of the Royal Meteorological Society*, *23*(1), 1-26.

Asante, F. and Amuakwa-Mensah, F. (2014). ‗Climate Change and Variability in Ghana: Stocktaking', *Climate,* 3(1), pp. 78–99.

Azhdari, A., Soltani, A. and Alidadi, M. (2018). Urban morphology and landscape structure effect on land surface temperature: Evidence from Shiraz, a semi-arid city. *Sustainable cities and society*, *41*, 853-864.

Bakar, S. A., Byzynski, G. and Ribeiro, C. (2016). Synergistic effect on the photocatalytic activity of N-doped TiO2 nanorods synthesised by novel route with exposed (110) facet. *Journal of Alloys and Compounds*, *666*, 38-49.

Barredo, J. I. (2009). Normalised flood losses in Europe: 1970–2006. *Natural Hazards and Earth System Sciences*, *9*(1), 97-104.

Basommi, L. P., Guan, Q. F., Cheng, D. D. and Singh, S. K. (2016). Dynamics of land use change in a mining area: a case study of Nadowli District, Ghana. *Journal of mountain science*, *13*(4), 633-642.

Bastiaanssen, W. G., Menenti, M., Feddes, R. A. and Holtslag, A. A. M. (1998). A remote sensing surface energy balance algorithm for land (SEBAL). 1. Formulation. *Journal of hydrology*, *212*, 198-212.

Beilin, R., Lindborg, R., Stenseke, M., Pereira, H. M., Llausàs, A., Slätmo, E. and Munro, N. (2014). Analysing how drivers of agricultural land abandonment affect biodiversity and cultural landscapes using case studies from Scandinavia, Iberia and Oceania. *Land use policy*, *36*, 60-72.

Belgiu, M. and Drăguţ, L. (2014). Comparing supervised and unsupervised multiresolution segmentation approaches for extracting buildings from very high resolution imagery. *ISPRS Journal of Photogrammetry and Remote Sensing*, *96*, 67-75.

Bense, V. F., Read, T. and Verhoef, A. (2016). Using distributed temperature sensing to monitor field scale dynamics of ground surface temperature and related substrate heat flux. *Agricultural and forest meteorology*, *220*, 207-215.

Bewket, W. (2002). Land cover dynamics since the 1950s in Chemoga watershed, Blue Nile basin, Ethiopia. *Mountain Research and Development*, *22*(3), 263-270.

Boafo, Y. A., Saito, O. and Takeuchi, K. (2014). Provisioning ecosystem services in rural savanna landscapes of Northern Ghana: An assessment of supply, utilization, and drivers of change. *J. Disaster Res*, *9*(4), 501-515.

Braimoh, A. K. and Vlek, P. L. G. (2004). The impact of land‐cover change on soil properties in northern Ghana. *Land Degradation & Development*, *15*(1), 65-74.

Braimoh, A.K. and Vlek, P.L.G. (2004). Land-Cover Change Analyses in the Volta Basin of Ghana. *Earth interactions*, *8*(21), 1-17.

Breiman, L. (2001). Random forests. *Machine learning*, *45*(1), 5-32.

Brunsell, N. A. and Gillies, R. R. (2003). Length scale analysis of surface energy fluxes derived from remote sensing. *Journal of Hydrometeorology*, *4*(6), 1212-1219.

Buyadi, S. N. A., Mohd, W. M. N. W. and Misni, A. (2013). Impact of land use changes on the surface temperature distribution of area surrounding the National Botanic Garden, Shah Alam. *Procedia-Social and Behavioral Sciences*, *101*, 516-525.

Buyadi, S. N. A., Mohd, W. M. N. W. and Misni, A. (2018). Urban Green Space Growth Impact on Surface Temperature Distribution. *Asian Journal of Environment-Behaviour Studies*, *3*(10), 198-207.

Calvas, B., Knoke, T., Castro, L. M., Hildebrandt, P., Weber, M., Stimm, B. and Aguirre, N. (2013). Sustainable agriculture and conservation payments are key factors in mitigating tropical forest loss. In *Ecosystem services, biodiversity and environmental change in a tropical mountain ecosystem of South Ecuador* (pp. 235-244). Springer, Berlin, Heidelberg.

Campbell, J. B. and Wynne R. H. (2011) *Introduction to Remote. Sensing* (5th Edition). New York: The Guilford Press.

Carlson, T. N. and Arthur, S. T. (2000). The impact of land use—land cover changes due to urbanization on surface microclimate and hydrology: a satellite perspective. *Global and planetary change*, *25*(1-2), 49-65.

Carlson, T. N., and Sanchez-Azofeifa, G. A. (1999). Satellite remote sensing of land use changes in and around San Jose, Costa Rica. *Remote Sensing of Environment*, *70*(3), 247-256.

Chander, G. and Markham, B. (2003). Revised Landsat-5 TM radiometric calibration procedures and postcalibration dynamic ranges. *IEEE Transactions on geoscience and remote sensing*, *41*(11), 2674-2677.

Chehata, N., Guo, L. and Mallet, C. (2009). Airborne lidar feature selection for urban classification using random forests. *International Archives of Photogrammetry, Remote Sensing and Spatial Information Sciences*, *38*(Part 3), W8.

Chen, J. M., Pavlic, G., Brown, L., Cihlar, J., Leblanc, S. G., White, H. P., Hall, R. J., Peddle, D. R., King, D. J., Trofymow, J. A., Swift, E., Van Dersandenj and Andpellikka, P. K. E. (2002). Derivation and validation of Canada-wide coarse resolutionleaf area index maps using highresolution satellite imagery and ground measure-ments.Remote Sensing of Environment,80, pp. 165–184.

Chen, X. L., Zhao, H. M., Li, P. X. and Yin, Z. Y. (2006). Remote sensing image-based analysis of the relationship between urban heat island and land use/cover changes. *Remote sensing of environment*, *104*(2), 133-146.

Chen, X. L., Zhao, H. M., Li, P. X. and Yin, Z. Y. (2006). Remote sensing image-based analysis of the relationship between urban heat island and land use/cover changes. *Remote sensing of environment*, *104*(2), 133-146.

Climate Change. doi: 10.1017/CBO9781107415324.

Cohen, J. E. (1995). Population growth and earth's human carrying capacity. *Science*, *269*(5222), 341-346.

Colditz, R. (2015). An evaluation of different training sample allocation schemes for discrete and continuous land cover classification using decision tree-based algorithms. *Remote Sensing*, *7*(8), 9655-9681.

Coll, C., Caselles, V., Sobrino, J. A. and Valor, E. (1994). On the atmospheric dependence of the split-window equation for land surface temperature. *Remote sensing*, *15*(1), 105-122.

Collins, J. M. (2011). ‗Temperature variability over Africa', *Journal of Climate*, 24(14), pp. 3649–3666.

Congalton, R. G. (1991). A review of assessing the accuracy of classifications of remotely sensed data. *Remote sensing of environment*, *37*(1), 35-46.

Cracknell, A. P. (1997). *Advanced very high resolution radiometer AVHRR*. CRC Press.

Dalponte, M., Ørka, H. O., Ene, L. T., Gobakken, T. and Næsset, E. (2013). Tree crown delineation and tree species classification in boreal forests using hyperspectral and ALS data. *Remote sensing of environment*, *140*, 306-317.

Dash, P., Göttsche, F. M. and Olesen, F. S. (2002). Potential of MSG for surface temperature and emissivity estimation: considerations for real-time applications. *International Journal of Remote Sensing*, *23*(20), 4511-4518.

Deng, C. and Wu, C. (2013). Examining the impacts of urban biophysical compositions on surface urban heat island: A spectral unmixing and thermal mixing approach. *Remote Sensing of Environment*, *131*, 262-274.

Dessie, G. and Kleman, J. (2007). Pattern and magnitude of deforestation in the South Central Rift Valley Region of Ethiopia. *Mountain research and development*, *27*(2), 162-169.

Dewan, A. M., Yamaguchi, Y. and Rahman, M. Z. (2012). Dynamics of land use/cover changes and the analysis of landscape fragmentation in Dhaka Metropolitan, Bangladesh. *GeoJournal*, *77*(3), 315-330.

Duan, S. B., Li, Z. L. and Leng, P. (2017). A framework for the retrieval of all-weather land surface temperature at a high spatial resolution from polar-orbiting thermal infrared and passive microwave data. *Remote Sensing of Environment*, *195*, 107-117.

Ebi, K. L., Exuzides, K. A., Lau, E., Kelsh, M. and Barnston, A. (2004). Weather changes associated with hospitalizations for cardiovascular diseases and stroke in California, 1983–1998. *International journal of biometeorology*, *49*(1), 48-58.

Enete, I. C. and Okwu, V. U. (2013). _Mapping Enugu City′s Urban Heat Island‘, *International Journal of Environmental Protection and Policy*, 1(4), p. 50.

Enete, I. C., Awuh, M. E., and Ikekpeazu, F. O. (2013). Assessment of Urban Heat Island (Uhi) situation in Douala Metropolis, Cameroon. *Journal of Geography and Earth Sciences*, *2*(1), 55-57.

European Environment Agency (2010). *THE EUROPEAN ENVIRONMENT STATE AND OUTLOOK 2010*.

Fathizad, H., Tazeh, M., Kalantari, S., and Shojaei, S. (2017). The investigation of spatiotemporal variations of land surface temperature based on land use changes using NDVI in southwest of Iran. *Journal of African Earth Sciences, 134*, 249-256.

Foody, G. M. and Mathur, A. (2002). Toward intelligent training of supervised image classifications: directing training data acquisition for SVM classification. *Remote Sensing of Environment*, *93*(1-2), 107-117.

Franc, G. B., and Cracknell, A. P. (1994). Retrieval of land and sea surface temperature using NOAA-11 AVHRR· data in north-eastern Brazil. *International Journal of Remote Sensing*, *15*(8), 1695-1712.

Friedl, M. A., McIver, D. K., Hodges, J. C., Zhang, X. Y., Muchoney, D., Strahler, A. H. and Baccini, A. (2002). Global land cover mapping from MODIS: algorithms and early results. *Remote Sensing of Environment*, *83*(1-2), 287-302.

Gallo, K. P. and Owen, T. W. (2002). A sampling strategy for satellite sensor-based assessments of the urban heat-island bias. *International Journal of Remote Sensing*, *23*(9), 1935-1939.

Gao, B. C. (1996). NDWI—A normalized difference water index for remote sensing of vegetation liquid water from space. *Remote sensing of environment*, *58*(3), 257-266.

Geist, H. J. and Lambin, E. F. (2002). Proximate Causes and Underlying Driving Forces of Tropical DeforestationTropical forests are disappearing as the result of many pressures, both local and regional, acting in various combinations in different geographical locations. *BioScience*, *52*(2), 143-150.

Ghana Energy Commission. (2014). Charcoal Price Tracking in Major Urban Centres of Ghana. Accra, Ghana.

Ghana Statistical Service (2012). 2010 Population and Housing Census Final Report, Ghana Statistical Service, Accra-Ghana.

Haas, J. and Ban, Y. (2014). Urban growth and environmental impacts in Jing-Jin-Ji, the Yangtze, River Delta and the Pearl River Delta. *International Journal of Applied Earth Observation and Geoinformation*, *30*, 42-55.

Hachem, S., Allard, M. and Duguay, C. (2009). Using the MODIS land surface temperature product for mapping permafrost: an application to Northern Quebec and Labrador, Canada. *Permafrost and Periglacial Processes*, *20*(4), 407-416.

Hajat, S., O'Connor, M. and Kosatsky, T. (2010). Health effects of hot weather: from awareness of risk factors to effective health protection. *The Lancet*, *375*(9717), 856-863.

Hansen, J., Ruedy, R., Sato, M. and Lo, K. (2010). Global surface temperature change. *Reviews of Geophysics*, *48*(4).

Hashemian, M. S. and Fatemi, S. B. (2004). Study of sampling methods for accuracy assessment of classified remotely sensed data. In *International congress for photogrammetry and remote sensing* (pp. 1682-1750).

Hegerl, G. C., Zwiers, F. W., Braconnot, P., Gillett, N. P., Luo, Y., Marengo Orsini, J. A. and Stott, P. A. (2007). Understanding and attributing climate change.

Hille, K. (2016). *2016 Climate Trends Continue to Break Records*. Available at: https://www.nasa.gov/feature/goddard/2016/climate-trends-continue-to-break-records (Accessed: 14 September 2018).

Hinkel, K. M., Eisner, W. R., Bockheim, J. G., Nelson, F. E., Peterson, K. M. and Dai, X. (2003). Spatial extent, age, and carbon stocks in drained thaw lake basins on the Barrow Peninsula, Alaska. *Arctic, Antarctic, and Alpine Research*, *35*(3), 291-300.

Hu, L. and Brunsell, N. A. (2013). The impact of temporal aggregation of land surface temperature data for surface urban heat island (SUHI) monitoring. *Remote Sensing of Environment*, *134*, 162-174.

IPCC (2014) *Climate Change 2014: Synthesis Report*, *5th Assessment Report: Mitigation of*

Ishola, K. A., Okogbue, E. C. and Adeyeri, O. E. (2016). A quantitative assessment of surface urban heat islands using satellite multitemporal data over Abeokuta, Nigeria. *International Journal of Atmospheric Sciences*, *2016*.

Jensen, J. R. (2000). Remote Sensing of the Environment: An Earth Resource Perspective. Pearson Education, Inc., Delhi, pp. 361–365.

Jensen, J. R. (2009). *Remote sensing of the environment: An earth resource perspective 2/e*. Pearson Education India.

Jiang, J. and Tian, G. (2010). Analysis of the impact of land use/land cover change on land surface temperature with remote sensing. *Procedia environmental sciences*, *2*, 571-575.

Jin, M. and Dickinson, R. E. (2000). A generalized algorithm for retrieving cloudy sky skin temperature from satellite thermal infrared radiances. *Journal of Geophysical Research: Atmospheres*, *105*(D22), 27037-27047.

Jung, H. C., Hamski, J., Durand, M., Hoque, A. Z., Hasan, M. A., Bhattacharya, P. and Breit, G. N. (2014). Study on satellite images based spectral emissivity, land surface temperature and land-cover in and around Kuju volcano, Central Kyushu, Japan. *Journal of Asian Earth Sciences*, *91*, 218-226.

Kalma, J. D., McVicar, T. R. and McCabe, M. F. (2008). Estimating land surface evaporation: A review of methods using remotely sensed surface temperature data. *Surveys in Geophysics*, *29*(4-5), 421-469.

Karikari, A. Y. and Ansa-Asare, O. D. (2006). Physico-chemical and microbial water quality assessment of Densu River of Ghana. *West African Journal of Applied Ecology*, *10*(1).

Karlson, M., Ostwald, M., Reese, H., Sanou, J., Tankoano, B. and Mattsson, E. (2015). Mapping tree canopy cover and aboveground biomass in Sudano-Sahelian woodlands using Landsat 8 and random forest. *Remote Sensing*, *7*(8), 10017-10041.

Karnieli, A., Agam, N., Pinker, R. T., Anderson, M., Imhoff, M. L., Gutman, G. G. and Goldberg, A. (2010). Use of NDVI and land surface temperature for drought assessment: Merits and limitations. *Journal of climate*, *23*(3), 618-633.

Kato, S. and Yamaguchi, Y. (2005). Analysis of urban heat-island effect using ASTER and ETM+ Data: Separation of anthropogenic heat discharge and natural heat radiation from sensible heat flux. *Remote Sensing of Environment*, *99*(1-2), 44-54.

Kepner, W. G., Watts, C. J., Edmonds, C. M., Maingi, J. K., Marsh, S. E. and Luna, G. (2000). A landscape approach for detecting and evaluating change in a semi-arid environment. In *Monitoring Ecological Condition in the Western United States* (pp. 179-195). Springer, Dordrecht.

Kerr, Y. H., Lagouarde, J. P., Nerry, F. and Ottlé, C. (2004). Land surface temperature retrieval techniques and applications: Case of the AVHRR. In *Thermal Remote Sensing in Land Surface Processing* (pp. 55-131). CRC Press.

Kicklighter, D. W., Cai, Y., Zhuang, Q., Parfenova, E. I., Paltsev, S., Sokolov, A. P. and Lu, X. (2014). Potential influence of climate-induced vegetation shifts on future land use and associated land carbon fluxes in Northern Eurasia. *Environmental Research Letters*, *9*(3), 035004.

Kleemann, M. E., Chikkaraddy, R., Alexeev, E. M., Kos, D., Carnegie, C., Deacon, W. and Tartakovskii, A. I. (2017). Strong-coupling of WSe 2 in ultra-compact plasmonic nanocavities at room temperature. *Nature communications*, *8*(1), 1296.

Kogan, F. N. (2001). Operational space technology for global vegetation assessment. *Bulletin of the American Meteorological Society*, *82*(9), 1949-1964.

Korem, A. (1985). Bush fire and agricultural development in Ghana. *220 pp.*

Kumi-Baoteng, B., Stemn, E. and Agyapong, A. E. (2015). Effect of Urban Growth on Urban Thermal Environment: A Case Study of Sekondi-Takoradi Metropolis of Ghana. Journal of Environment and Earth Science, 5(2), 32-41.

Kustas, W. and Anderson, M. (2009). Advances in thermal infrared remote sensing for land surface modeling. *Agricultural and Forest Meteorology*, *149*(12), 2071-2081.

Landsberg, H. E. (1981). *The urban climate* (Vol. 28). Academic press.

Levin, N. (1999). Fundamentals of remote sensing. *1st Hydrographic Data Management Course, IMO—International Maritime Academy, Trieste*, *76*.

Li, X., Zhou, W., Ouyang, Z., Xu, W. and Zheng, H. (2009). Spatial pattern of greenspace affects land surface temperature: evidence from the heavily urbanized Beijing metropolitan area, China. *Landscape ecology*, *27*(6), 887-898.

Li, Z. L., Tang, B. H., Wu, H., Ren, H., Yan, G., Wan, Z. and Sobrino, J. A. (2013). Satellitederived land surface temperature: Current status and perspectives. *Remote sensing of environment*, *131*, 14-37.

Lillesand, T. M., Kiefer, R. W. and Chipman, J. W. (2008). Digital image interpretation and analysis. *Remote sensing and image interpretation*, *6*, 545-81.

Lim, H. S., Jafri, M., Abdullah, K. and Alsultan, S. (2012). Application of a simple mono window land surface temperature algorithm from Landsat ETM over Al Qassim, Saudi Arabia. *Sains Malaysiana*, *41*(7), 841-846.

Liu, H. and Weng, Q. (2008). Seasonal variations in the relationship between landscape pattern and land surface temperature in Indianapolis, USA. *Environmental Monitoring and Assessment*, *144*(1-3), 199-219.

Liu, L. and Zhang, Y. (2011). Urban heat island analysis using the Landsat TM data and ASTER data: A case study in Hong Kong. *Remote Sensing*, *3*(7), 1535-1552.

Luo, D., Jin, H., Marchenko, S. S. and Romanovsky, V. E. (2018). Difference between nearsurface air, land surface and ground surface temperatures and their influences on the frozen ground on the Qinghai-Tibet Plateau. *Geoderma*, *312*, 74-85.

Magee, N., Curtis, J. and Wendler, G. (1999). The urban heat island effect at Fairbanks, Alaska. *Theoretical and applied climatology*, *64*(1-2), 39-47.

Makinde, E. O. and Agbor, C. F. (2019). Geoinformatic assessment of urban heat island and land use/cover processes: a case study from Akure. *Environmental Earth Sciences*, *78*(15), 483.

Mannstein, H. (1987). Surface energy budget, surface temperature and thermal inertia. In *Remote sensing applications in meteorology and climatology* (pp. 391-410). Springer, Dordrecht.

Manu, A., Twumasi, Y. A. and Coleman, T. L. (2006). _Is It the Result of Global Warming or Urbanization ? The Rise in Air Temperature in Two Cities in Ghana Is It the Result of Global Warming or Urbanization ? The Rise in Air Temperature in Two Cities in Ghana', *5th FIG Regional Conference*.

Mathew, A., Khandelwal, S. and Kaul, N. (2016). Spatial and temporal variations of urban heat island effect and the effect of percentage impervious surface area and elevation on land surface temperature: Study of Chandigarh city, India. *Sustainable Cities and Society*, *26*, 264277.

Matthies, M., Giupponi, C. and Ostndorf, B. (2008). Environmental decision support systems: current issues, methods and tools. Environmental Model-ling and Software (22), 123e127.

Mellor, A., Boukir, S., Haywood, A. and Jones, S. (2015). Exploring issues of training data imbalance and mislabelling on random forest performance for large area land cover

classification using the ensemble margin. *ISPRS Journal of Photogrammetry and Remote Sensing*, *105*, 155-168.

Mensah, C. (2017). The United Nations Commission on Sustainable Development. In *Greening international institutions* (pp. 21-37). Routledge.

Millard, K. and Richardson, M. (2015). On the importance of training data sample selection in random forest image classification: A case study in peatland ecosystem mapping. *Remote sensing*, *7*(7), 8489-8515.

Ministry of Local Government (1992). *Strategic plan for the Greater Accra Metropolitan Area*. Volume 1. Context report.

Mora, C., Dousset, B., Caldwell, I. R., Powell, F. E., Geronimo, R. C., Bielecki, C. R. and Lucas, M. P. (2017). Global risk of deadly heat. *Nature Climate Change*, *7*(7), 501.

Mushore, T. D., Mutanga, O., Odindi, J. and Dube, T. (2017). Linking major shifts in land surface temperatures to long term land use and land cover changes: A case of Harare, Zimbabwe. *Urban climate*, *20*, 120-134.

Neteler, M. (2010). Estimating daily land surface temperatures in mountainous environments by reconstructed MODIS LST data. *Remote sensing*, *2*(1), 333-351.

Niang, I., Ruppel, O. C., Abdrabo, M. A., Essel, A., Lennard, C., Padgham, J. and Urquhart, P. (2014). Africa Climate Change 2014: Impacts, Adaptation, and Vulnerability. Part B: Regional Aspects. Contribution of Working Group II to the Fifth Assessment Report of the Intergovernmental Panel on Climate Change ed VR Barros *et al.*

Nichol, J. E. and To, P. H. (2012). Temporal characteristics of thermal satellite images for urban heat stress and heat island mapping. *ISPRS journal of photogrammetry and remote sensing*, *74*, 153-162.

Niemeyer, J., Rottensteiner, F. and Soergel, U. (2014). Contextual classification of lidar data and building object detection in urban areas. *ISPRS journal of photogrammetry and remote sensing*, *87*, 152-165.

Ofori‐Sarpong, E. (1986). The 1981–1983 drought in Ghana. *Singapore journal of tropical geography*, *7*(2), 108-127.

Oke, T. R. (1982). The energetic basis of the urban heat island. *Quarterly Journal of the Royal Meteorological Society*, *108*(455), 1-24.

Oke, T. R. (1997). Applied Climatology: Principles and Practice (RD Thompson and A. Perry, Eds.).

Pal, S. and Ziaul, S. K. (2017). Detection of land use and land cover change and land surface temperature in English Bazar urban centre. *The Egyptian Journal of Remote Sensing and Space Science*, *20*(1), 125-145.

Peng, J., Ma, J., Liu, Q., Liu, Y., Li, Y. and Yue, Y. (2018). Spatial-temporal change of land surface temperature across 285 cities in China: An urban-rural contrast perspective. *Science of the Total Environment*, *635*, 487-497.

Prata, A. J. (1993). Land surface temperatures derived from the advanced very high resolution radiometer and the along‐track scanning radiometer: 1. Theory. *Journal of Geophysical Research: Atmospheres*, *98*(D9), 16689-16702.

Prata, A. J., Caselles, V., Coll, C., Sobrino, J. A. and Ottle, C. (1995). Thermal remote sensing of land surface temperature from satellites: Current status and future prospects. *Remote Sensing Reviews*, *12*(3-4), 175-224.

Pu, R., Gong, P., Michishita, R. and Sasagawa, T. (2006). Assessment of multi-resolution and multi-sensor data for urban surface temperature retrieval. *Remote Sensing of Environment*, *104*(2), 211-225.

Qian, J., Wu, X., Cao, Y., Ai, X. and Yang, H. (2013). High capacity and rate capability of amorphous phosphorus for sodium ion batteries. *Angewandte Chemie International Edition*, *52*(17), 4633-4636.

Qin, Z. and Karnieli, A. (1999). Progress in the remote sensing of land surface temperature and ground emissivity using NOAA-AVHRR data. *International journal of remote sensing*, *20*(12), 2367-2393.

Qin, Z., Karnieli, A. and Berliner, P. (2001). A mono-window algorithm for retrieving land surface temperature from Landsat TM data and its application to the Israel-Egypt border region. *International journal of remote sensing*, *22*(18), 3719-3746.

Quattrochi, D. A. and Goel, N. S. (1995). Spatial and temporal scaling of thermal infrared remote sensing data. *Remote Sensing Reviews*, *12*(3-4), 255-286.

Quattrochi, D. A., Luvall, J. C., Rickman, D. L., Estes Jr., M. G., Laymon, C. A. and Howell, B. F. (2000). A decision support information system for urban landscape management using thermal infrared data. Photogrammetric Engineering and Remote Sensing, 66, 1195– 1207.

Rajeshwari, A. and Mani, N. D. (2014). Estimation of land surface temperature of Dindigul district using Landsat 8 data. *International Journal of Research in Engineering and Technology*, *3*(5), 122-126.

Räsänen, A., Rusanen, A., Kuitunen, M. and Lensu, A. (2013). What makes segmentation good? A case study in boreal forest habitat mapping. *International journal of remote sensing*, *34*(23), 8603-8627.

Raynolds, M. K., Comiso, J. C., Walker, D. A. and Verbyla, D. (2008). Relationship between satellite-derived land surface temperatures, arctic vegetation types, and NDVI. *Remote Sensing of Environment*, *112*(4), 1884-1894.

Rodriguez-Galiano, V. F., Ghimire, B., Rogan, J., Chica-Olmo, M. and Rigol-Sanchez, J. P. (2012). An assessment of the effectiveness of a random forest classifier for land-cover classification. *ISPRS Journal of Photogrammetry and Remote Sensing*, *67*, 93-104.

Román‐Cuesta, R. M., Carmona‐Moreno, C., Lizcano, G., New, M., Silman, M., Knoke, T. and Vuille, M. (2014). Synchronous fire activity in the tropical high Andes: an indication of regional climate forcing. *Global change biology*, *20*(6), 1929-1942.

Rosa, L. P., Dos Santos, M. A., Matvienko, B., dos Santos, E. O. and Sikar, E. (2004). Greenhouse gas emissions from hydroelectric reservoirs in tropical regions. *Climatic Change*, *66*(1-2), 9-21.

Saha, S., Chant, D., Welham, J. and McGrath, J. (2005). A systematic review of the prevalence of schizophrenia. *PLoS medicine*, *2*(5), e141.

Saleh, S. A. H. (2011). Impact of urban expansion on surface temperature in Baghdad, Iraq using remote sensing and GIS techniques. *Canadian Journal on Environmental, Construction and Civil Engineering*, *2*(8), 193-202.

Sandholt, I., Rasmussen, K. and Andersen, J. (2002). A simple interpretation of the surface temperature/vegetation index space for assessment of surface moisture status. *Remote Sensing of environment*, *79*(2-3), 213-224.

Schmugge, T., Hook, S. J. and Coll, C. (1998). Recovering surface temperature and emissivity from thermal infrared multispectral data. *Remote Sensing of Environment*, *65*(2), 121-131.

Sellers, P. J., Hall, F. G., Asrar, G., Strebel, D. E. and Murphy, R. E. (1988). The first ISLSCP field experiment (FIFE). *Bulletin of the American Meteorological Society*, *69*(1), 22-27.

Serdeczny, O., Adams, S., Baarsch, F., Coumou, D., Robinson, A., Hare, W. and Reinhardt, J. (2017). Climate change impacts in Sub-Saharan Africa: from physical changes to their social repercussions. *Regional Environmental Change*, *17*(6), 1585-1600.

Serneels, S. and Lambin, E. F. (2001). Proximate causes of land-use change in Narok District, Kenya: a spatial statistical model. *Agriculture, Ecosystems & Environment*, *85*(1-3), 65-81.

Shao, F. (2006). Research on change information extraction of remote sensing image based on ANN, Master Dissertation, Shandong University of Science and Technology, China.

Shiferaw, A. and Singh, K. L. (2011). Evaluating the Land Use and Land Cover Dynamics in Borena Woreda South Wollo Highlands, Ethiopia. *Ethiopian Journal of Business and Economics (The)*, *2*(1).

Sieferie, R. P. (2001). The Subterranean Forest: Ecology Systems and the Industrial Revolution.

Small, C. (2006). Comparative analysis of urban reflectance and surface temperature. *Remote Sensing of Environment*, *104*(2), 168-189.

Snyder, W. C., Wan, Z., Zhang, Y. and Feng, Y. Z. (1998). Classification-based emissivity for land surface temperature measurement from space. *International Journal of Remote Sensing*, *19*(14), 2753-2774.

Sobrino, J. A., Jimenez-Munoz, J. C. and Paolini, L. (2004). Land surface temperature retrieval from LANDSAT TM 5. *Remote Sensing of environment*, *90*(4), 434-440.

Sobrino, J. A., Jimenez-Munoz, J. C. and Paolini, L. (2004). Land surface temperature retrieval from LANDSAT TM 5. *Remote Sensing of environment*, *90*(4), 434-440.

Sobrino, J., Coll, C. and Caselles, V. (1991). Atmospheric correction for land surface temperature using NOAA-11 AVHRR channels 4 and 5. *Remote sensing of environment*, *38*(1), 19-34.

Srivastava, P. K., Majumdar, T. J. and Bhattacharya, A. K. (2010). ‗Study of land surface temperature and spectral emissivity using multi-sensor satellite data', *Journal of Earth System Science*, 119(1), pp. 67–74.

Stefanski, M. D., Sloo, D. and Matsuoka, Y. (2013). *U.S. Patent No. 8,544,285*. Washington, DC: U.S. Patent and Trademark Office.

Stocker, T. F., Qin, D., Plattner, G. K., Tignor, M., Allen, S. K., Boschung, J. and Midgley, P. M. (2013). Climate change 2013: The physical science basis.

Stow, D. A., Weeks, J. R., Toure, S., Coulter, L. L., Lippitt, C. D. and Ashcroft, E. (2013). Urban vegetation cover and vegetation change in Accra, Ghana: Connection to housing quality. *The Professional Geographer*, *65*(3), 451-465.

Streutker, D. R. (2003). Satellite-measured growth of the urban heat island of Houston, Texas. *Remote Sensing of Environment*, *85*(3), 282-289.

Stumpf, A. and Kerle, N. (2011). Object-oriented mapping of landslides using Random Forests. *Remote sensing of environment*, *115*(10), 2564-2577.

Su, Z. (2002). The Surface Energy Balance System (SEBS) for estimation of turbulent heat fluxes. *Hydrology and earth system sciences*, *6*(1), 85-100.

Sun, L. and Schulz, K. (2015). The improvement of land cover classification by thermal remote sensing. *Remote sensing*, *7*(7), 8368-8390.

Sun, R., Chen, A., Chen, L. and Lü, Y. (2012). Cooling effects of wetlands in an urban region: the case of Beijing. *Ecological Indicators*, *20*, 57-64.

Tedesco, M. (2015). *Remote sensing of the cryosphere*. John Wiley and Sons.

Tefera, M. M. (2011). Land-use/land-cover dynamics in Nonno district, central Ethiopia. *Journal of Sustainable development in Africa*, *13*(1), 123-141.

Tegene, B. (2002). Land-cover/land-use changes in the derekolli catchment of the South Welo Zone of Amhara Region, Ethiopia. *Eastern Africa Social Science Research Review*, *18*(1), 120.

Tekle, K. and Hedlund, L. (2000). Land cover changes between 1958 and 1986 in Kalu District, southern Wello, Ethiopia. *Mountain research and development*, *20*(1), 42-52.

Topouzelis, K. and Psyllos, A. (2012). Oil spill feature selection and classification using decision tree forest on SAR image data. *ISPRS journal of photogrammetry and remote sensing*, *68*, 135-143.

Trigo, I. F., Monteiro, I. T., Olesen, F. and Kabsch, E. (2008). An assessment of remotely sensed land surface temperature. *Journal of Geophysical Research: Atmospheres*, *113*(D17).

Tsutsumida, N. and Comber, A. J. (2015). Measures of spatio-temporal accuracy for time series land cover data. *International Journal of Applied Earth Observation and Geoinformation*, *41*, 46-55.

Uhlmann, S. and Kiranyaz, S. (2014). Classification of dual-and single polarized SAR images by incorporating visual features. *ISPRS journal of photogrammetry and remote sensing*, *90*, 1022.

UNEP (2006). Africa‘s Lakes: Atlas of Our Changing Environment. Nairobi, Kenya: United Nations Environment Programme, Division of Early Warning and Assessment (DEWA) EarthPrint. 90 p. http://na.unep.net/AfricaLakes/ .

UN/HABITAT (2001). Cities in a Globalizing World: Global Report on Human Settlements 2001. Earthscan, London, UK.

Václavík, T. and Rogan, J. (2009). Identifying trends in land use/land cover changes in the context of post-socialist transformation in central Europe: a case study of the greater Olomouc region, Czech Republic. *GIScience & Remote Sensing*, *46*(1), 54-76.

Van Den Bergh, J. C. and Botzen, W. J. (2014). A lower bound to the social cost of CO 2 emissions. *Nature climate change*, *4*(4), 253.

van Leeuwen, T. T., Frank, A. J., Jin, Y., Smyth, P., Goulden, M. L., van der Werf, G. R. and Randerson, J. T. (2011). Optimal use of land surface temperature data to detect changes in tropical forest cover. *Journal of Geophysical Research: Biogeosciences*, *116*(G2).

Voogt, J. A. (2004). Urban heat islands: hotter cities. America Institute of Biological Sciences.

Voogt, J. A. and Oke, T. R. (1997). _Complete Urban Surface Temperatures', *Journal of Applied Meteorology*, 36(9), pp. 1117–1132.

Voogt, J. A. and Oke, T. R. (2003). Thermal remote sensing of urban climates. *Remote sensing of environment*, *86*(3), 370-384.

Walther, G. R., Hughes, L., Vitousek, P., and Stenseth, N. C. (2002). Consensus on climate change. *Trends in Ecology & Evolution*, *20*(12), 648-649.

Wang, G., Wei, Y., Qiao, S., Lin, P. and Chen, Y. (2018). *Generalized inverses: theory and computations* (Vol. 53). Singapore: Springer.

Waske, B. and Braun, M. (2009). Classifier ensembles for land cover mapping using multitemporal SAR imagery. *ISPRS Journal of Photogrammetry and Remote Sensing*, *64*(5), 450-457.

Wellington, H.N.A. (2009). Gated cages, glazed boxes and dashed housing hopes: In remembrance of the dicey future of Ghanaian housing. Proceedings of the 2009 National Housing Conference held in Accra, Ghana on 7-8 October, 2009, MWRW and H/CSIRBRRI/GIA.

Weng, Q. (2001). A remote sensing? GIS evaluation of urban expansion and its impact on surface temperature in the Zhujiang Delta, China. *International journal of remote sensing*, *22*(10), 1999-2014.

Weng, Q. (2001). A remote sensing? GIS evaluation of urban expansion and its impact on surface temperature in the Zhujiang Delta, China. *International journal of remote sensing*, *22*(10), 1999-2014.

Weng, Q. (2009). Thermal infrared remote sensing for urban climate and environmental studies: Methods, applications, and trends. *ISPRS Journal of Photogrammetry and Remote Sensing*, *64*(4), 335-344.

Weng, Q. and Fu, P. (2014). Modeling annual parameters of clear-sky land surface temperature variations and evaluating the impact of cloud cover using time series of Landsat TIR data. *Remote Sensing of Environment*, *140*, 267-278.

Weng, Q., Lu, D. and Schubring, J. (2004). Estimation of land surface temperature–vegetation abundance relationship for urban heat island studies. *Remote sensing of Environment*, *89*(4), 467-483.

Widyasamratri, H., Souma, K., Suetsugi, T., Ishidaira, H., Ichikawa, Y., Kobayashi, H. and Inagaki, I. (2013). Air temperature estimation from satellite remote sensing to detect the effect of urbanization in Jakarta, Indonesia. *Journal of Emerging Trends in Engineering and Applied Sciences*, *4*(6), 800-805.

World Health Organization. (2007). Improving Public Health Responses to Extreme Weather / EuroHEAT Improving Public Health Responses to Extreme Weather / Heat-Waves EuroHEAT Meeting Report. 1–86. https://doi.org/http://www.euro.who.int/__data/assets/pdf_file/0018/112473/E91350.pdf.

World Meteorological Organization (2017). ―WMO Statement on the Status of the Global Climate in 2017.‖ World Meteorological Organization, 2017. WMO_1108_EN_web_000.pdf.WMO statement on the status of the global climate in 2017. In World Meteorological Organization. Retrieved from http://www.wmo.int/pages/mediacentre/press_releases/documents/WMO_1108_EN_web_000.pdf.

Xiao, H. L. and Weng, Q. H. (2007). The impact of land use and land cover changes on land surface temperature in a karst area of China. J Environ Manag 85:245–257

Yang, Y., Long, D. and Shang, S. (2013). Remote estimation of terrestrial evapotranspiration without using meteorological data. *Geophysical Research Letters*, *40*(12), 3026-3030.

Yankson, P. W. K. and Gough, K. V. (1999). The environmental impact of rapid urbanization in the peri-urban area of Accra, Ghana. *Geografisk Tidsskrift-Danish Journal of Geography*, *99*(1), 89-100.

Yeboah, F., Awotwi, A., Forkuo, E. K. and Kumi, M. (2017). Assessing the land use and land cover changes due to urban growth in Accra, Ghana. *Journal of Basic and Applied Research International*, *22*(2), 43-50.

Yeboah, S., Zhang, R., Cai, L., Li, L., Xie, J., Luo, Z. and Antille, D. L. (2017). Soil water content and photosynthetic capacity of spring wheat as affected by soil application of nitrogen-enriched biochar in a semiarid environment. *Photosynthetica*, *55*(3), 532-542.

Yuan, F. and Bauer, M. E. (2007). Comparison of impervious surface area and normalized difference vegetation index as indicators of surface urban heat island effects in Landsat imagery. *Remote Sensing of environment*, *106*(3), 375-386.

Zhang, Q., Zhou, A., Zhao, S., Suganthan, P. N., Liu, W. and Tiwari, S. (2008). Multiobjective optimization test instances for the CEC 2009 special session and competition. *University of Essex, Colchester, UK and Nanyang technological University, Singapore, special session on performance assessment of multi-objective optimization algorithms, technical report, 264*.

Zhang, R., Tian, J., Su, H., Sun, X., Chen, S. and Xia, J. (2008). Two improvements of an operational two-layer model for terrestrial surface heat flux retrieval. *Sensors, 8*(10), 61656187.

Zhao, W., Li, S., Yao, H., Zhang, S., Zhang, Y., Yang, B. and Hou, J. (2017). Molecular optimization enables over 13% efficiency in organic solar cells. *Journal of the American Chemical Society, 139*(21), 7148-7151.

Zheng, Z. (2006). *U.S. Patent Application No. 11/096,153*.

Zhou, X. and Wang, Y. C. (2011). _Dynamics of Land Surface Temperature in Response to Land-Use/Cover Change', *Geographical Research*, 49(1), pp. 23–36.

Appendices

Appendix A: Landsat Satellite Images

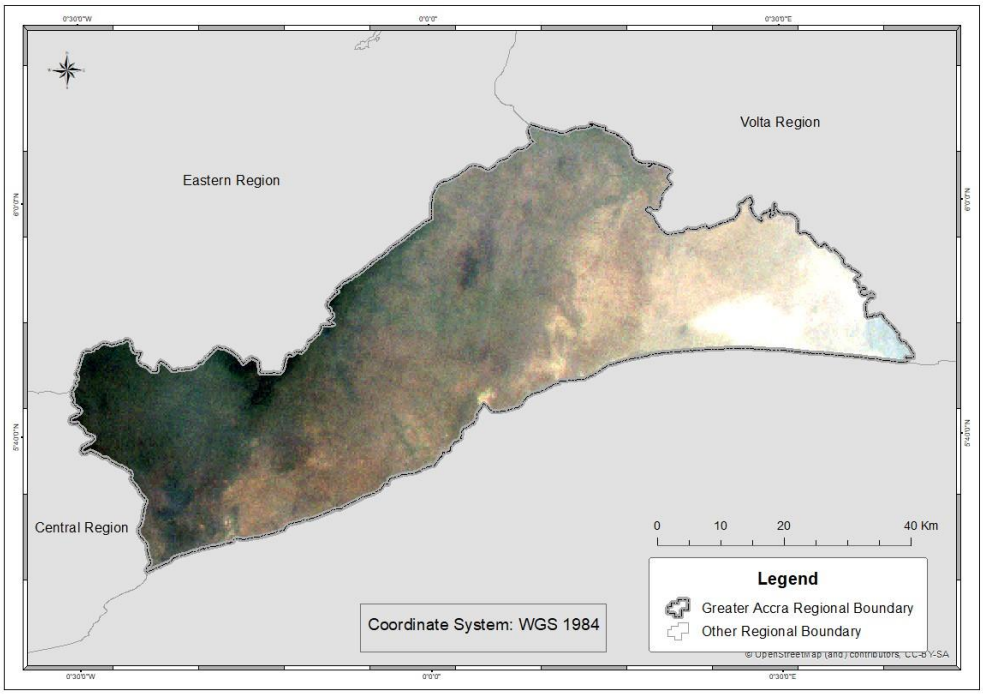

Figure A-1: Map of True Colour Band Combination of 1986, for Land use/Land cover Classification

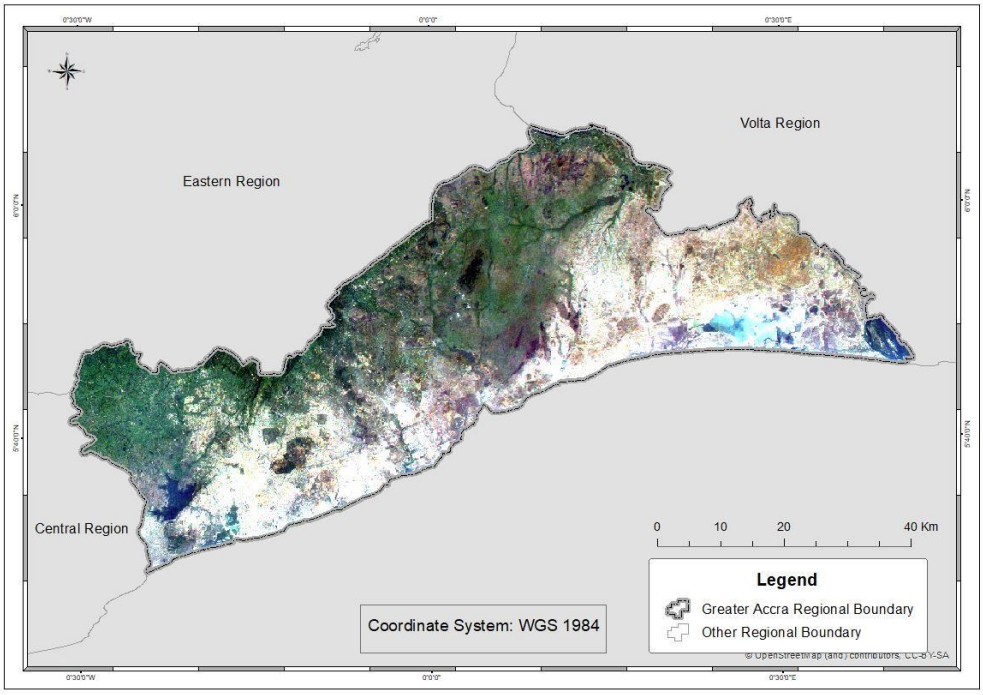

Figure A-2: Map of True Colour Band Combination of 2002, for Land use/Land cover Classification

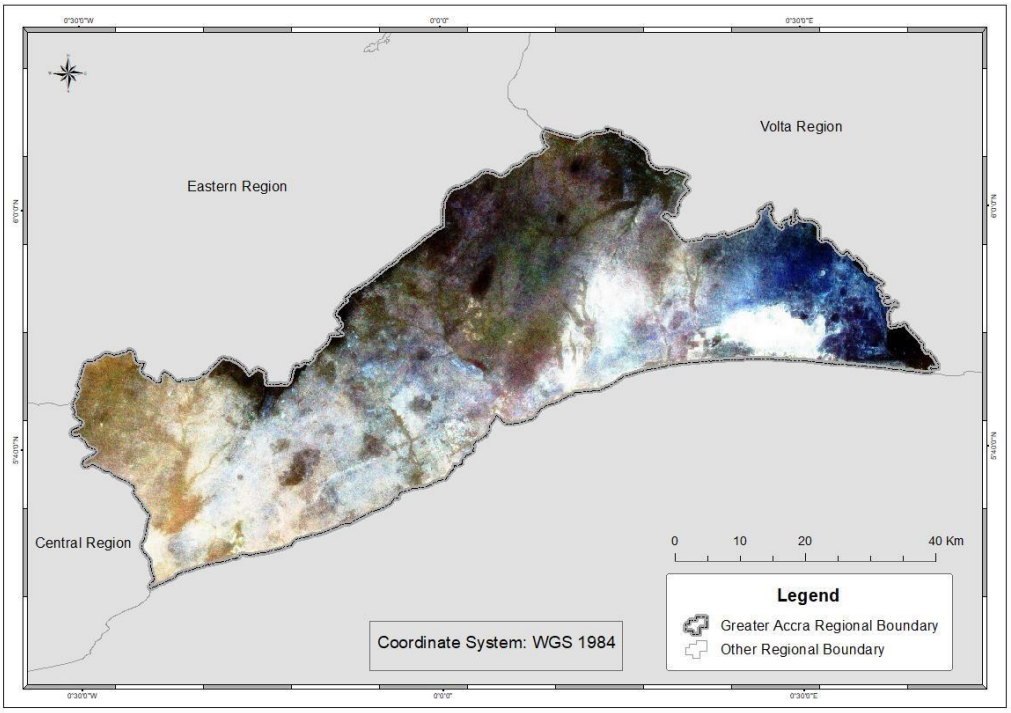

Figure A-3: Map of True Colour Band Combination of 2018, for Land use/Land cover Classification

Appendix B: Change Detection Statistics

Pixel Count | Percentage | Area (Square Meters) | Reference

		Initial State						
		Unclassified	Bareland8.shp	Vegetation.shp	Water.shp	Builtup_Land_Final2.shp	Row Total	Class Total
Final State	Unclassified	0.000	0.000	0.000	0.000	0.000	0.000	0.000
	water	0.000	0.742	0.331	60.210	0.047	100.000	100.000
	Vegetation7	0.000	33.281	83.009	12.816	12.115	100.000	100.000
	Biultup4	0.000	12.011	3.622	1.915	57.663	100.000	100.000
	Bareland6	100.000	53.966	13.037	25.058	30.175	100.000	100.000
	Class Total	100.000	100.000	100.000	100.000	100.000		
	Class Changes	100.000	46.034	16.991	39.790	42.337		
	Image Difference	-100.000	307.875	16.206	-23.829	362.931		

Figure B-1: Percentage Change Detection Statistics between 1986 and 2002 for Change Analysis

Change Detection Statistics (Initial State: 2002_v3_subset, Final State: 2018_v2)

File Options Help

Pixel Count | Percentage | Area (Square Km) | Reference

Initial State

Final State	water	Bareland6	Biultup4	Vegetation7	Row Total	Class Total
Unclassified	0.000	0.000	0.000	0.000	0.000	100.000
Water4_final	78.341	2.732	0.292	0.197	100.000	100.000
Vegetation3_final	7.535	15.134	16.105	73.098	100.000	100.000
Bareland6_final	13.461	48.905	26.693	16.326	100.000	100.000
Builtup	0.662	33.229	56.910	10.380	100.000	100.000
Class Total	100.000	100.000	100.000	100.000		
Class Changes	21.659	51.095	43.090	26.902		
Image Difference	20.981	-15.123	155.046	-15.367		

Figure B-2: Percentage Change Detection Statistics between 2002 and 2018 for Change Analysis

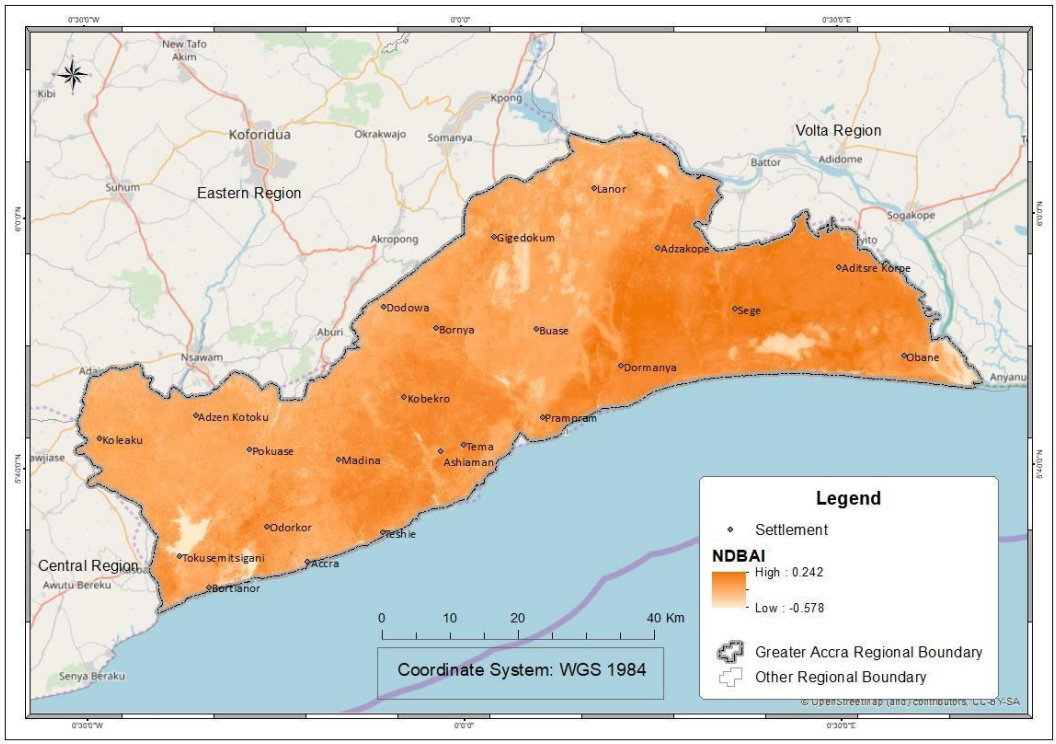

Appendix C: Map of LULC Indices

Figure C-1: Normalized Difference Bareness Index Map of 1986, for Correlation Analysis

Figure C-2: Normalized Difference Built-up Index Map of 1986, for Correlation Analysis

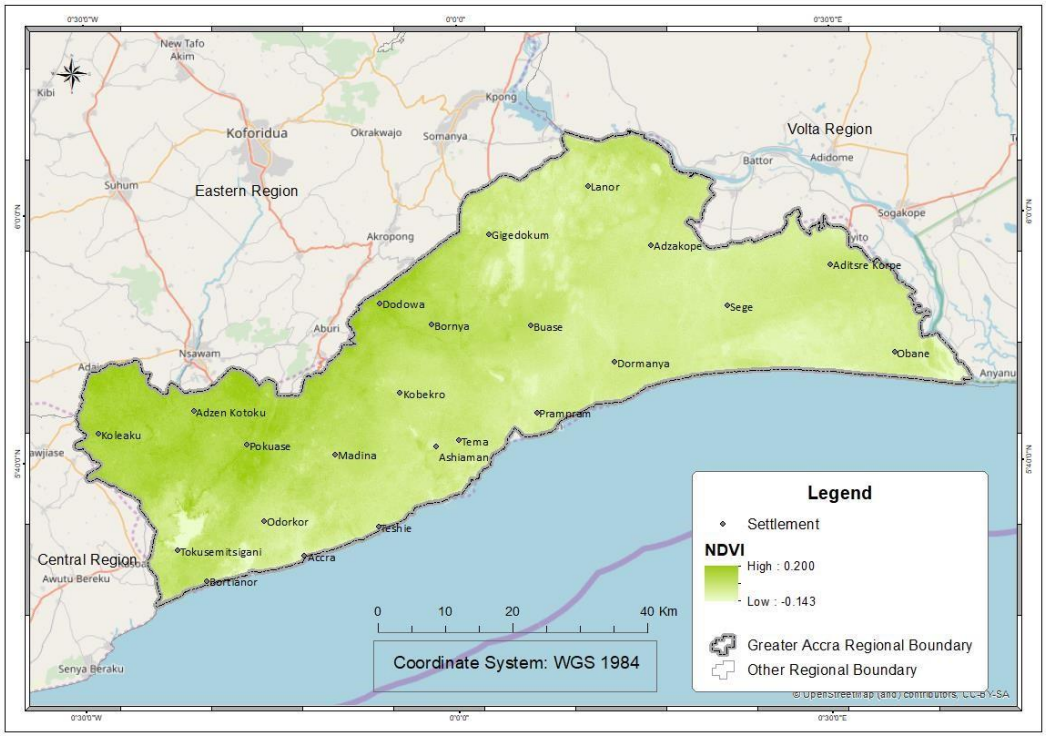

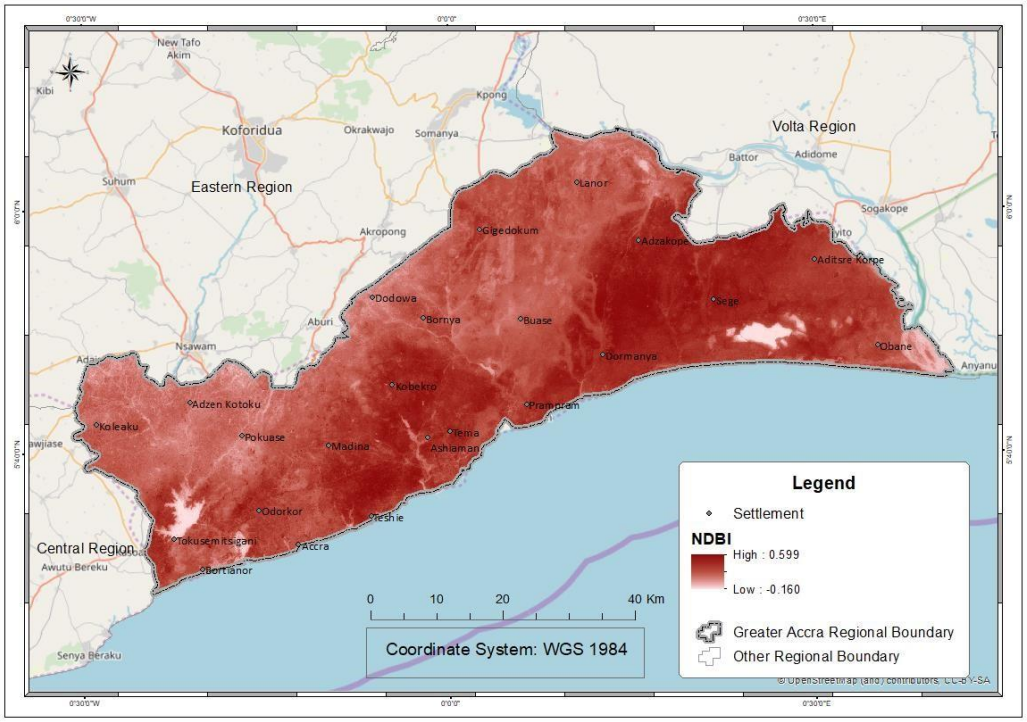

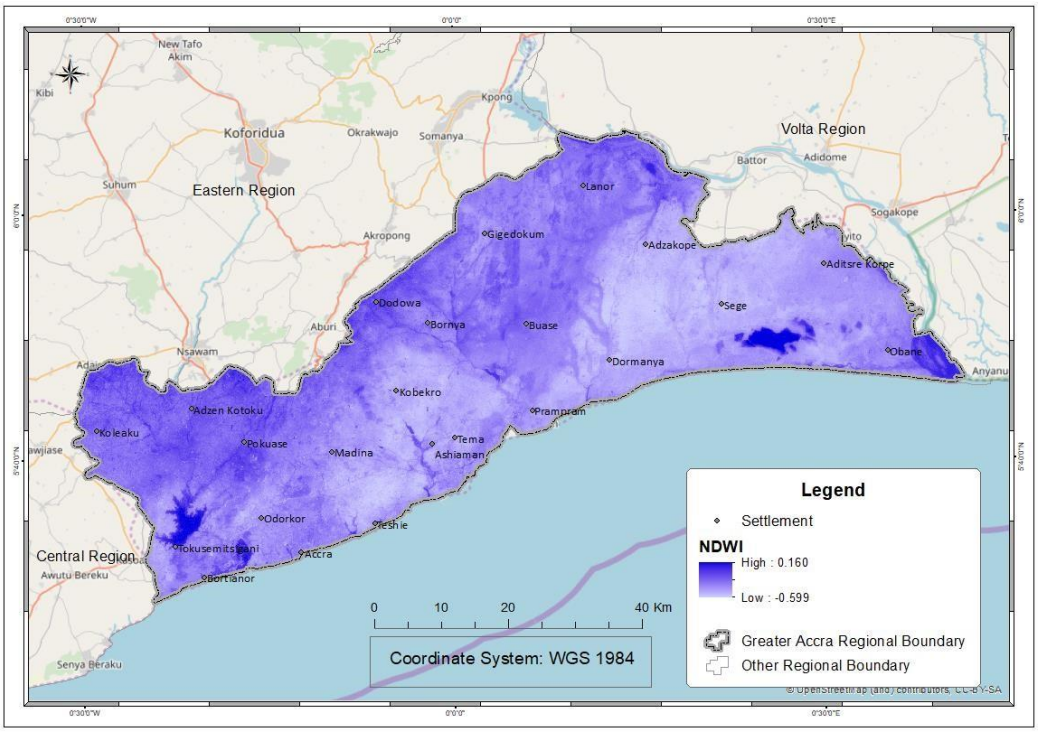

Figure C-3: Normalized Difference Vegetation Index Map of 1986, for Correlation Analysis

Figure C-4: Normalized Difference Water Index Map of 1986, for Correlation Analysis

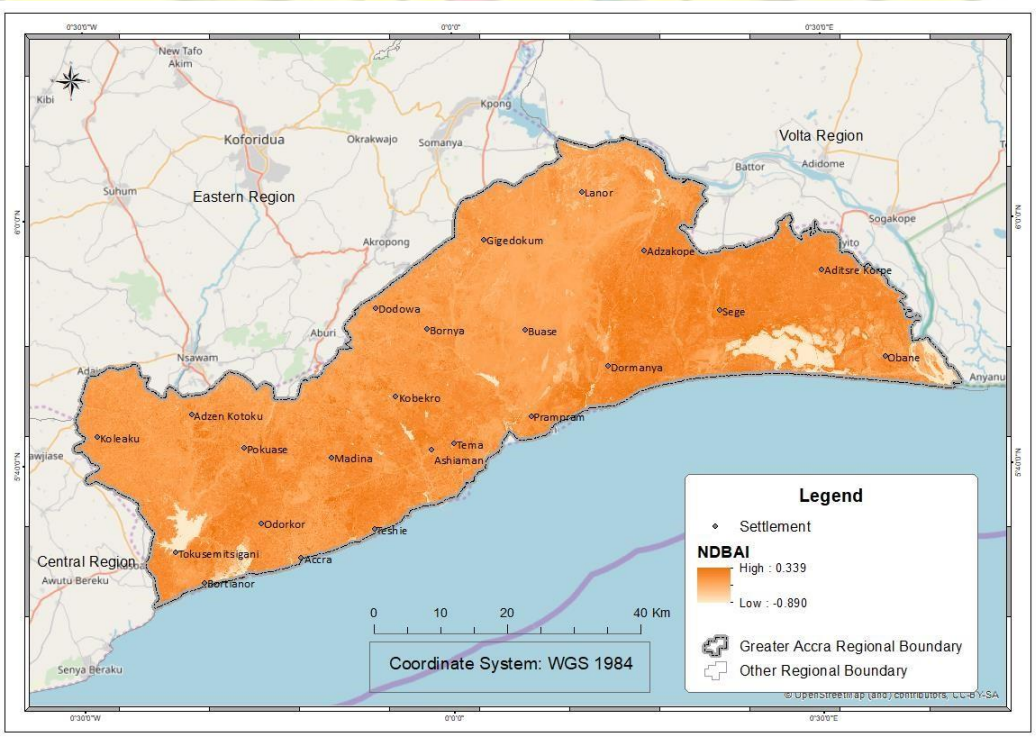

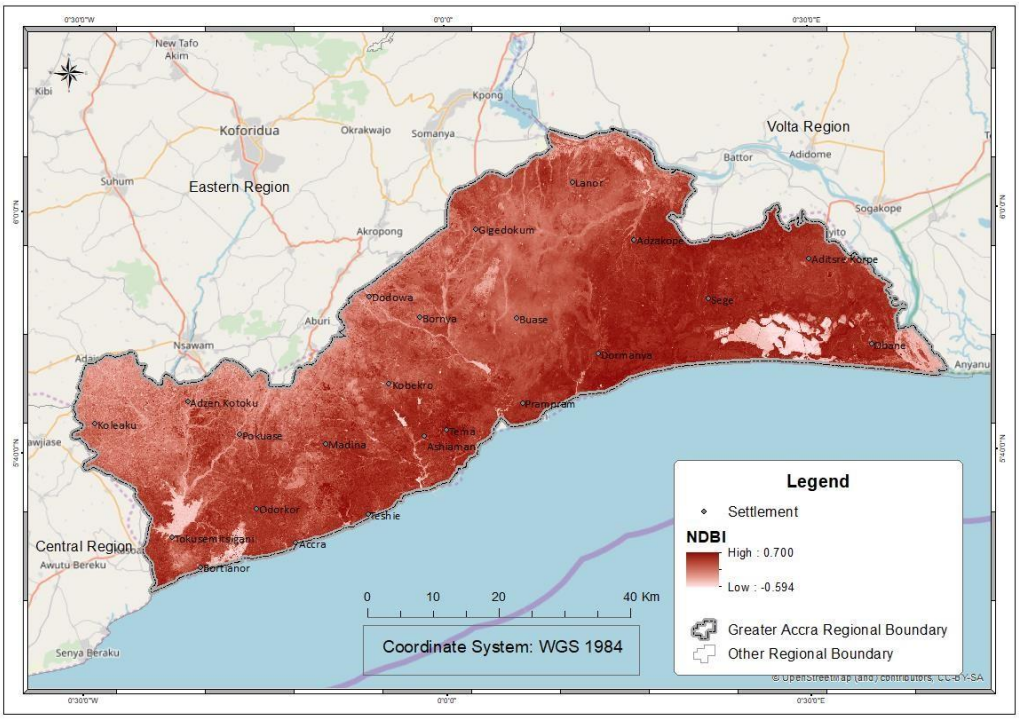

Figure C-5: Normalized Difference Bareness Index Map of 2002, for Correlation Analysis

Figure C-6: Normalized Difference Built-up Index Map of 2002, for Correlation Analysis

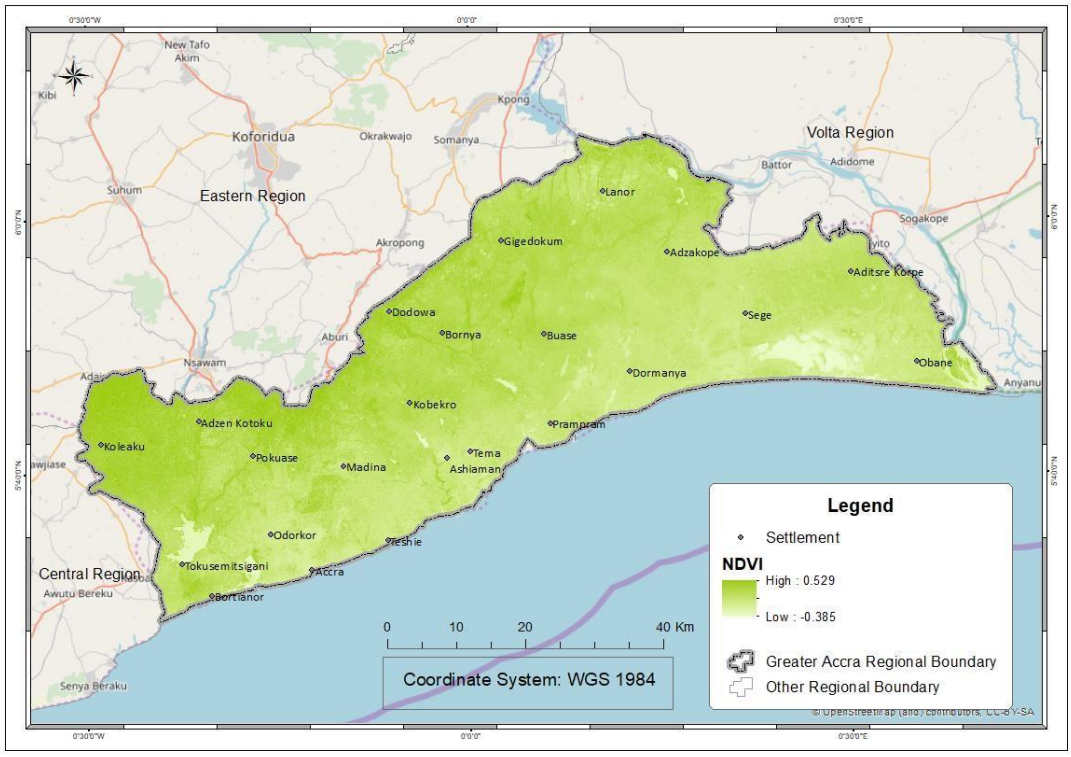

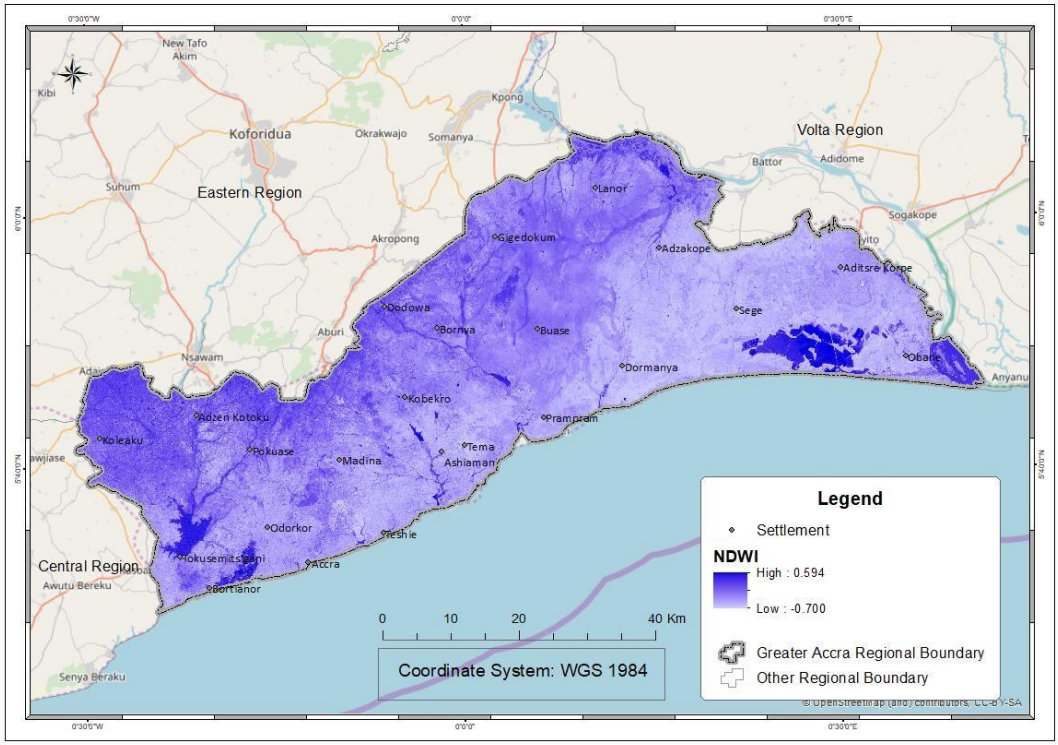

Figure C-7: Normalized Difference Vegetation Index Map of 2002, for Correlation Analysis

Figure C-8: Normalized Difference Water Index Map of 2002, for Correlation Analysis

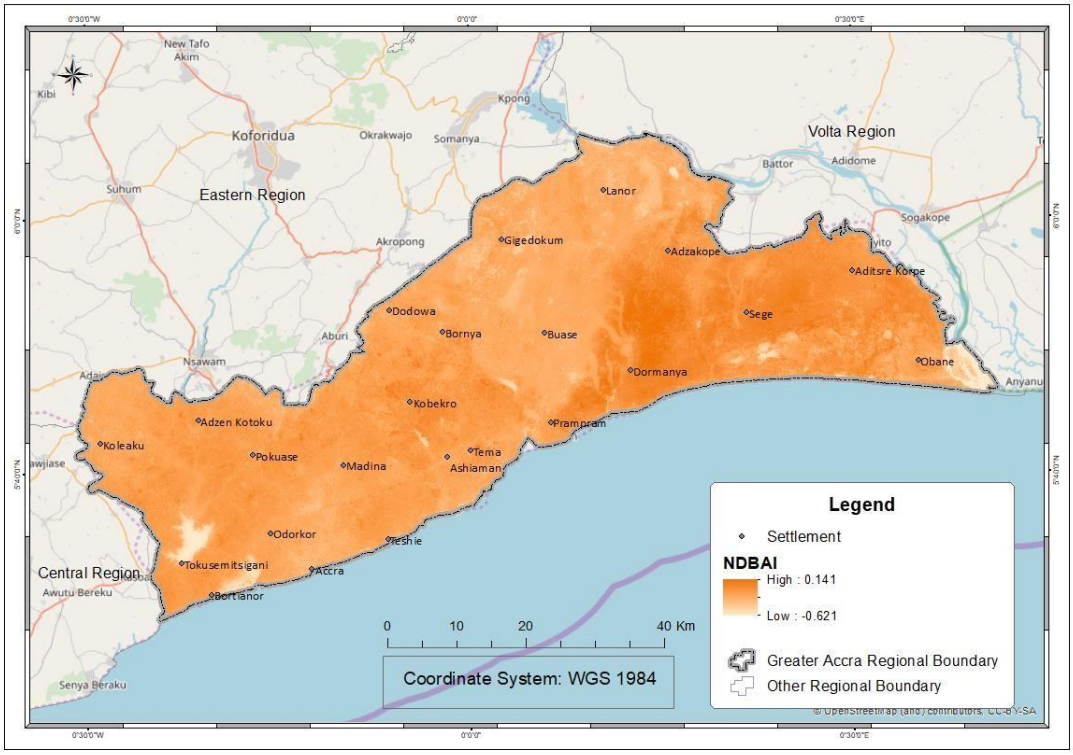

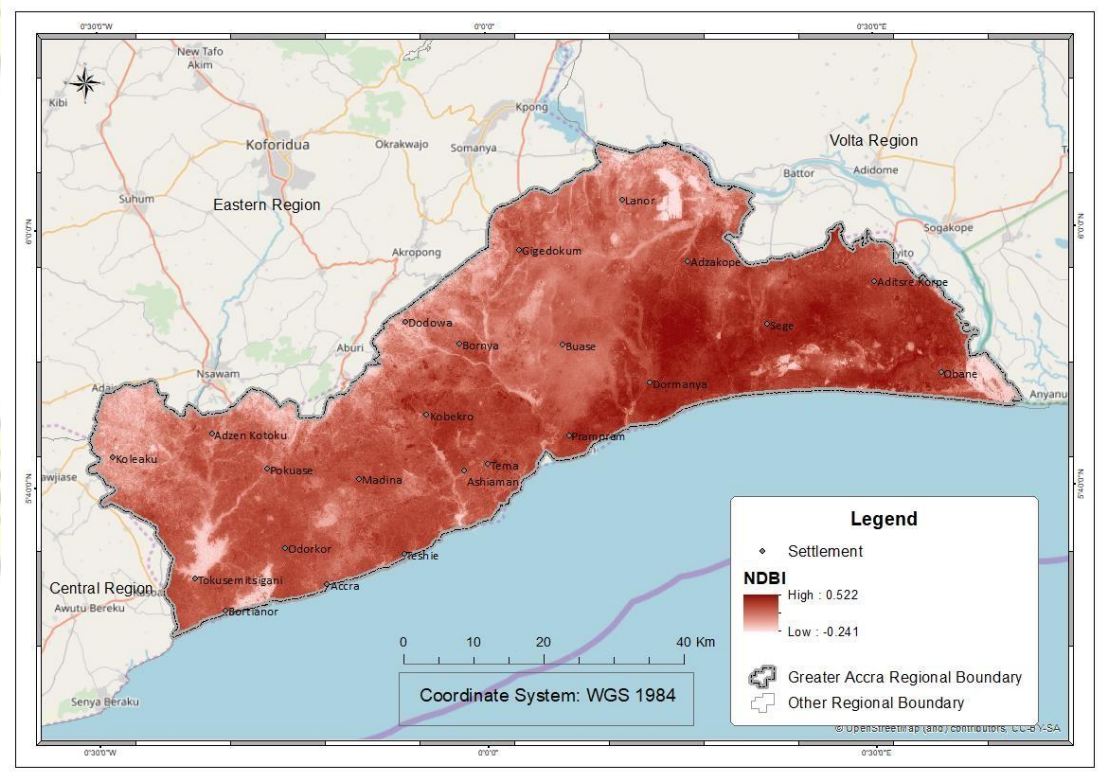

Figure C-9: Normalized Difference Bareness Index Map of 2018, for Correlation Analysis

Figure C-10: Normalized Difference Built-up Index Map of 2018, for Correlation Analysis

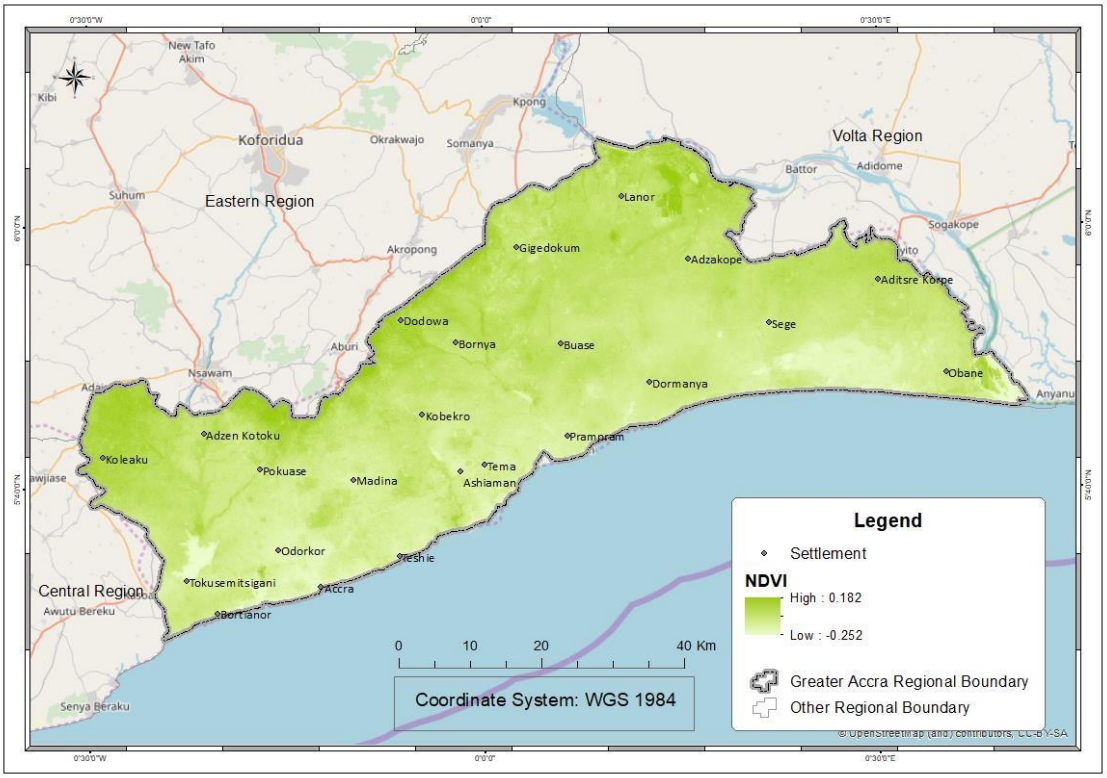

Figure C-11: Normalized Difference Vegetation Index Map of 2018, for Correlation Analysis

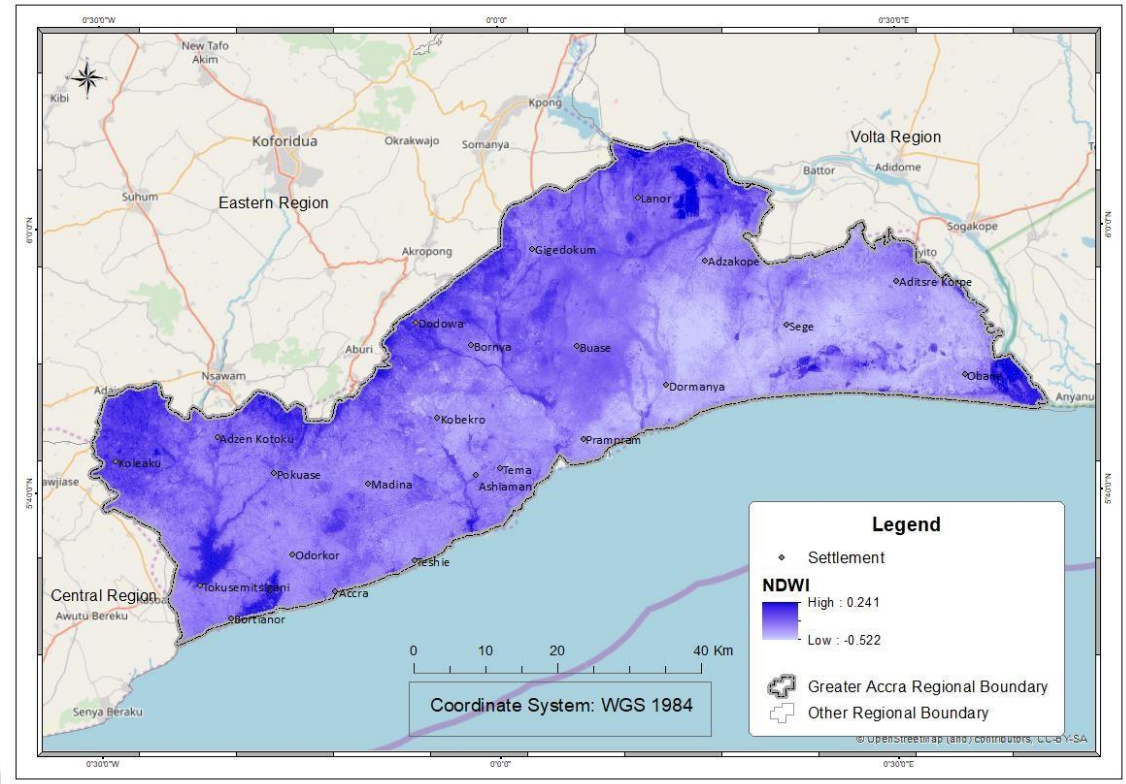

Figure C-12: Normalized Difference Water Index Map of 2018, for Correlation Analysis

Appendix D: Ground truth Images

Figure D-1: Image of Urban development around Kwabenya for Accuracy Assessment

Figure D-2: Image of Bare and Open Land around Afienya for Accuracy Assessment

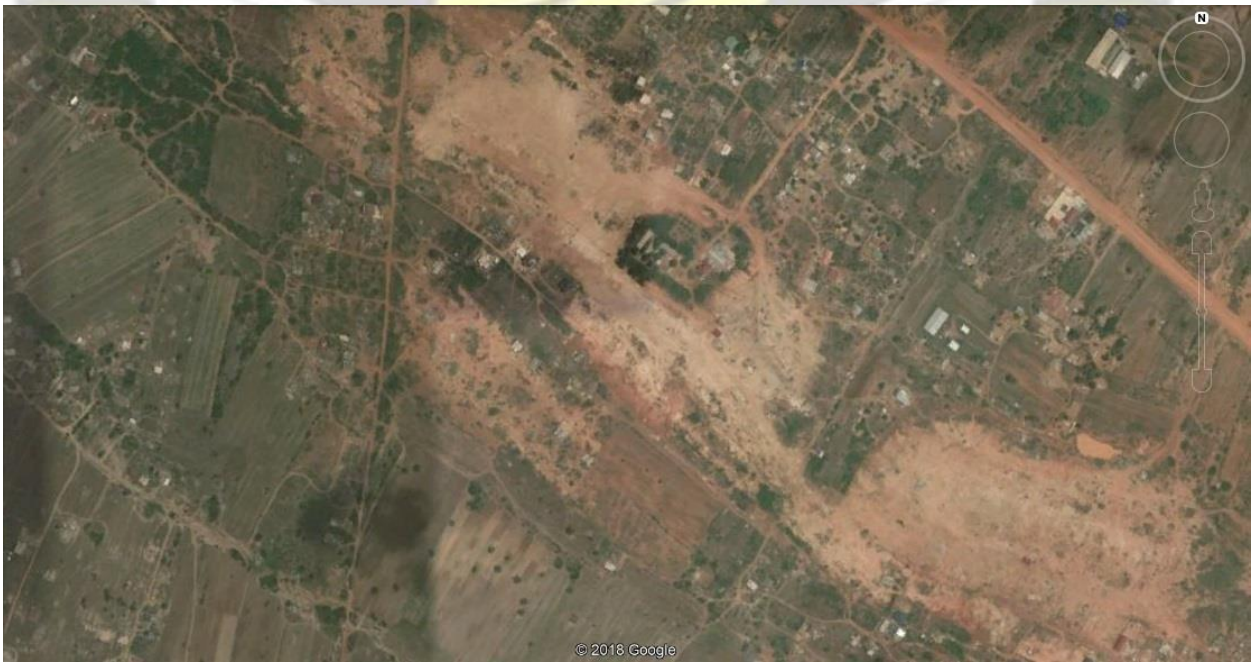

Figure D-3: Image of Built up Development around Pambros for Accuracy Assessment